POSITION-SENSITIVE DEVICES AND SENSOR SYSTEMS FOR OPTICAL TRACKING AND DISPLACEMENT SENSING APPLICATIONS

ANSSI MÄKYNEN

Department of Electrical Engineering

OULU 2000

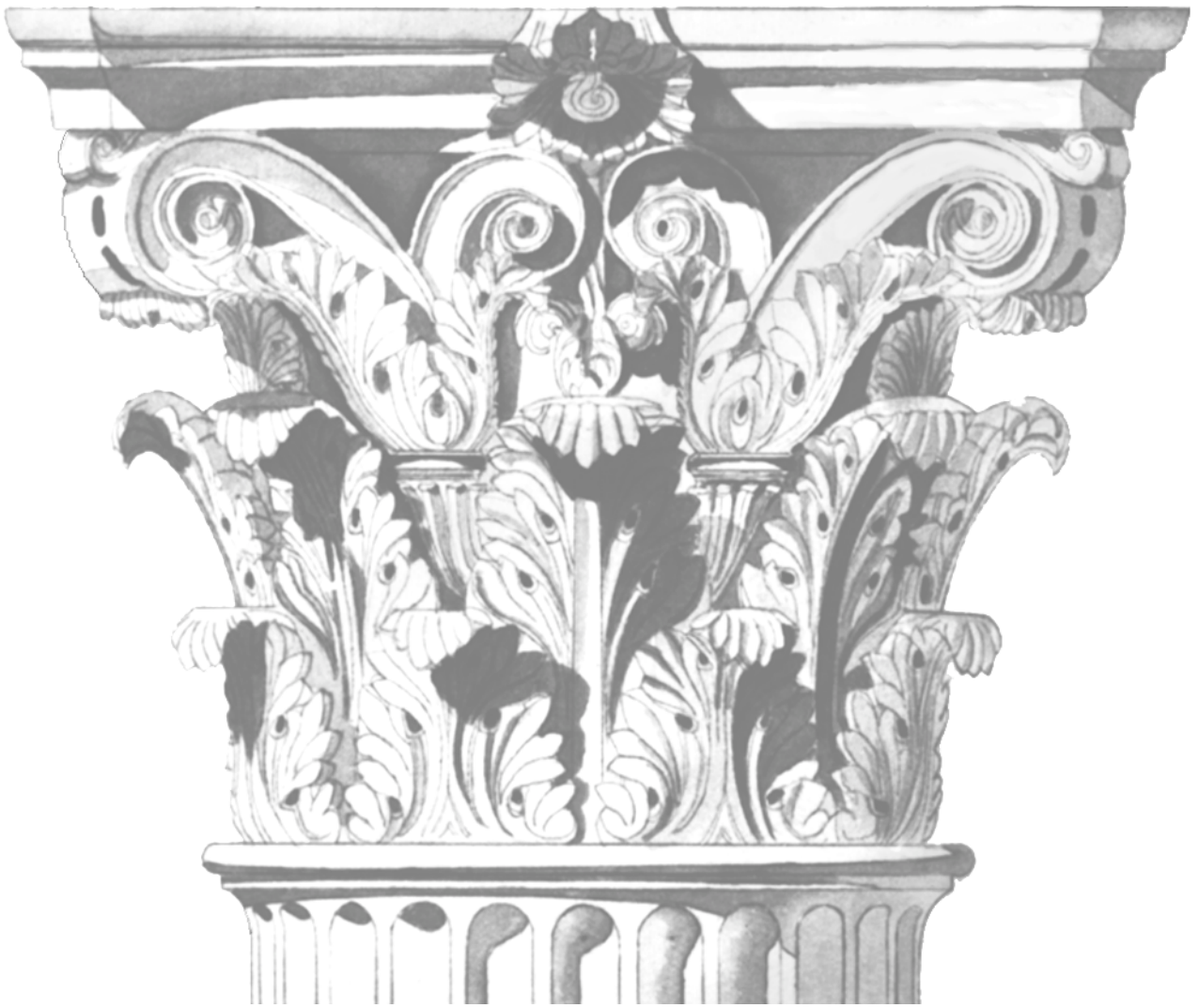

ANSSI MÄKYNEN

POSITION-SENSITIVE DEVICES AND SENSOR SYSTEMS FOR OPTICAL TRACKING AND DISPLACEMENT SENSING APPLICATIONS

Academic Dissertation to be presented with the assent of the Faculty of Technology, University of Oulu, for public discussion in Raahensali (Auditorium L 10), Linnanmaa, on November 3rd, 2000, at 12 noon.

OULUN YLIOPISTO, OULU 2000

Manuscript received 25 September 2000
Accepted 11 October 2000

Communicated by
Doctor Kalevi Hyyppä
Professor Erkki Ikonen

ISBN 951-42-5780-4

ALSO AVAILABLE IN PRINTED FORMAT

ISBN 951-42-5779-0
ISSN 0355-3213 (URL: http://herkules.oulu.fi/issn03553213/)

OULU UNIVERSITY LIBRARY
OULU 2000

Mäkynen, Anssi, Position-sensitive devices and sensor systems for optical tracking and displacement sensing applications
Department of Electrical Engineering, University of Oulu, P.O.Box 4500, FIN-90014 University of Oulu, Finland
2000
Oulu, Finland
(Manuscript received 25 September 2000)

Abstract

This thesis describes position-sensitive devices (PSDs) and optical sensor systems suitable for industrial tracking and displacement sensing applications. The main application areas of the proposed sensors include automatic pointing of a rangefinder beam and measuring the lateral displacement of an object.

A conventional tracking sensor is composed of a laser illuminator, a misfocused quadrant detector (QD) receiver and a corner cube retroreflector (CCR) attached to the target. The angular displacement of a target from the receiver optical axis is detected by illuminating the target and determining the direction of the reflection using the QD receiver. The main contribution of the thesis is related to the modifications proposed for this conventional construction in order to make its performance sufficient for industrial applications that require a few millimetre to submillimetre accuracy. The work includes sensor optical construction modifications and the designing of new types of PSDs. The conventional QD-based sensor, although electrically very sensitive, is not considered optimal for industrial applications since its precision is severely hampered by atmospheric turbulence due to the misfocusing needed for its operation. Replacing the CCR with a sheet reflector is found to improve the precision of the conventional sensor construction in outdoor beam pointing applications, and is estimated to allow subcentimetre precision over distances of up to 100 m under most operating conditions. Submillimetre accuracy is achievable in close-range beam pointing applications using a small piece of sheet reflector, coaxial illumination and a focused QD receiver. Polarisation filtering is found to be effective in eliminating the main error contributor in close-range applications, which is low reflector background contrast, especially in cases when a sheet reflector has a specularly reflecting background.

The tracking sensor construction is also proposed for measuring the aiming trajectory of a firearm in an outdoor environment. This time an order of magnitude improvement in precision is achieved by replacing the QD with a focused lateral effect photodiode (LEP). Use of this construction in cases of intermediate atmospheric turbulence allows a precision better than 1 cm to be achieved up to a distance of 300 m. A method based on averaging the positions of multiple reflectors is also proposed in order to improve the precision in turbulence-limited cases. Finally, various types of custom-designed PSDs utilising a photodetector array structure are presented for long-range displacement sensing applications. The goal was to be able to replace the noisy LEP with a low-noise PSD without compromising the low turbulence sensitivity achievable with the LEP. An order of magnitude improvement in incremental sensitivity is achievable with the proposed array PSDs.

Keywords: 3D coordinate measurement, CMOS photodetectors, atmospheric turbulence, laser spot tracking

Acknowledgements

The research work for this doctoral thesis was carried out at the Electronics Laboratory of the University of Oulu during the years 1988 – 1998.

I wish to express my deepest gratitude to my supervisors, Prof. Juha Kostamovaara and Prof. Risto Myllylä, for their unlimited patience and skilful scientific guidance. I am also grateful to Prof. Timo Rahkonen, Prof. Harri Kopola, Dr. Kari Määttä and Dr. Tarmo Ruotsalainen for their help and support. I thank all my co-workers for the pleasant working atmosphere. I also wish to thank Markku Koskinen and Esa Jansson from Noptel and Ilkka Kaisto from Prometrics for their help and for the sincere interest they showed towards my work.

I wish to thank Prof. Erkki Ikonen and Dr. Kalevi Hyyppä for examining my thesis, and Mr. Malcolm Hicks and Mr. Janne Rissanen for revising the English of my papers and this thesis.

The financial support received from the Oulu University Research Foundation, Walter Ahlström Foundation, Tauno Tönning Foundation, Emil Aaltonen Foundation, Northern Finland Cultural Fund and Seppo Säynäjäkangas Scientific Foundation is gratefully acknowledged.

Finally, I would express my warmest thanks to my family, Anne, Aliisa and Aino, for their patience and support during these years.

Oulu, October 2000 Anssi Mäkynen

List of original papers

The research work for this doctoral thesis was carried out at the Electronics Laboratory of the University of Oulu in several projects during the years 1988-1998. These projects were funded by the University of Oulu, TEKES, Noptel Oy and Prometrics Ltd. This thesis is a summary of the results presented in the following journal and conference papers:

I Kostamovaara J, Mäkynen A & Myllylä R (1988) Method for industrial robot tracking and navigation based on time-of-flight laser rangefinding and the position sensitive detection technique. Proc. SPIE International Conference on Industrial Inspection, Hamburg, FRG, 1010: 92–99.

II Mäkynen A, Kostamovaara J & Myllylä R (1989) Position sensitive detection techniques for manufacturing accuracy control. Proc. SPIE International Conference on Optics, Illumination, and Image Sensing for Machine Vision IV, Philadelphia, Pensylvania, USA, 1194: 243–252.

III Mäkynen A, Kostamovaara J & Myllylä R (1994) Tracking laser radar for 3-D shape measurements of large industrial objects based on time-of-flight laser rangefinding and position-sensitive detection techniques. IEEE Transactions on Instrumentation and Measurement, 43(1): 40–49.

IV Mäkynen A, Kostamovaara J & Myllylä R (1991) Position-sensitive detector applications based on active illumination of a cooperative target. In: Tzafestas SG (ed) Engineering Systems with Intelligence: Concepts, Tools and Applications. International Series on Microprosessor-based and Intelligent Systems Engineering 9: 265–274. Kluwer Academic Publishers, The Netherlands.

V Mäkynen A, Kostamovaara J & Myllylä R (1995) Laser-radar-based three dimensional sensor for teaching robot paths. Optical Engineering 34(9): 2596–2602.

VI Mäkynen A, Kostamovaara J & Myllylä R (1995) A high-resolution lateral displacement sensing method using active illumination of a cooperative target and a focused four-quadrant position-sensitive detector. IEEE Transactions on Instrumentation and Measurement 44(1): 46–52.

VII Mäkynen A, Kostamovaara J & Myllylä R (1996) Positioning resolution of the position-sensitive detectors in high background illumination. IEEE Transactions on Instrumentation and Measurement 45(1): 324–326.

VIII Mäkynen A, Kostamovaara J & Myllylä R (1997) Displacement sensing resolution of position-sensitive detectors in atmospheric turbulence using retroreflected beam. IEEE Transactions on Instrumentation and Measurement 46(5): 1133–1136.

IX Mäkynen A & Kostamovaara J (1997) Accuracy of lateral displacement sensing in atmospheric turbulence using a retroreflector and a position-sensitive detector. Optical Engineering 36(11): 3119–3126.

X Mäkynen A, Rahkonen T & Kostamovaara J (1994) CMOS photodetectors for industrial position sensing. IEEE Transactions on Instrumentation and Measurement 43(3): 489–492.

XI Mäkynen A, Ruotsalainen T & Kostamovaara J (1997) High accuracy CMOS position-sensitive photodetector (PSD). Electronics Letters 33(2): 128–129.

XII Mäkynen A & Kostamovaara J (1998) Linear and sensitive CMOS position-sensitive photodetector. Electronics Letters 34(12): 1255–1256.

XIII Mäkynen A, Rahkonen T & Kostamovaara J (1998) A binary photodetector array for position sensing. Sensors and Actuators A 65(1): 45–53.

XIV Mäkynen A, Ruotsalainen T, Rahkonen T & Kostamovaara J (1998) High performance CMOS position-sensitive photodetectors (PSDs). Proc. IEEE International Symposium on Circuits and Systems, Monterey, California, USA, 6: 610–616.

XV Mäkynen A & Kostamovaara J (1998) An application-specific PSD implemented using standard CMOS technology. Proc. 5th IEEE International Conference on Electronics, Circuits and Systems, Lissabon, Portugal, 1: 397–400.

Papers I to IV describe optical tracking techniques developed for aiming a rangefider beam towards a stationary or moving object. The research work was done by the author, who also prepared the manuscripts for papers II, III and IV. Paper I was prepared by Prof. Juha Kostamovaara who also originally introduced the author to the reflected beam sensing principle. Paper V reports a laser rangefinding method for target orientation measurements. The idea was provided by Professors Juha Kostamovaara and Risto Myllylä, and the circuit techniques for the rangefinder electronics were mostly adapted from the earlier work of Dr. Kari Määttä. The research itself and the preparation of manuscripts were carried out by the author. Paper VI describes a sensing method and experimental results obtained with a sensor prototype designed for close-range lateral displacement sensing. The original idea, research work and preparation of manuscript were the author's. Papers VII, VIII and IX describe the effect of atmospheric turbulence and background illumination on the displacement sensing precision of a reflected beam sensor in an outdoor environment. The idea of using reflected beam techniques for aim point trajectory measurement was originally provided by Prof. Kostamovaara. The ideas related to precision improvement, the actual research work and the writing of the manuscript were the responsibility of the author. Papers X to XV are concerned with the construction and performance of position-sensitive photodetectors implemented using standard CMOS technology. The circuit and layout design work was done jointly by Prof. Timo Rahkonen (Papers X and XIII), Dr. Tarmo Ruotsalainen (Paper XI and XIV) and the author (Papers XII and XV). The second prototype of the digital PSD was designed by Marko Malinen, Dipl. Eng. (not reported in the papers but included in the summary). The idea of a segmented photodiode array with tracking capability (Paper XII) and that of a phototransistor area array (Paper XI) were provided by the author. Prof. Rahkonen originally suggested the digital sensing principle (Paper XIII) and Dr. Ruotsalainen the discrete electrode structure used in the 2-axis lateral effect photodiode (Paper XIV). All device testing and manuscript preparation for Papers X to XV were the work of the author.

List of terms, symbols and abbreviations

The terms describing the performance of sensors are defined according to the IEEE Standard Dictionary of Electrical and Electronics Terms (IEEE 1996):

- **Accuracy** is the degree of correctness with which a measured value agrees with the true value
- **Random error** is a component of error whose magnitude and direction vary in a random manner in a sequence of measurements made under nominally identical conditions
- **Systematic error** is the inherent bias of a measurement process or of one of its components
- **Differential non-linearity** is the percentage departure of the slope of the plot of output versus input from the slope of a reference line
- **Integral non-linearity** is the maximum*) non-linearity (deviation) over the specified operating range of a system, usually expressed as a percentage of the maximum of the specified range
- **Precision** is the quality of coherence or repeatability of measurement data, customarily expressed in terms of the standard deviation of an extended set of measurement results
- **Resolution** describes the degree to which closely spaced objects in an image can be distinguished from one another
- **Incremental sensitivity** is a measure of the smallest change in stimulus that produces a statistically significant change in response.

*) standard deviation is used here

2D	two-dimensional
3D	three-dimensional
A/D	analogue-to-digital
AMS	Austria Mikro Systeme
APD	avalanche photodiode
BiCMOS	bipolar CMOS
CCD	charge-coupled device
CCR	corner cube retroreflector

CMOS	complementary MOS
FOV	field-of-view
FWHM	full width at half maximum
HeNe	helium neon
HPRI	priority encoder
IC	integrated circuit
IEEE	Institute of Electrical and Electronics Engineers, Inc.
LED	light-emitting diode
LEP	lateral effect photodiode, refers here mainly to a commercially manufactured high-quality 2-axis duolateral construction with a 10 kΩ interelectrode resistance
MOS	metal oxide semiconductor
NEP	noise equivalent power
NMOS	n-channel MOS
op amp	operational amplifier
PIN	p-i-n photodiode
PMOS	p-channel MOS
PSD	position-sensitive photodetector
QD	quadrant detector
rms	root-mean-square
RX	receiver
SFR	signal-to-fluctuation ratio related to one quadrant of a receiver aperture or to one CCR, defined here as the average signal level divided by the rms value of its fluctuations
SNR	signal-to-noise ratio, here the ratio between rms values
SPIE	International Society for Optical Engineering
SRG	shift register
TDC	time-to-digital converter
TIM	time interval measurement
TOF	time of flight
TX	transmitter

A	aperture averaging factor defined as $\sigma_{Ier}^2/\sigma_{Ipr}^2$
a	radius of curvature of the active area boundary of a pincushion LEP; contact (quadrant) of a PSD
B	noise equivalent bandwidth
b	contact (quadrant) of a PSD
C_d	total capacitance of a PSD
C_n	refractive index structure coefficient, describes the strength of atmospheric turbulence
C_{pix}	input capacitance of a digital pixel
c	correlation coefficient of the illumination fluctuations between crosswise quadrants of a receiver aperture or between the reflections from separate CCRs; contact (quadrant) of a PSD; speed of light

D	lateral extent of the measurement field at the target distance, equals sheet reflector diameter (or side length) in the case of a focused QD receiver
d	lateral extent of a PSD measurement span, equals the diameter (or side length) of the light spot on a QD and the side length of the LEP active area; contact (quadrant) of a PSD
d_s	light spot diameter (or side length) on a PSD
E_{DPSD}	optical signal energy needed for one measurement result in the case of a digital PSD
E_{LEP}	optical signal energy needed for one measurement result in the case of a LEP
E_{pix}	optical signal energy needed for triggering a digital pixel
f	focal length of receiver optics
$f/\#$	f-number, defined as f/ϕ
G	gain of a sheet reflector over a perfect Lambertian surface
H	diameter of the illuminated area relative to that of the reflector defined as $L\theta/D$
I_b	current due to background illumination at the input of a digital pixel
I_s	current due to the optical signal at the input of a digital pixel
I_t	threshold current of a digital pixel
i_a, i_b, i_c, i_d	average signal currents of the contacts (quadrants) a, b, c and d of a PSD
i_n	rms value of current noise density
i_{namp}	rms value of current noise density of an op amp
i_{nLEP}	rms value of current noise density of a LEP receiver
i_{nb}	rms value of current noise density due to background illumination
i_{nRf}	rms value of current noise density of R_f
i_{nRie}	rms value of current noise density of R_{ie}
$i_n(-1)$,$i_n(0)$,$i_n(+1)$	rms value of total current noise density of noise sources having the same correlation coefficient (–1, 0, +1) between opposite receiver channels
K	slope of the error characteristics of a tracking sensor
K_F	fill factor of a photodetector array, here the photodetector area divided by the total area of the array
k	Boltzmann's constant; wave number defined as $2\pi/\lambda$
k_{LEP}, k_{QD}	scale factors of a LEP and QD, convert the relative displacement values to absolute ones
k_n	noise sensitivity of a PSD, scales the effect of SNR on relative precision
L	reflector distance from the receiver lens
L'	image plane distance from the receiver lens
L_0	outer scale of turbulence, describes the largest turbulent cell size
m	magnification of optics
n	number of CCRs; number of measurement results averaged; refractive index
P_b	background illumination power falling on a PSD

P_{ill}	total power used to illuminate the measurement field
P_t	optical power producing a signal current which equals the threshold current I_t
P_{pix}	optical signal power falling on a digital pixel
P_r	total optical signal power received
p	total pixel width (pitch) of a digital PSD
q	light spot diameter expressed in terms of pixel width p; electron charge
R	sheet resistance, Ω/□
R_f	feedback resistance of a transimpedance preamplifier
R_{ie}	resistance between opposite electrodes of a LEP, called here interelectrode resistance
r	boundary resistance of a pincushion LEP, Ω/cm
S	responsivity of a photodetector
$\Delta S/S_{syst}$	relative system responsivity difference in the areas occupied by the reflector and its image, illumination, reflector reflectivity and photodetector responsivity non-uniformities are taken into account here
SW_x, SW_y	signals for switching CMOS LEP contacts on/off
T	absolute temperature
t	time
t_m	time interval between successive measurements
Δt	time interval between start and stop pulses of a TOF rangefinder
U_{dd}	operating voltage of a digital pixel
U_{in}	voltage at the input node of a digital pixel
U_T	threshold voltage of a MOS transistor
ΔU	voltage change needed at the input node of a digital pixel to trigger it
u_n	rms value of voltage noise density
u_{namp}	rms value of voltage noise density of an op amp
V	wind speed perpendicular to a measurement beam
V_α	output signal of a tracking sensor used to drive gimballed optics
w	beam diameter
X, X_t	measured and true displacements of a reflector from the centre of a measurement field
x, y	measured displacements of a light spot centroid from the centre of a PSD
α	angle between the target line-of-sight and receiver optical axis
β	current gain of a phototransistor
χ	input signal for a tracker describing the desired angle between an arbitrary reference axis and the target line-of-sight
Δ	lateral distance separating two reflector centroids at the target
δ	relative misfocus defined as detector axial displacement from the image plane divided by the distance of the image plane from the receiver lens
ε_c	estimate for the lateral displacement sensing error at the target distance due to finite reflector background contrast

ε_{srd}	upper bound estimate for the error due to the system responsivity difference
φ	constant in the equation defining the angle-of-arrival variance of the received beam
λ	wavelength of optical radiation
ϕ	receiver lens (entrance pupil) diameter
γ	aperture diameter divided by the diffraction patch size $\sqrt{L\lambda}$
θ	illumination beam divergence (full angle), typically equals the angular FOV of the receiver
$\pm\theta_{aq}$	angular divergence of the acquisition FOV, θ_{aq} equals half of the angular FOV
$\pm\theta_{tr}$	angular divergence of the tracking FOV
ρ_0	spherical wave coherence length, describes the path-integrated strength of atmospheric turbulence
ρ_{av}	average reflectivity of the illuminated background
ρ_Δ	difference in reflectivities of illuminated background half circles
σ	standard deviation of measurement results describing the precision of a sensor system at the target distance; standard deviation of the integral non-linearity of a LEP at its active surface, unit is metre
σ_{AOA}	standard deviation of lateral displacement results at the target distance due to angle-of-arrival fluctuations
σ_{DPSD}	standard deviation of lateral displacement results of the digital PSD at its active surface
σ_{IFrec}	standard deviation of lateral displacement results at the target distance due to spatially uncorrelated intensity fluctuations at the receiver aperture
σ_{IFref}	standard deviation of lateral displacement results at the target distance due to uncorrelated intensity fluctuations of reflections from separate reflectors
σ_{LEP}, σ_{QD}	standard deviation of lateral displacement results of the LEP and QD at their active surfaces
σ_{min}	estimate for the smallest possible standard deviation of lateral displacement results achievable with a LEP at its active surface
σ_{PSD}	standard deviation of lateral displacement results of a PSD at its active surface
σ_{PTPSD}	standard deviation of lateral displacement results of the phototransistor PSD at its active surface
σ_{TRPSD}	standard deviation of lateral displacement results of the tracking PSD at its active surface
σ_α^2	angular variance of angle-of-arrival fluctuations
σ_{Ier}^2	normalised illumination variance for an extended receiver
σ_{Ipr}^2	normalised illumination variance for a point receiver
τ	transmittance of an optical path from a light source to a photodetector
ξ	rotational angle of a pointer
Ψ	angle between tracker's reference axis and its optical axis
ζ	depth angle of a pointer

Contents

Abstract
Acknowledgements
List of original papers
List of terms, symbols and abbreviations
Contents
1. Introduction 21
1.1. Applications of position-sensitive devices (PSDs) 22
1.2. A conventional laser spot tracker 22
1.3. Content and main contributions of the work 24
2. Reflected beam sensor 26
2.1. Operating principle and outline of construction 26
2.2. Position-sensitive detectors (PSDs) 27
2.2.1. Operating principles 27
2.2.2. Lateral transfer characteristics 29
2.3. Limits of measurement accuracy 29
2.3.1. Precision of the LEP and QD receivers 29
2.3.1.1. Noise sensitivity 30
2.3.1.2. Predominant internal noise sources 31
2.3.1.3. Comparison of the PSD receivers 32
2.3.2. Reflectors and their influence on measurement accuracy 32
2.4. Proposed sensor constructions 33
2.4.1. A focused QD receiver and sheet reflector 33
2.4.2. A focused LEP receiver and CCR 34
2.4.3. Conclusions 35
3. Sensors for tracking rangefinders 36
3.1. Tracking rangefinder 36
3.1.1. Rangefinding 3D coordinate meter 36
3.1.2. Pulsed time-of-flight (TOF) rangefinder 37
3.1.3. The tracking rangefinder and its applications 38
3.2. A simplified tracker model 40
3.3. A tracking sensor for vehicle positioning 41
3.3.1. Tracking rangefinders for vehicle positioning 42
3.3.2. Proposed sensor construction 42

3.3.3. Precision in outdoor environment ... 43
3.3.4. Conclusions ... 44
3.4. A tracking sensor for an automatic 3D coordinate meter ... 45
3.4.1. Advantages of automatic pointing ... 45
3.4.2. Rangefinding coordinate meters capable of automatic pointing ... 46
3.4.3. QD versus camera-based tracking ... 46
3.4.4. Operating principle and design goals ... 47
3.4.5. Sensor parameters and tracking accuracy ... 48
3.4.6. Sensor construction ... 49
3.4.6.1. Combining the rangefinder and tracking sensor optics ... 49
3.4.6.2. Parallel versus coaxial illumination ... 50
3.4.7. Performance of the tracking sensor prototypes ... 51
3.4.8. Conclusions ... 52
3.5. Improving reflector background contrast by polarisation filtering ... 53
3.5.1. Applications of polarisation filtering and related work ... 53
3.5.2. Operating principle ... 53
3.5.3. Applicability to a tracking coordinate meter ... 55
3.6. A rangefinder for measuring object position and orientation ... 55
3.6.1. Interactive teaching of robot paths and environments ... 56
3.6.2. Sensor systems for position and orientation measurements ... 56
3.6.3. Sensor construction ... 57
3.6.4. Active target rangefinder ... 58
3.6.4.1. Operating principle ... 58
3.6.4.2. Miscellaneous phenomena and constructional details ... 59
3.6.4.3. Measured performance ... 60
3.6.5. Discussion ... 60
4. Sensors for lateral displacement measurements ... 61
4.1. A reflected beam sensor for close-range displacement sensing ... 62
4.1.1. Methods for small displacement sensing ... 63
4.1.2. Main properties of the sensing principle ... 63
4.1.3. Performance of the experimental sensor ... 65
4.1.3.1. Precision ... 65
4.1.3.2. Accuracy of scaling ... 65
4.1.3.3. Effect of receiver misfocus and reflector misorientation ... 66
4.1.3.4. Linearity of the lateral transfer characteristics ... 67
4.1.4. Conclusions and discussion ... 67
4.2. A reflected beam sensor for long-range displacement sensing ... 69
4.2.1. Requirements for a shooting practice sensor ... 69
4.2.2. Possible sensor constructions ... 70
4.2.3. Construction of the proposed sensor ... 70
4.2.4. Effect of noise on measurement precision ... 71
4.2.5. Atmospheric turbulence ... 71
4.2.6. Effect of atmospheric turbulence on measurement precision ... 73
4.2.6.1. Angle-of-arrival fluctuations ... 73
4.2.6.2. Effect of illumination fluctuations ... 74
4.2.7. Turbulence-limited precision of QD and LEP-based sensors ... 76

4.2.8. Experimental results ... 76
4.2.8.1. Turbulence-limited precision of a QD-based sensor ... 77
4.2.8.2. Turbulence-limited precision of a LEP-based sensor ... 77
4.2.9. Improving turbulence-limited precision ... 78
4.2.9.1. Averaging successive measurement results ... 78
4.2.9.2. Averaging using multiple reflectors ... 79
4.2.10. Sensor construction for the best precision ... 81
5. Custom-designed position-sensitive devices ... 82
5.1. Earlier work on PSDs manufactured using IC technologies ... 83
5.2. Conventional 2-axis LEP ... 84
5.2.1. Evolution ... 84
5.2.2. Performance of a duolateral LEP ... 85
5.2.3. Precision optimisation and its practical restrictions ... 86
5.2.4. Receiver power consumption ... 87
5.3. Aims of the PSD experiments ... 87
5.4. Array PSDs employing LEP-type current division ... 88
5.4.1. A photodiode array PSD ... 88
5.4.2. A phototransistor PSD ... 88
5.4.3. Effect of a discrete photodetector array on accuracy ... 89
5.4.4. Lowering the digitising error by spatial filtering ... 90
5.5. An array PSD employing QD-type current division ... 91
5.6. An array PSD composed of digital pixels ... 92
5.6.1. Accuracy of binary detection ... 92
5.6.2. Optimal pixel size ... 93
5.6.3. Construction and operating principles of a digital pixel ... 93
5.6.4. Sensitivity in pulsed mode ... 95
5.6.5. Sensitivity comparison with LEP ... 96
5.7. Suitability of CMOS technology for PSD realisations ... 96
5.7.1. Properties of CMOS photodetectors ... 97
5.7.2. 2-axis LEP realisations using CMOS ... 98
5.7.3. Effect of crosstalk on spatial digitisation error ... 98
5.8. PSD prototypes ... 99
5.8.1. Single-axis LEPs ... 99
5.8.2. 2-axis LEP ... 100
5.8.3. Photodiode array PSD ... 101
5.8.4. Phototransistor PSD ... 102
5.8.5. Tracking PSD ... 103
5.8.6. Digital PSDs ... 104
5.9. Comparison of the performance of the PSDs ... 106
5.9.1. Effects of technology and device scaling ... 108
5.9.2. Applicability to long-range displacement sensing ... 108
6. Discussion ... 110
6.1.Ways to reduce the effect of atmospheric turbulence ... 110
6.2. Improving reflector background contrast ... 111
6.3. Custom-designed PSDs ... 112
7. Summary ... 114
References ... 118
Original papers

1. Introduction

Various kinds of optical sensor systems for tracking and displacement sensing are needed in industrial and commercial applications. Typical examples include centring and focusing of the pick-up laser beam in optical data storage devices and distance measurement on the optical triangulation principle. This thesis describes optical position-sensitive detection techniques developed for automatic pointing of a laser beam towards a target and for measuring 2D displacement of a target from a reference point. The beam pointing technique was developed for industrial dimensional accuracy control and has been used as such in a commercial 3D coordinate meter (Prometrics Ltd. 1993a). The displacement sensing techniques have been applied in optical shooting practice to measure the aiming trajectory of a firearm (Noptel Oy 1997). The sensing method used is the same in both applications. Target point displacement from the receiver optical axis is detected by illuminating a reflector attached to the target and detecting the direction of reflection using a position-sensitive photodetector (PSD). The results are then used either to drive the servomotors of a measuring head in the case of the coordinate meter, or to evaluate the displacement of the aim point from the target centre in optical shooting practice.

The sensing method, called here the reflected beam method, is similar to that of laser spot trackers used in aerospace and military applications since the 1960s. The main contributions of the work are related to the modifications proposed to the operating principle and construction of the conventional laser spot tracker in order to make it suitable for the industrial tracking and displacement sensing applications described above. This work has included modifications in optical construction and the designing of new types of PSDs.

Typical PSD applications and the operating principle of the conventional laser spot tracker are explained first, after which the content and main contributions of the work are briefly described. Related work will be presented separately in each chapter.

1.1. Applications of position-sensitive devices (PSDs)

Optical position-sensitive detectors are simple photodiodes capable of detecting the centroid position of a light spot projected on their surface. The position information is calculated from the relative magnitudes of a few photocurrent signals provided by the PSD. In a quadrant detector (QD), photocurrents are derived by projecting a light spot on four photodiodes placed close to each other on a common substrate, while the lateral effect photodiode (LEP) is a single photodiode in which embedded resistive layers are used to generate the position-sensitive signal currents.

PSDs are widely used in commercial and industrial applications where low-cost or high-speed position sensing is needed. LEPs are probably mostly used in optical distance meters based on the triangulation principle (Stenberg 1999). Such sensors are used in various kinds of height, thickness and vibration measurements needed in industrial fabrication processes, for example, as well as in inexpensive cameras to provide the target distance for the autofocus mechanism (Seikosha Corp. 1994, Sharp Corp. 1997). In addition to distance measurements, triangulating sensors are used for switching various domestic devices such as electric fans, air conditioners, water taps and sanitary facilities on and off by detecting the presence of a human body (Seikosha Corp. 1994, Sharp Corp. 1997, Symmons Industries Inc. 1999). Other applications include miscellaneous types of position, motion, vibration, alignment, levelling and angle measurements and beam tracking applications (New 1974, Hutcheson 1976, Feige *et al.* 1983, Schuda 1983, Lau *et al.* 1985, SiTek Electro Optics 1996, Spiess *et al.* 1998).

QDs are mostly used as centring indicators rather than as linear position sensors. Large quantities of them are used in CD-ROMs and audio players, for example, to centre and focus the pick-up laser beam on the disc track to be read (Pohlmann 1992). Other uses include various kinds of precision instrumentation and robotic, military and aerospace tracking applications (Kelly & Nemhauser 1973, Light 1982, Brown *et al.* 1986, Gerson *et al.* 1989, Mayer & Parker 1994, Nakamura *et al.* 1994, Degnan & McGarry 1996).

Imaging detectors such as CCDs are sometimes used for light spot position sensing instead of PSDs, particularly in instrumentation applications requiring the utmost accuracy and sensitivity. It is obvious that the mass production of low-cost CMOS imagers and the rapid development of digital signal processing ICs together will partially replace PSDs in some of the traditional applications described above. It should be noted, however, that it is not easy to replace a two-dimensional PSD with an imaging detector in applications where the measurement speed exceeds the standard video frame rate or where a low signal processing load (low power consumption) is required. The sensors presented in the present thesis belong to this category.

1.2. A conventional laser spot tracker

Optical laser spot tracking resembles the techniques used in a military tracking radar devices. Monopulse radar tracking based on target illumination with a diverging electromagnetic beam and four adjacent receiver lobes was first proposed in 1928 and

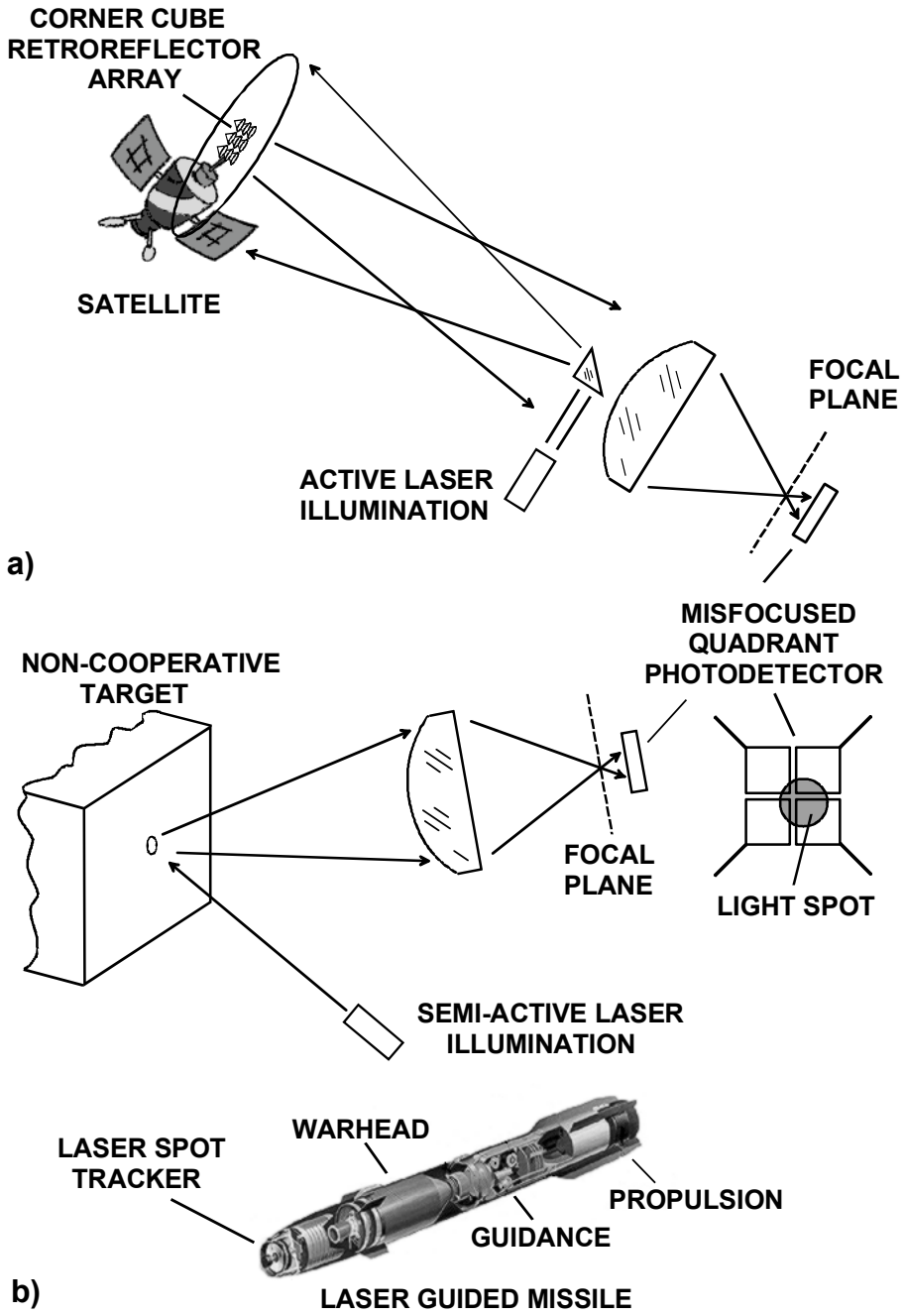

Fig. 1. The proposed industrial tracking and displacement sensors resemble the active laser spot trackers used a) in satellite laser ranging systems and b) in laser guided missiles and bombs.

has been used since the 1950s for missile homing purposes, for example (Kingsley & Quegan 1992). Optical tracking became possible after the invention of lasers. Due to the much shorter wavelength, optical tracking provided better precision and smaller device size than conventional radar, and thus small-size, light-weight missile homing systems with pinpoint accuracy became possible, for example.

The reflected beam sensors proposed in this thesis are in principle similar to the laser spot trackers used in aerospace and military applications (Fig. 1), which use active illumination and a misfocused QD receiver to measure the angular displacement of a laser spot from the optical axis of the receiver. Receiver misfocusing is needed to enlarge the tracking FOV and consequently to maintain continuous, stable tracking (Yanhai 1986, Gerson *et al.* 1989). In aerospace applications targets such as spacecraft, satellites and aeroplanes are equipped with corner cube reflectors (CCRs) and the illuminating beam overfills the target as in conventional radar trackers (Ammon & Russel 1970, Cooke & Speck 1971, Kinnard *et al.* 1978, Kunkel *et al.* 1985, Degnan & McGarry 1997). Similar techniques have also been experimented with for geophysical measurements (Degnan *et al.* 1983, Cyran 1986). In military applications the target is typically non-cooperative, and semi-active illumination as depicted in Fig. 1b is used (Martin Marietta Aerospace 1974, Walter 1976, Johnson RE 1979, Sparrius 1981, Gerson *et al.* 1989).

1.3. Content and main contributions of the work

The laser spot trackers used in aerospace and military applications are not suitable as such for industrial applications. Thus the main contributions of this work are related to the modifications to be made to the operating principle and the construction of a conventional tracking sensor in order to provide adequate performance for industrial tracking and displacement sensing applications, which typically require an operating range from a few metres to a few hundreds of metres together with subcentimetre or submillimetre measurement accuracy. The content and main contributions of the work are described below.

The operating principles, constructions and fundamental performance constraints of the two reflected beam sensor constructions proposed in this thesis for tracking and displacement sensing are presented in Chapter 2, and tracking sensors for the automatic pointing of a laser beam towards a stationary or moving target, together with rangefinding techniques for target orientation measurement, are proposed in Chapter 3. The conventional laser spot tracker proves to be very susceptible to atmospheric turbulence due to the receiver misfocusing used, and thus shows inadequate precision for outdoor tracking applications requiring subcentimetre accuracy. Improved precision is obtained by replacing the corner cube reflector with a sheet reflector.

A tracking sensor is implemented for a 3D coordinate meter in order to point its measurement beam automatically towards a marked point on the object surface. A practical sensor implementation based on a focused QD receiver, coaxial illumination and a small sheet reflector provides comparable accuracy with manual aiming when the object to be measured has diffuse reflectance properties. The practical operating

environment may also include specularly reflecting objects, however, in which case sufficient tracking accuracy may not be achieved, due to strong background reflections. The polarisation filtering proposed for reducing this error has proved to be effective and technically feasible.

The last part of Chapter 3 deals with a rangefinding method proposed for object distance and orientation measurement. Small fibre-coupled transmitters are attached to the target object and their distance from a tracking receiver is measured using a pulsed TOF rangefinder. The distance results are then used to determine the orientation of the object with respect to the optical axis of the receiver. The functionality of the method is demonstrated by implementing a pointing device for robot teaching purposes.

The properties and performance of two reflected beam sensor constructions designed for displacement sensing applications are described in Chapter 4. The first of these utilises a focused QD receiver and a square-shaped sheet reflector to measure small displacements accurately from a distance of a few metres. Unlike the conventional tracking sensor, the proposed construction provides position information which is proportional to linear rather than angular displacement, and scaling which is range-invariant and solely determined by the size of the reflector. Experimental results suggest that the proposed sensing principle is feasible in practice.

The second sensor system, based on a focused LEP receiver and a CCR, is proposed for long-range outdoor measurements such as the aim point trajectory measurement needed in optical shooting practice. Ways of minimising receiver sensitivity to atmospheric turbulence, which determines the measurement precision out of doors, are studied. The turbulence sensitivities of the misfocused QD receiver and the LEP receiver are compared, and it is found that the LEP receiver is less sensitive to atmospheric fluctuations, since it can be focused, and that regardless of its higher noise it provides better precision. Further precision improvement by adjusting the parameters of the receiver optics or by averaging successive measurement results is found to be inefficient in a turbulence-limited case. A method for improving turbulence-limited precision based on multiple laterally separated reflectors is proposed and its functionality demonstrated.

Chapter 5 describes several types of PSD designed particularly for the reflected beam sensor used in long-range displacement sensing applications. The prototypes show that PSDs based on a dense photodetector array allow equally low sensitivity to atmospheric turbulence to be achieved as with the LEP but with much better linearity and incremental sensitivity.

The main results of the work are discussed in Chapter 6, and a summary is given in Chapter 7.

2. Reflected beam sensor

2.1. Operating principle and outline of construction

A reflected beam sensor, as depicted in Fig. 2, is composed of an optical transceiver and a reflector. The transmitter illuminates the measurement field with a uniform beam, the divergence θ of which equals the angular field-of-view (FOV) of the receiver, and the light reflected from the target is focused on the PSD located at the focal plane of the receiver optics. The angular displacement of the reflector with respect to the optical axis of the receiver is

$$\alpha \approx \frac{x}{f}, \tag{1}$$

where x is the displacement of the reflector image from the centre of the PSD and f the focal length of the receiver optics.

A block diagram of a typical signal processing circuitry is depicted in Fig. 3. The illuminator (LED, laser diode etc.) is on/off-modulated in order to distinguish the signal from background illumination. The PSD provides four current signals the relative amplitudes of which are proportional to the light spot position on its surface. These current signals are amplified and their amplitudes detected using four identical signal conditioning channels, each of which consists of a transimpedance preamplifier, postamplifier, synchronous demodulator and A/D converter. To cope with signal level variations, the postamplifier may include variable gain, or the transmitter power may be variable. Position calculation is performed numerically.

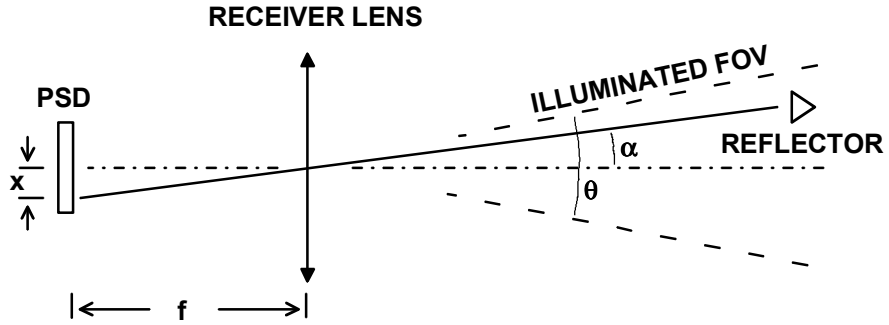

Fig. 2. Operating principle of a reflected beam sensor.

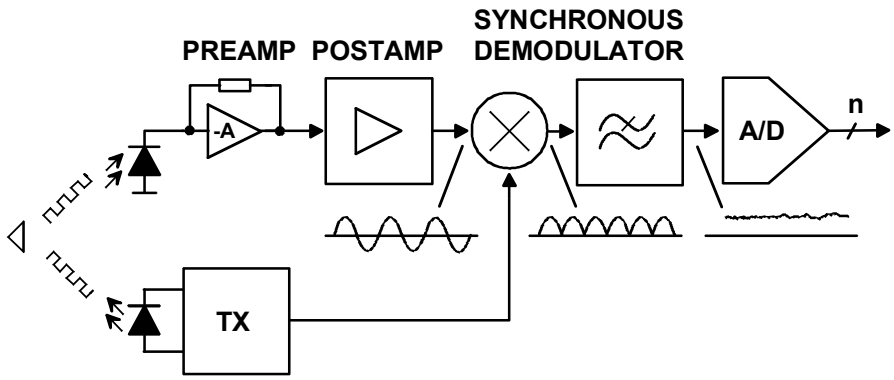

Fig. 3. Block diagram of the signal processing circuitry of a reflected beam sensor.

2.2. Position-sensitive detectors (PSDs)

2.2.1. Operating principles

The two PSDs considered in this study are the lateral effect photodiode (LEP) and the quadrant detector (QD), both of which are capable of measuring lateral displacement in two dimensions. The QD (Fig. 4a) consists of four photodiodes (quadrants) positioned symmetrically around the centre of the detector and separated by a narrow gap. The position information is derived from the optical signal powers received by the quadrants the electrical contribution of which then serves to define the relative position of the light spot with respect to the centre of the device.

The LEP (Fig. 4b) consists of a single large-area photodiode, which has a uniform resistive sheet on its cathode and similarly on its anode, and two extended ohmic contacts on each of the two sheets. The contacts are positioned at the opposite edges of the sheets, and the contact pairs of the sheets are oriented perpendicularly to each other. The photon-generated current carriers divide between the contacts in proportion to the

resistance of the current paths between the illuminated region and the contacts. The position of a light spot centroid can be deduced from the currents of the contact pairs, since the resistances are directly proportional to the lengths of the current paths.

Calculation of the spot position is based on the same principle in both cases: subtracting the opposite signals in the direction of the measured axis and dividing this result by the sum of the same signals. This provides scaling which is insensitive to signal level variations and whose minimum and maximum values are -1 and +1, respectively. If the coordinate system is chosen, as shown in Fig. 4, the single axis displacement of the light spot from the centre of the detector for a QD and an LEP are

$$x = k_{QD}\frac{(i_a + i_b) - (i_c + i_d)}{i_a + i_b + i_c + i_d} \text{ and } x = k_{LEP}\frac{i_b - i_d}{i_b + i_d}, \tag{2}$$

respectively, where i_a, i_b, i_c and i_d are the average currents of the contacts (quadrants) a, b, c and d, and k_{LEP} and k_{QD} are scale factors which convert the relative displacement values to absolute ones. Corresponding equations can be deduced for the perpendicular direction.

Despite the apparent similarity, there are two important differences that affect the properties of the PSDs, and consequently their suitability for different sensing applications. The first is the effect of spot size and shape on the extent of the measurement span and the behaviour of the lateral transfer characteristics within this span, and the second is the difference in their noise levels and correspondingly in the achievable precision.

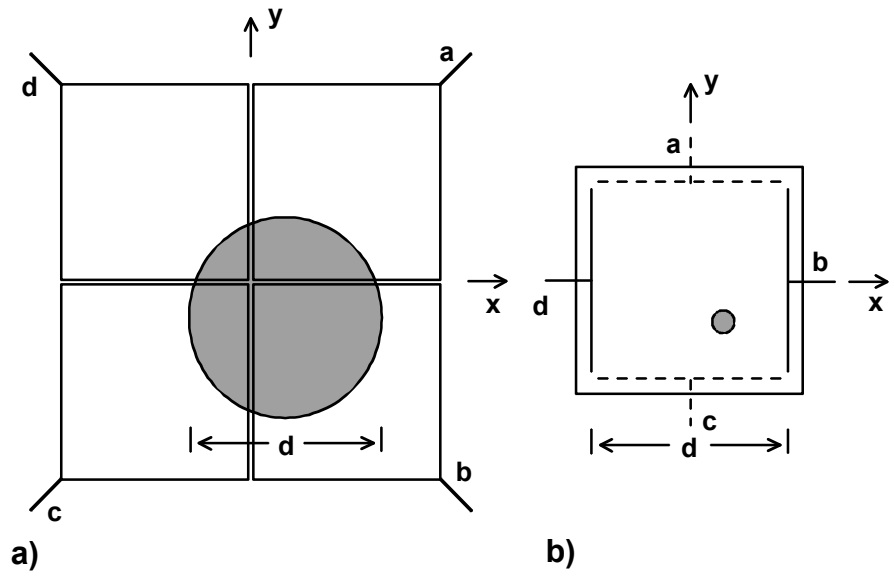

Fig. 4. Outline of a) a QD and b) a LEP having an equal measurement span width d.

2.2.2. Lateral transfer characteristics

In the case of the QD the linear extent of the measurement span d and the scale factor k_{QD} are determined by the size of the light spot, as the QD will provide position information only up to the point where the edge of the spot reaches the detector gap. Misfocusing is typically used to adjust the spot size so that it corresponds to the desired measurement span. The method employed here was to use a sheet reflector whose size equals the desired measurement field at the target and to focus it accurately on the QD.

The lateral transfer characteristics of a QD depend on the spatial irradiance distribution of the light spot. The transfer characteristics for a uniform circular spot are non-linear, because spot movement is not proportional to the percentage of the area which shifts between adjacent quadrants. Consequently, QDs are commonly used as tracking and centring devices rather than as linear position sensors. Note, however, that there exist several ways of linearising QD transfer characteristics (Paper VI, Kazovsky 1983, Carbonneau & Dubois 1986) and that they may therefore be used for linear displacement measurements as well. The scale factor k_{QD} for a uniform circular spot near the centre of the measurement span is $d_s\pi/8$, where d_s is the diameter of the spot (Kazovsky 1983, Yanhai 1986, Young *et al.* 1986).

The measurement span of the LEP is determined by the size of its active area. It provides accurate position information independent of the size of the light spot, because its signals are a direct measure of the position of the spot centroid from the edges of the detector. Thus, unlike with the situation with the QD, there is no need to adjust the spot size by misfocusing. The transfer characteristics of a LEP are linear and the scale factor k_{LEP} is d/2, where d is the width of the LEP active area.

2.3. Limits of measurement accuracy

The limits for the measurement accuracy are set by the achievable signal to noise ratio (SNR) and the reflector background contrast, defined as the ratio of the powers of the signals received from the reflector and the illuminated background. The former determines the achievable precision and the latter the lower bound for systematic errors.

2.3.1. Precision of the LEP and QD receivers

The incremental sensitivity of the LEP and QD receivers depends on the lateral transfer characteristics and signal current distribution (head-or-tail-current v. head-and-tail current) of the PSDs, on noises originating from the PSDs, preamplifier and background, and on the noise correlation between signal channels. The results of the analysis, including the above factors, are presented in the following. First the relation between the SNR and precision is determined (noise sensitivity), and then the dominating noise sources are evaluated, and finally the precisions of the LEP and QD receivers are compared under conditions of low and high background illumination.

2.3.1.1. Noise sensitivity

A general form for the equation determining the relation between SNR and precision is

$$\frac{\sigma_{PSD}}{d} \approx \frac{k_n}{SNR}, \tag{3}$$

where σ_{PSD} is the standard deviation of measured light spot displacement due to noise, d the lateral extent of the measurement span on the PSD surface and k_n the noise sensitivity factor determined by the lateral transfer characteristics of the PSD and the noise correlation between the separate receiver channels (Yanhai 1986, Young *et al.* 1986).

In the case of the QD receiver, the noises related to different quadrants are non-correlated, due to the fully isolated operation of the receiver channels, and therefore noise sensitivity is the same for all noise sources (Paper VII). Thus the relative precision of a QD receiver is

$$\frac{\sigma_{QD}}{d} \approx \frac{\pi}{4}\frac{i_n\sqrt{B}}{P_r S}, \tag{4}$$

where i_n is the root-mean-square (rms) value of the current noise density at the input of a single receiver channel, B the noise equivalent bandwidth, P_r the total signal power received and S the responsivity of the quadrants.

The LEP has low resistance between opposite electrodes (interelectrode resistance R_{ie}), which means that it is inherently much noisier than the QD, and that there exist noise components which correlate in opposite channels. Due to the different magnitudes of correlation, the effects of the various noise sources on precision are different. By dividing the noise sources into groups according to their correlation coefficients (-1, 0, +1) and noting that both head and tail currents are utilised in the 2-axis duolateral LEP, its relative precision becomes

$$\frac{\sigma_{LEP}}{d} \approx \frac{\sqrt{B}}{2P_r S}\sqrt{\left(2i_n(-1)\right)^2 + \left(\sqrt{2}i_n(0)\right)^2 + \left(\frac{2}{\sqrt{3}}i_n(+1)\right)^2}, \tag{5}$$

where

$$i_n(-1) = \sqrt{\frac{4kT}{R_{ie}} + \frac{2u_{namp}^2}{R_{ie}^2}}, \; i_n(0) = \sqrt{i_{namp}^2 + \frac{4kT}{R_f}} \text{ and } i_n(+1) = \frac{\sqrt{2qP_bS}}{2}.$$

P_b is the average power of the background illumination falling on the detector and other symbols are as depicted in Fig. 5.

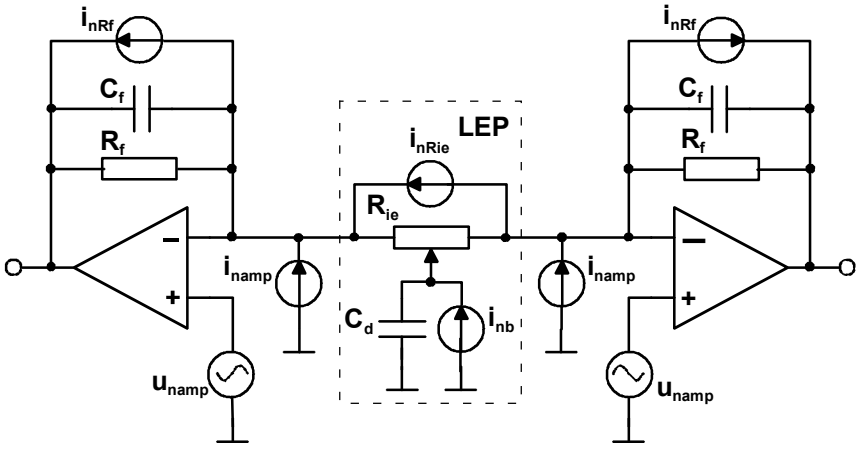

Fig. 5. Main noise sources of a LEP receiver.

2.3.1.2. Predominant internal noise sources

The noise of the signal processing circuitry originates from the PSD and the transimpedance preamplifier, which is typically constructed using an operational amplifier (op amp) (Fig. 5). When properly designed, the op amp makes essentially no contribution to the total noise of the preamplifier, and if shot noise due to background illumination is also neglected, the main noise contributors are the thermal noise of the feedback resistance R_f in the case of the QD and that of the interelectrode resistance R_{ie} in the case of the LEP.

The value of the feedback resistance of a QD receiver is basically fixed by the desired preamplifier bandwidth, the unity-gain bandwidth of the op amp and the photodiode capacitance (Burr-Brown Corp. 1994, Graeme 1996). The phase lag caused by the photodiode capacitance is compensated for with the feedback capacitance to provide stable operation. The feedback capacitance then determines the bandwidth of the preamplifier together with the feedback resistance, and in this way fixes the value of the feedback resistance and the noise level accordingly. In discrete implementations, however, the total stray capacitance across the feedback resistor is typically 1 to 2 pF, which is more than enough to compensate for the QD capacitance (<20 pF/quadrant), and thus the value of feedback resistance is determined simply by this stray capacitance and the bandwidth required. Assuming that the highest frequency needed to cover the modulation frequency and the signal band around it is 10 kHz, results in a 10 MΩ feedback resistance. Despite voltage noise gain peaking, the noise specifications required from the op amp are feasible in practice (u_{namp}<20 nV/√Hz, i_{namp}<20 fA/√Hz).

The noise level of the LEP receiver is determined by the interelectrode resistance, the value of which is typically fixed around 10 kΩ in the case of a 2-axis LEP. Due to a low value for the interelectrode resistance and the detector capacitance (C_d<100 pF) voltage noise peaking makes no contribution below 10 kHz, and thus the noise specification for the op amp stays within reasonable limits (u_{namp}<5 nV/√Hz, i_{namp}<1 pA/√Hz).

2.3.1.3. Comparison of the PSD receivers

Assuming negligible background illumination, the ratio between the achievable precisions of the QD and LEP receivers becomes

$$\frac{\sigma_{QD}}{\sigma_{LEP}} \approx \frac{\pi}{4}\sqrt{\frac{R_{ie}}{R_f}}\,. \tag{6}$$

Using the derived values for R_{ie} (10 kΩ) and R_f (10 MΩ), we see that a QD receiver provides roughly 40 times better precision. The situation is reversed, however, when a high level of background illumination is present, the QD being noisier since it collects more background light due to the larger active area needed for providing the same size of the measurement field as with the LEP (Fig. 4) (Paper VII). Assuming a square-shaped QD, the precision ratio becomes $\sqrt{3}\pi/2$ (~2.7) when background shot noise dominates. Note, however, that the inherent noise level of a LEP is so high that background illumination makes essentially no contribution to its total noise in typical outdoor measurement conditions, and that the precision of a QD receiver, although being limited by background noise, is still very much better than that of a LEP (Mäkynen *et al.* 1991).

2.3.2. Reflectors and their influence on measurement accuracy

The reflectors used in reflected beam sensors include discrete corner cube retroreflectors (CCRs) and continuous retroreflective arrays (sheet reflectors) composed of small (30 to 300 μm) corner cubes or glass spheres. A CCR has low losses and is capable of reflecting rays accurately in the direction from which they came. Beam spreading due to diffraction and the parallelism error (~3 arcsec) is negligible within the Fresnel range (~0.5 km for a typical CCR diameter), and thus a point source illumination produces a returned beam with a diameter twice that of the CCR within this range. The CCR diameter is typically large enough for the receiver aperture to be fully illuminated by the reflected beam, and therefore the received signal level is roughly the same as would be obtained if the receiver were positioned in the illuminating beam at a distance twice that of the CCR.

The reflectance properties of the sheet reflectors are best characterised by the gain G that they provide over the intensity reflected from a perfect Lambertian surface. The gains of commercially available sheet reflectors such as those used in traffic signs vary typically from 200 to 3000.

The properties of the reflectors determine the received signal level and the target background contrast, and thus have a considerable effect on the measurement accuracy achievable with a particular sensor system. Assuming coaxial illumination, a uniform Lambertian background, circular reflectors and fully illuminated receiver lens, it can be concluded that in the case of the CCR the contrast is essentially constant irrespective of its distance L, and that the received signal level is proportional to $1/L^2$. With the sheet reflector the contrast and the received signal level have a very much greater dependence

on distance, being proportional to $1/L^2$ and $1/L^4$, respectively. Use of a typical angular FOV of 10 mrad reveals that one CCR provides about 30 times better contrast and a 40 times higher signal level than a typical sheet reflector (G~1000) even though the sheet reflector is allowed to cover half of the angular FOV (1/4 of the illuminated area) at all distances.

The pronounced distance dependence and the lower gain compared with a CCR mean that sheet reflectors are best suited for applications where the reflector can occupy a considerable area of the illuminated field and in which a limited depth range at relatively short distances is used. This means that sheet reflectors are inherently more suitable for use with a QD receiver due to its better incremental sensitivity and due to the fact that the large reflector size needed to achieve adequate SNR and contrast usually provides a suitable measurement field size without misfocusing the receiver. CCRs are obviously more suitable for long-range applications, due to their highly efficient reflectance properties, and the fact that they usually provide enough signal also for the noisier LEP receiver. The effective aperture area of a CCR is typically halved at an observation angle of ±25°, where sheet reflectors provide ±25° to ±45° half-gain observation angles.

2.4. Proposed sensor constructions

The first sensor, comprising a focused QD receiver and a small piece of sheet reflector, was developed for short-range industrial tracking and displacement sensing applications. The second sensor is composed of a focused LEP receiver and a CCR, and has been employed for aim point trajectory measurement in long-range shooting practice performed outdoors.

2.4.1. A focused QD receiver and sheet reflector

This sensor is typically used in an indoor-like environment where the background illumination is low and the achievable precision at the target distance is thus roughly

$$\sigma \approx \frac{\pi\theta^2 L^4 \sqrt{4kTB/R_f}}{\tau\phi^2 GDP_{ill}S}, \tag{7}$$

where τ is the transmittance, ϕ receiver aperture diameter, D reflector (measurement field) diameter, P_{ill} total illumination power and other symbols are as before (Paper VI). Introducing some practical values (P_{ill}=1 mW, R_f=10 MΩ, G=1000, τ=0.5, ϕ=50 mm, θ =10 mrad, S=0.5 A/W), we see that the sensor is capable of providing submicron precision when a small (1 cm^2) piece of sheet reflector is used with a bandwidth of a few kHz and measurement distance of several metres.

In tracking applications no systematic error is caused by the background reflections as long as the background reflectivity is uniform, since the centroid positions of the reflector image and the background are the same. A non-uniform background reflectivity causes error, however, which can be roughly approximated by assuming that the half circles of the illuminated background (Lambertian) have different but uniform reflectivities. With such an assumption the relative tracking error at the target becomes

$$\frac{\varepsilon_c}{D} \approx \frac{\pi}{8} \frac{\rho_\Delta H^2}{2\rho_{av} H^2 + G}, \tag{8}$$

where ρ_Δ is the difference in the reflectivities of the half planes and ρ_{av} the average reflectivity of the illuminated background, and where H describes the size of the reflector relative to the illuminated field ($H=L\theta/D$) (Paper VI). An upper bound for the error is obtained by assuming that $\rho_\Delta=1$ and $\rho_{av}=0.5$. According to Eq. (8), the sensor is susceptible to significant systematic errors if the reflector is small compared with the illuminated area. Better than 1% accuracy, which is typically adequate for industrial tracking applications, is achievable if the diameter of the sheet reflector (G~1000) is larger than 1/5 of that of the illuminated area ($H \leq 5$).

2.4.2. A focused LEP receiver and CCR

The noise level of a properly designed LEP receiver having a modest FOV (~10 mrad) is determined by its interelectrode resistance in all practical operating environments, and thus the precision achievable with the sensor at the target distance is roughly

$$\sigma \approx \frac{4D^3 \sqrt{4kTB / R_{ie}}}{\tau \phi^2 n P_{ill} S}, \tag{9}$$

where D is the diameter of the measurement field at the target and n the number of CCRs (Paper IX). Using transceiver parameters suitable for a shooting practice application, for example (R_{ie}=10 kΩ, B=30 Hz, ϕ=50 mm, P_{ill}=1 mW, τ=0.5 and S=0.5 A/W), indicate that about one millimetre precision is achievable with one CCR when the diameter of the measurement field is a few metres and the reflector is positioned within the Fresnel diffraction range (typically < 0.5 km).

The relative error due to finite reflector background contrast, assuming a uniform Lambertian background of reflectivity ρ, is correspondingly

$$\frac{\varepsilon_c}{X_t} = \frac{X_t - X}{X_t} \approx \frac{\theta^2 \rho}{n}, \tag{10}$$

where X and X_t represent the measured and true spot displacements from the centre of the measurement field. Thus a FOV of 10 mrad should provide less than 0.01% error.

2.4.3. Conclusions

According to the above, highly precise measurements should be possible with the proposed sensor constructions. The lateral extent of the measurement field is typically 10^3 to 10^6 times that of the smallest resolvable displacement, and the sensing distance typically 10^6 to 10^8 times that level. The corresponding ratios related to the systematic error due to finite contrast are of the same order. The performance of practical sensor implementations in tracking and displacement sensing applications is discussed in the following chapters.

3. Sensors for tracking rangefinders

The sensor subsystems for tracking rangefinders designed for industrial 3D position-sensing applications that are described here include two tracking sensor constructions for automatic coordinate meters and a sensor which uses pulsed time-of-flight (TOF) rangefinding techniques for target orientation measurement. The applications of such tracking rangefinders include vehicle positioning, checking the dimensional accuracy of large objects and interactive teaching of robot paths and environments using a pointing tool. A tracking sensor developed for a dimensional accuracy control application has been used as such in a commercial 3D coordinate meter (Prometrics Ltd. 1993a), but the other applications mentioned have served merely as a framework for feasibility studies, without any actual plans for implementing sensor systems in such applications.

3.1. Tracking rangefinder

3.1.1. Rangefinding 3D coordinate meter

The 3D coordinates of an object point can be readily measured using a rangefinder which includes a gimballed measurement head. The polar coordinates of a target point are obtained by using the rangefinder to measure the distance from it and accurate angle encoders to measure the two orthogonal angles of the rangefinder optical axis. Using the pulsed TOF rangefinding technique, millimetre-level accuracy and a measuring time of less than one second within an operating range of tens of metres are achievable without reflectors. The measuring principle is well suited for industrial applications, and thus coordinate meters for checking the dimensional accuracy of ship building blocks (Prometrics Ltd. 1993b, Kaisto *et al.* 1994), and wearing in the hot refractory linings of converters in ironworks (Määttä *et al.* 1993, Spectra-Physics VisionTech 1996) have been developed (Fig. 6).

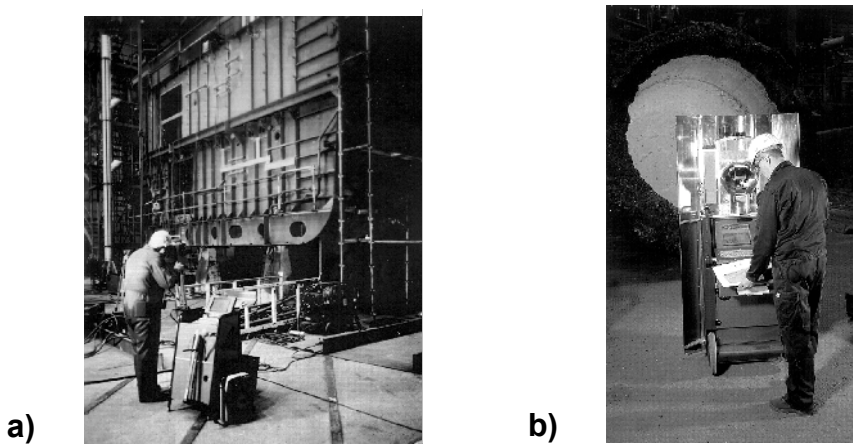

Fig. 6. Industrial applications of rangefinding 3D coordinate meters. a) Dimensional accuracy control of building blocks for ships and b) wearing control for the refractory linings of converters in ironworks.

3.1.2. Pulsed time-of-flight (TOF) rangefinders

The distance determination method used in the above coordinate meters is pulsed time-of-flight (TOF) rangefinding, i.e. it is based on measurement of the transit time required for a short light pulse to reach the target and to return to the receiver. The construction of a pulsed TOF rangefinder is presented in Fig. 7. The transmitter (TX) laser diode emits narrow (~10 ns), high power (1 to 100 W) light pulses with a repetition frequency of a few kHz, and the receiver (RX) consists of an avalanche photodiode (APD) connected to the input of a transimpedance preamplifier, postamplifiers and a timing discriminator. The receiver bandwidth is typically around 150 MHz. The timing discriminator produces accurate logic-level timing pulses for the time interval measurement unit from the start and stop pulses received. The large amplitude variation of the pulses received from the target is compensated for by using optical and electrical gain control methods such as neutral density filters and pin-diode attenuators. The laser diode and the APD are connected to the transceiver optics by means of optical fibres. The time interval between the start and stop pulses is measured using a time-to-digital (TDC) converter, which includes a digital clock combined with an analogue interpolator. The distance measurement precision, accuracy and measurement time are typically about 1 mm (standard deviation), ±3 mm and <1 s, respectively. Such performance is achievable up to tens of metres from natural targets. In accurate 3D coordinate measurements, non-cooperative adhesive marks are used to aid manual aiming and to guarantee good accuracy in all cases irrespective of object reflectance properties. Good spatial resolution is achieved by minimising the spot size at the target by using small-diameter fibres (~100 μm) and focused transceiver optics (Määttä 1995).

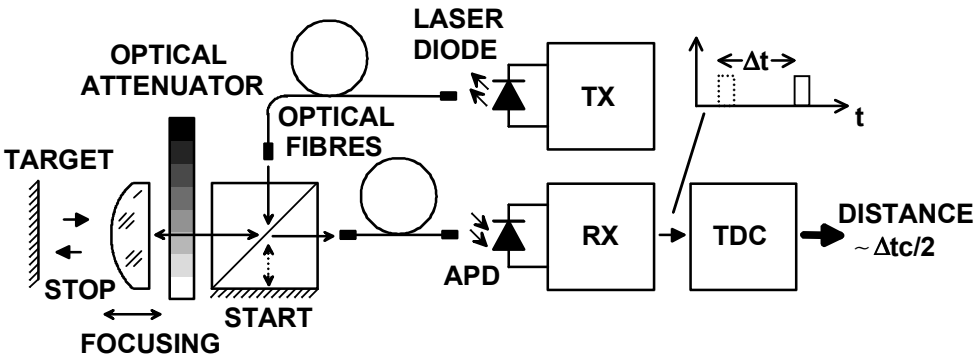

Fig. 7. Construction of a pulsed TOF laser rangefinder.

3.1.3. The tracking rangefinder and its applications

A tracking rangefinder is a pulsed TOF rangefinder which is capable of automatically and continuously pointing itself towards a desired target and which is used for 3D position and orientation measurements. As with manually operated coordinate meters, target position is acquired using the measured range of the target and the two orthogonal angles of the rangefinder optical axis. Pointing is facilitated by a tracking sensor and a servo system (Fig. 8). The target, which could be the object itself or a special pointing tool, is equipped with reflectors.

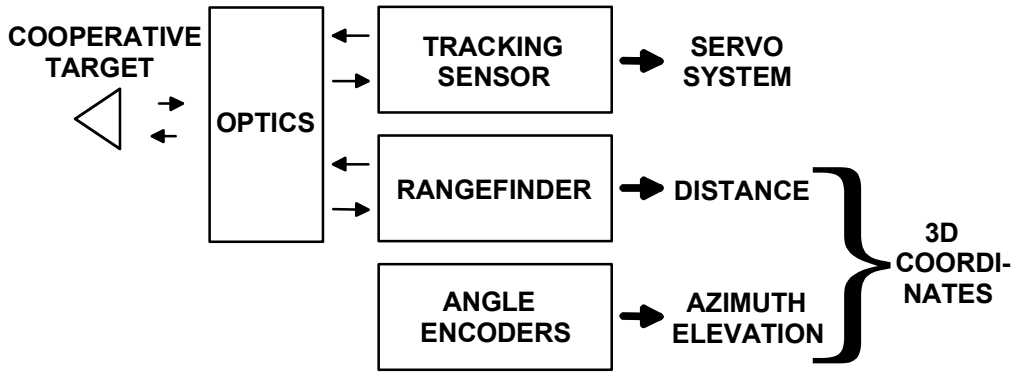

Fig. 8. Operating principle of a tracking rangefinder.

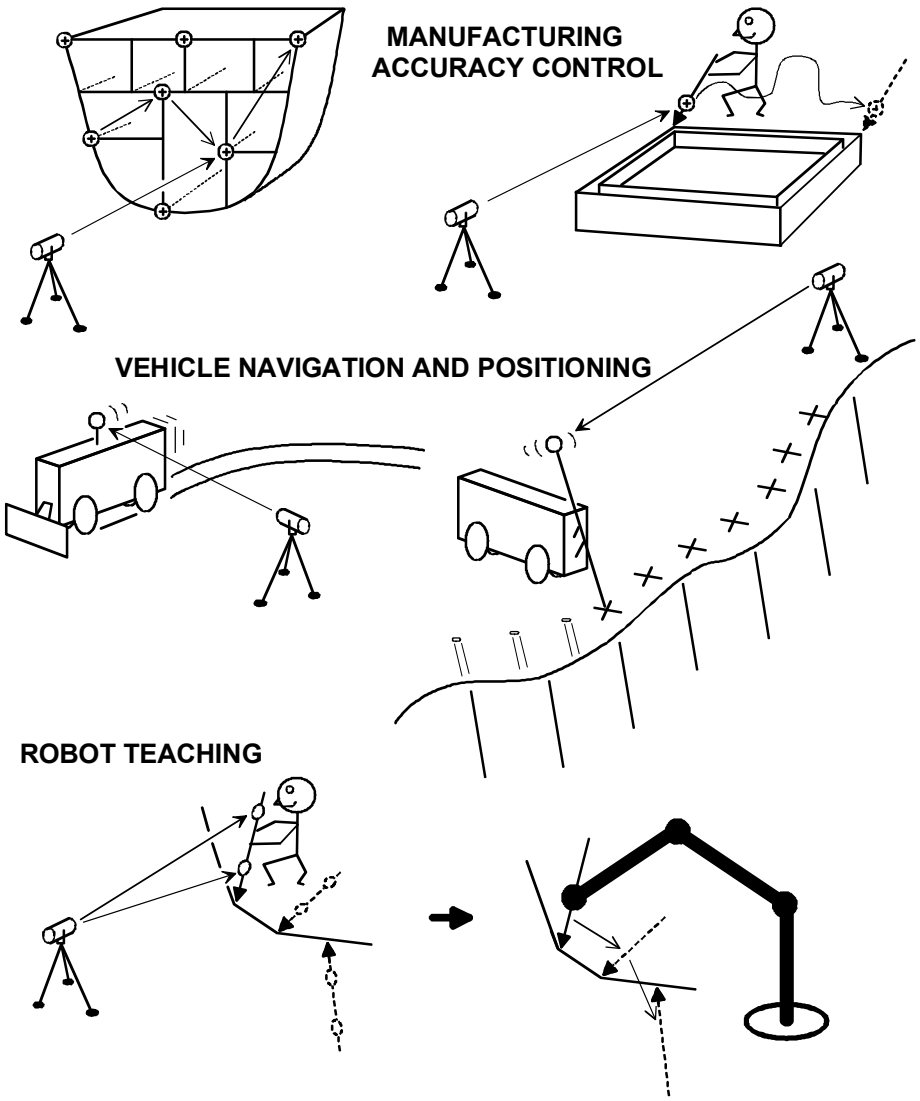

Fig. 9. Examples of tracking rangefinder applications. Checking the dimensions of large industrial objects, vehicle navigation and positioning, and interactive robot teaching.

To fully utilise the millimetre accuracy provided by the laser rangefinder and the angle encoders, the tracking sensor should provide an accuracy that is comparable with these subsystems. The upper bound for the tracking error is readily set by the accuracy of the angle encoders, being better than ±0.05 mrad, which corresponds to ±0.5 mm and ±5 mm lateral displacements at distances of 10 m and 100 m, respectively (Nishimura 1986).

Examples of possible ways of using a tracking rangefinder for 3D position and orientation measurements, as illustrated in Fig. 9, include checking the dimensions of large industrial objects such as building blocks for ships or moulds for pre-cast concrete, for example. The tracking rangefinder could also be used for vehicle navigation and positioning in outdoor areas of limited size, such as construction or mining sites. A typical task could be to ensure that a vehicle such as a heavy bulldozer follows a certain route in its working environment. Another type of task could be the accurate positioning and orientation of a tool on a working machine, such as a boring tool used for blast hole drilling in an open pit. The last category includes applications in which not only the 3D coordinates are to be measured but also the target orientation. The application presented here includes determination of the position and orientation of a manually operated pointing tool intended for robot teaching.

Tracking sensor constructions proposed for vehicle positioning and checking the dimensions of large industrial objects, and also TOF rangefinding techniques for measuring target orientation, will be described below.

3.2. A simplified tracker model

Trackers are systems which facilitate continuous pointing to a remote target by responding to the light reflected from it. To accomplish pointing, a typical non-imaging tracker used in aerospace and military applications includes a misfocused QD receiver to provide the error signal, gimballed transceiver optics to allow the tracker to follow the target motion, and a servo-system for controlling transceiver movements. Two modes of operation are generally recognised: acquisition mode and tracking mode. The tracker points or scans a prescribed space sector in the acquisition mode, looking for a target, and after finding it switches to the tracking mode.

A block diagram of a simple tracking system is presented in Fig. 10 (Gerson *et al.* 1989). The QD provides a monotonously changing error signal V_α within its tracking FOV (measurement field), defined by the angle $\pm\theta_{tr}$, and a constant error signal elsewhere in the FOV ($\theta_{tr}<\alpha<\theta_{aq}$). Integration in the feedback path represents the angular motion of the transceiver. The following conclusions can be drawn from the simplified model:

- A stationary target can be acquired if it is within the receiver FOV.
- The tracker can point to a stationary target with zero steady-state error.
- The rotational velocity of the receiver is proportional to the error signal V_α within the tracking FOV and saturates to $K\theta_{tr}$ rad/s when the pointing error exceeds θ_{tr}.
- The tracking system can track a moving target with constant error up to a rotational velocity of $K\theta_{tr}$ rad/s.
- The target angular velocity can only momentarily be larger than $K\theta_{tr}$ rad/s.
- If the angle error ever exceeds θ_{aq}, the target will be lost.
- The upper bound of the accuracy of a tracker is set by the accuracy of the tracking sensor.

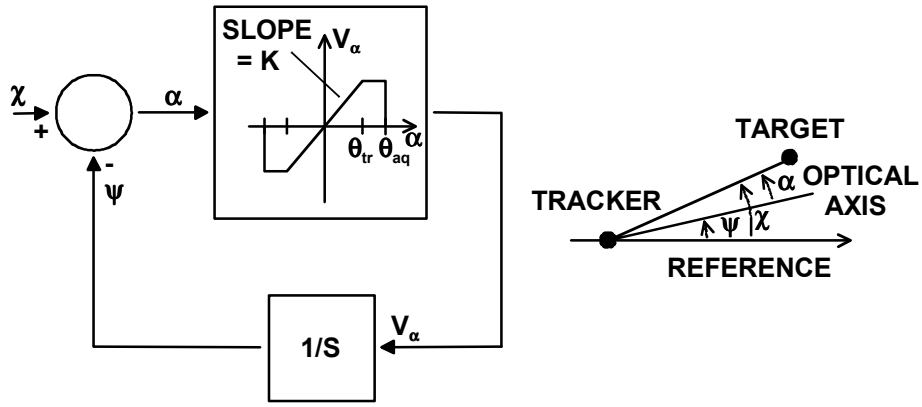

Fig. 10. Block diagram of a simple tracking system.

According to the above, the sizes of the tracking and acquisition FOVs have a significant effect on tracker performance. The optimal size of the acquisition FOV depends on the search strategy and the angular velocity of the target, and can be readily adjusted by choosing an appropriate detector area and receiver focal length. The tracking FOV, in turn, should be large enough to allow sudden rapid movements of the target which the pointing system is not capable of following to take place without losing the target. The angular coverage of the tracking FOV can typically be adjusted by changing the spot size by misfocusing the receiver. With a stationary target, however, stable tracking is achieved irrespective of the size of the tracking FOV, and misfocusing is not usually needed.

3.3. A tracking sensor for vehicle positioning

The conventional tracking sensor construction including a misfocused QD receiver and a CCR target is highly susceptible to atmospheric turbulence and has a tracking precision which is a good deal worse than that of a rangefinder or angle encoder, for example. A reflected beam sensor construction using a sheet reflector instead of the CCR is proposed in Paper I since this is found to improve tracking precision in turbulence-limited cases. The idea of using a sheet reflector for precision improvement is believed to be new.

Tracking rangefinders for vehicle positioning purposes will be reviewed first, after which the proposed sensor construction and its performance in a turbulent outdoor environment will be presented. Finally, conclusions are put forward.

3.3.1. Tracking rangefinders for vehicle positioning

Tracking rangefinders such as the Navitrack 1000 Polar positioning system (IBEO GmbH 1987) and the Atlas Polarfix Range-azimuth position fixing system (Smith 1983, Mackenthun & Muller 1987) provide 2D positional data on slowly moving objects with decimetre accuracy up to distances of a few kilometres. The systems are designed for hydrographic applications, such as the positioning of survey vessels working on a sea coast. A reflected beam sensor composed of CCR reflectors and a scanning receiver are used to track the target.

It is claimed that autotracking total stations such as the Geodimeter 600 ATS (Spectra Precision AB 1998a) and the Leica TCA (Leica Geosystems AG 1999a) provide 3D positional data on a moving target with an accuracy of a few millimetres up to distances of hundreds of metres. They are intended for the position tracking and guidance of heavy machines and their tools at construction and mining sites. Reflected beam techniques including CCR targets and CCD or QD receivers are used for tracking. The Geodimeter includes two coaxially positioned QDs with active area diameters of 3 mm and 0.2 mm and the Leica includes a CCD.

3.3.2. Proposed sensor construction

The proposed tracking sensor is composed of a misfocused QD receiver and a 15 cm spherical target covered with a high-gain sheet reflector (G~3000). The reflector was made spherical so that the reflected beam would appear to originate from the same point irrespective of the direction of observation and thus to allow the target free movement without pointing errors. An illumination power of a few mW, misfocused receiver optics with a 10 mrad tracking FOV and 100 Hz bandwidth were used in the experiments. The applicability of these more or less intuitively chosen values was verified by constructing a system and making tracking experiments at the local pulp mill, where a slowly moving bulldozer (< 10 km/h) used to feed a discharger with wood chips was tracked.

Excluding the effect of atmospheric turbulence, the tracking error of the proposed sensor construction due to noise and finite reflector background contrast was calculated to be equal to or smaller than those of the angle encoders and the rangefinder up to a distance of about 100 m. The experimental results concerning the effect of atmospheric turbulence on tracking precision in case of a CCR and the proposed sheet reflector target are summarised below.

3.3.3. Precision in outdoor environment

The measured precision achieved using a CCR and a spherical sheet reflector in outdoor (distance 40 m) and indoor (distance 20 m) environments is assessed in Tables 1 and 2 of Paper I, which are reproduced here in modified form (Tables 1 and 2). The full width at half maximum (FWHM) values describing the angular spreading of the results are adjusted for standard deviations and scaled so that the tracking FOV is effectively equal in both cases (~10 mrad). Results affected by too low a signal level have also been removed. The strength of the atmospheric turbulence in the above measurement situations was estimated by comparing the measured results with those presented in Papers VIII and IX, according to which the measurement conditions indoors and outdoors represent typical weak and intermediate (between weak and strong) turbulence conditions, respectively.

It can be concluded from the results in Tables 1 and 2 that the precision achievable with a misfocused QD receiver is determined by the strength of the atmospheric turbulence for both reflector types, even in weak turbulence. The results also show that a sheet reflector provides an improvement in precision by a factor of two in weak atmospheric turbulence and by a factor of 20 in intermediate turbulence relative to the CCR.

Table 1. Angular precision of a misfocused QD receiver (ϕ~50 mm, θ~10 mrad) in weak atmospheric turbulence for a reflector distance of 20 m. A relative signal level of 10 corresponds to illumination powers of 2.8 and 0.7 mW in the cases of a sheet reflector and a CCR, respectively.

Relative signal level	Standard deviation, µrad	
	Sheet reflector	CCR
10	2.5	6.5
4.3	-	6.5
1	2.9	7.6
0.5	4.0	8.7

Table 2. Angular precision in intermediate atmospheric turbulence for a reflector distance of 40 m. A relative signal level of 3.5 corresponds to illumination powers of 8 and 0.8 mW in the cases of a sheet reflector and a CCR, respectively.

Relative signal level	Standard deviation, µrad	
	Sheet reflector	CCR
3.5	9.4	190
1.7	9.4	223
0.9	10	180
0.4	10	162
0.2	11	171

The distance range within which the sheet reflector provides a comparable performance to the rangefinder and angle encoders can be readily estimated using the results of Papers VIII and IX, which show that the turbulence-limited precision with a misfocused QD receiver is directly proportional to the strength of the turbulence and the extent of the measurement field. At a distance of 100 to 150 m, strong, intermediate and weak atmospheric turbulence cause standard deviations which are approximately >5%, 2% and <0.5% of the extent of the tracking FOV, respectively. Using these estimates and assuming that a sheet reflector provides the measured improvements in precision at longer distances (>40 m) as well, the following conclusions can be reached. A CCR would provide subcentimetre precision up to a distance of 100 m only in weak atmospheric turbulence, whereas the sheet reflector is capable of providing the same precision also in intermediate atmospheric turbulence.

The main reason for the deterioration in precision in atmospheric turbulence proved to be the sensitivity of the misfocused receiver to spatially uncorrelated illumination fluctuations across its aperture. Due to the misfocusing, fluctuations present at the receiver aperture are projected directly on the light spot on the QD surface, thereby causing fluctuations in the centroid of the spot. These illumination fluctuations could be observed visually with a CCR, but not when a sheet reflector was used. The reason for the negligible fluctuations is believed to be the averaging effect of multiple overlapping beams reflected from the sheet reflector. A sheet reflector having a diameter of 10 cm, for example, reflects approximately 100 000 individual beams originating from the small-diameter CCRs (<0.3 mm) or glass spheres of the sheet.

3.3.4. Conclusions

The precision of a conventional tracking sensor composed of a misfocused QD receiver and a CCR is severely hampered by atmospheric turbulence, and thus provides much worse accuracy in outdoor conditions than the proposed construction which uses a sheet reflector instead of the CCR. The sensor construction was estimated to provide subcentimetre accuracy up to a distance of 100 m in intermediate atmospheric turbulence, and thus tracking accuracy compatible with those of the pulsed TOF rangefinder and angle encoders should be achievable in most outdoor conditions[1].

The results reported in Papers VIII, IX and section 4.2 show that the effect of intensity fluctuations can also be eliminated by focusing the receiver. A sensor composed of a focused LEP receiver and a CCR target provides the same precision in intermediate atmospheric turbulence as the proposed sensor construction. Note, however, that the spherical sheet reflector provides a much wider observation angle than a single CCR, and that the reflected beam originates exactly from the centre point of the reflector irrespective of the direction of observation, which may not be the case if a spherical assembly of discrete CCRs with comparable angular coverage were used instead.

[1] Typical environmental conditions associated with intermediate atmospheric turbulence are described in section 4.2.8.

3.4. A tracking sensor for an automatic 3D coordinate meter

A coordinate meter composed of a millimetre-accurate pulsed TOF rangefinder with gimballed measuring head and accurate angle encoders has proved suitable for checking the dimensional accuracy of large industrial objects such as building blocks for ships. Its main advantages are that only one measurement device and measurement location is needed, which makes it flexible, fast and economic to use as compared with traditional methods based on theodolites, for example. The measurement beam of such a coordinate meter is aimed towards the desired target point manually using a visible pointer beam or magnifying telescope. Since manual aiming is laborious and time-consuming, the possibility of implementing a tracking sensor for automatic pointing was studied (Horsmon & Lupica 1990, Manninen & Jaatinen 1992).

The basic construction of the proposed tracking sensor based on a focused QD and a sheet reflector and the limitations of its theoretical performance were already explained in section 2.4.1. The practical sensor implementation and test results are reviewed here. Preliminary results concerning the optical construction of the tracking sensor are provided in Paper II and the detailed construction and test results of the tracking sensor prototypes developed for an automatic 3D coordinate meter in Paper III (Manninen *et al.* 1992, Prometrics Ltd. 1993a, Kaisto *et al.* 1994).

The advantages and possibilities afforded by automatic pointing in dimensional accuracy control applications are explained first. Existing systems capable of automatic or semiautomatic pointing in coordinate measurement applications are then reviewed. After that the justifications for introducing reflected beam techniques based on the QD receiver are given. The design goal is defined next, and finally, before conclusions, the implemented sensor construction and its performance are described.

3.4.1. Advantages of automatic pointing

Checking the dimensions of a ship block may require the measurement of about 50 target points, for example, and the total execution time in such a case will be about 1.5 hours when a manually operated coordinate meter is used. Marking the target points and performing the measurements will both take up approximately one third of the total time, and the remaining third will be used for operations such as system set-up, calibration, recording etc. Most of the measurement execution time (>30 s/point) is spent on aiming, while the coordinate measurement itself is relatively fast (<5 s/point) (Horsmon & Lupica 1990). Thus, automatic pointing could basically reduce the total execution time of a typical set of measurements by 1/3 relative to manually performed measurements. Since manual aiming also tends to be prone to errors, automatic pointing capable of precise and reliable operation would potentially result in better overall measurement accuracy, too.

Automatic pointing also makes it possible to place the coordinate meter in positions from which manual aiming is practically impossible but from which measurements can be made more easily and faster. The coordinate meter can be installed on the ceiling of a production hall, for example, where it can be moved from one measurement position to

another by means of a conveyor track. The set-up, calibration and measurement execution of such system are in principle fully automatic and thus the total measurement execution time can be less than half of that of manual coordinate measurements. Such a system using the tracking sensor described in Paper III has been implemented for facade panel inspection in a precast concrete factory (Heikkilä 1996).

Another possible measuring system utilising automatic pointing includes a manually operated tool with a reflector attached to it. A coordinate meter could track the tool continuously as it is moved in its working space and measurements could be performed simply by placing the tool at the desired object points one after another. This principle might prove useful in applications where permanent target marking is not possible and in which only a few relatively easily accessible points are to be measured. A similar concept has recently been introduced for land surveying applications (Spectra Precision AB 1998b, Leica Geosystems AG 1999a).

3.4.2. Rangefinding coordinate meters capable of automatic pointing

Motorised total stations such as the Leica TCM provide semiautomatic pointing. They are capable of pointing close to the target on the basis of its nominal position, but fine pointing is always performed manually. There also exist industrial total stations such as the Leica TDA5005 which provide fully automatic tracking and pointing at CCR targets (Leica Geosystems AG 1998).

Rangefinders capable of automatic pointing are also found in the field of robotic performance measurements (Lau *et al.* 1988). Here the tracking technique is based on transmitting a narrow collimated laser beam to a CCR attached to the target and detecting the lateral shift of the beam reflected from the CCR using a PSD. Trackers are equipped with a laser interferometer for distance measurements and provide extremely high accuracy (< 0.1 mm) within working volumes of a few metres (Lau *et al.* 1985, Mayer & Parker 1994, Nakamura *et al.* 1994, Spiess *et al.* 1998, Automated Precision Inc. 1996, Leica Geosystems AG 1999b).

None of the above coordinate meters is particularly suitable for automated dimensional accuracy control, however, which is the target application here.

3.4.3. QD versus camera-based tracking

The tracking sensors proposed for industrial coordinate measuring systems, such as electronic servo theodolites (Gottwald 1988) or rangefinding coordinate meters (Ailisto 1997), have been based on camera systems composed of a CCD camera, image processor and image analysis software. The measurement points on the object surface are marked with reflectors or with a bright laser spot transmitted from a separate station. The light reflected from the marked point is detected by the image sensor, which then provides the error signals for the servo system. An accuracy of 0.05 mm within a 3 m cube with a measurement speed of 5 to 7 seconds per point has been reported by Gottwald & Berner

(1987) and Gottwald (1988). Ailisto (1997) proposed a vision-based tracking system for a rangefinding 3D coordinate meter, and achieved submillimetre pointing accuracy within a distance range of 4.5 to 16 m at an execution speed of 20 s/point.

The general advantage of a camera-based tracker over a non-imaging QD tracker is the possibility to perform versatile processing operations on the image and thus to satisfy performance requirements that are beyond the capabilities of non-imaging trackers. Such capabilities are essential in military applications, for example, where targets of low contrast are to be tracked under difficult atmospheric conditions (Gerson *et al.* 1989). In industrial accuracy control applications, however, measurement points are typically marked with special adhesive marks to assure good aiming and measuring accuracy under all circumstances. This makes it readily possible to use non-imaging trackers for automatic pointing simply by replacing the non-cooperative marks used to aid manual aiming with similar cooperative ones.

The main motivation for introducing the QD-based tracker for automatic coordinate measurements was originally its fast operating speed and high precision. A few kHz bandwidth and submicron precision are basically achievable with a reflected beam sensor composed of a QD receiver and a small piece of sheet reflector. In principle, this makes it possible to construct a highly accurate pointing system, the speed of which is limited only by the servo system, and thereby to reduce the measurement execution time essentially to that needed for the coordinate measurement itself. Such an operating speed is not as easily achievable in the case of a camera-based tracker, due to the limited frame rate of image sensors and the much greater amount of data processing needed (Ailisto 1997).

3.4.4. Operating principle and design goals

The operating principle of the pointing system resembles that of automated total stations. During measurement execution the nominal coordinates included in the design database of the measured object are used to point the transceiver optics roughly towards the target, after which the tracking system is used to point the rangefinder beam accurately at the centre of a cooperative mark placed at the desired measurement point. The operating range depends on the application, varying typically from 3 to 30 m in assessing the manufacturing accuracy of ship blocks, for example. The pointing accuracy should be comparable to manual measurements, in which aiming accuracy comparable to or better than that provided by angle encoders is typically achieved. Thus automatic pointing should have an accuracy of better than 0.5 mm at 10 m, for example. Finally, the time needed for pointing should obviously be much shorter than that taken for manual aiming (~ 30 s) and preferably short by comparison with that needed for the coordinate measurement itself (< 5 s).

3.4.5. Sensor parameters and tracking accuracy

The reasoning behind the determination of an appropriate size for the tracking and acquisition FOVs and the reflector to fulfil the design goals are explained in this section. Due to the stationary target, it is possible in principle to achieve stable and accurate pointing irrespective of the extent of the tracking FOV and the speed of the servo system. This means that misfocusing is not needed in order to adjust the size of the tracking FOV. The size of the acquisition FOV depends in turn on the search strategy and on the degree of positional uncertainty of the reflector being searched for. The principle used here for finding the reflector was simply to make the acquisition FOV large enough to cover this positional uncertainty when the receiver was pointed towards nominal reflector position. With ship block measurements, for example, the nominal coordinate values and the position of the actual mark typically differ a few cm at the most, which means that the acquisition field should cover a lateral field of a few centimetres throughout the operating range (Manninen & Jaatinen 1992).

A reflector and acquisition FOV of fixed sizes can be used if the reflector distance variation is limited to about 1:2. If the reflector has a larger distance variation, the contrast at longer distances will become low and increase the possibility of pointing errors. The first sensor prototype, for example, has a 17 mrad acquisition FOV, resulting in a 3.5 to 8.5 cm lateral FOV within the specified 2 to 5 m operating range. Assuming typical receiver parameters a reflector of 10 mm in diameter and of gain 1000 should provide submicron precision and smaller than 0.3 mm systematic error in the case of a diffuse background. The second prototype, intended for checking the dimensional accuracy of facade panels, had an 8 mrad FOV and an operating range from 6 to 12 m. Use of a 20 mm reflector (G~1000) resulted in acceptable accuracy in this case, but when larger distance ranges are needed, the size of the reflector (or FOV) must be varied according to the distance. The desired performance within the distance range of 3 to 30 m needed in shipyard applications, for example, could be achieved using the optical construction of the first prototype and a high-gain reflector (G~3000) with a diameter that is varied from 1 to 5 cm according to the distance to be measured.

According to the above, a suitable combination of FOV and reflector size can readily be found to fulfil the design goal set for manufacturing accuracy control applications. The performance of the pointing system is also affected by the sensor construction, however, and by the various non-idealities of practical components. Constructional details affecting the pointing accuracy are explained next, and an analysis of the error contributions due to component non-idealities can be found in section 4.1.3. Note also that the background of the reflective marks may not be diffuse but specular, and thus larger pointing errors than those predicted by the diffuse model are possible in practice. A method for eliminating errors due to specular reflections is proposed in section 3.5.

3.4.6. Sensor construction

3.4.6.1. Combining the rangefinder and tracking sensor optics

The construction of the coordinate meter optics is depicted in Fig. 11. The tracking sensor optics was to be coaxial with the rangefinder so that the rangefinder beam could be accurately pointed towards the centre of the target regardless of distance. The two systems were combined using coaxial receivers with a common focusing lens and beam splitters to divide the incoming radiation between the rangefinder and the QD. A common problem with such a coaxial system is low transmission and high crosstalk, both of which may notably degrade the performance of the subsystems. Wavelength-selective beam splitters were used to optimise transmission, and narrow band (250 Hz with -40 dB/dec roll-off) synchronous detection in the QD receiver to suppress the disturbances of the received rangefinder pulses due to crosstalk.

After the acquisition phase both receivers are automatically focused at the target mark. Focusing optimises the spatial resolution of the rangefinder and the precision of the tracking sensor by minimising the beam width of the rangefinder and the lateral extent of the tracking FOV at all distances, respectively. Focusing also makes the tracking sensor less sensitive to non-uniform receiver lens illumination due to dust and dirt, for example, which in a misfocused case would cause a pointing error.

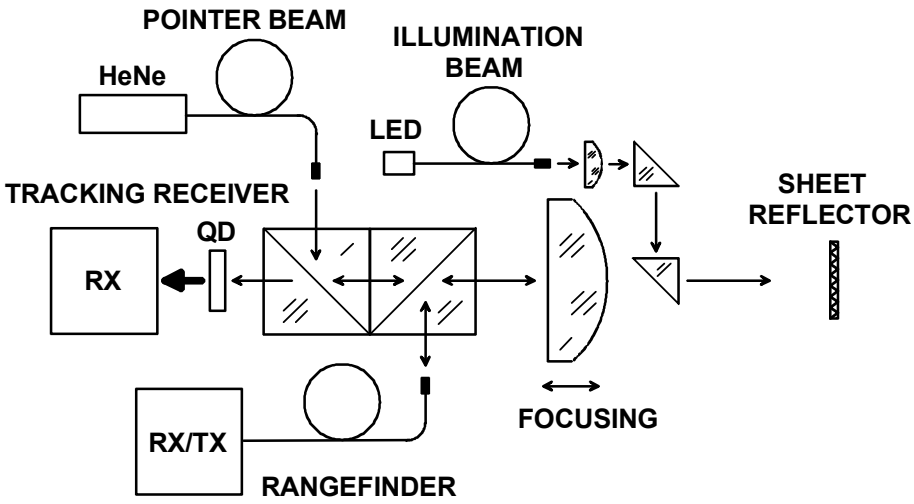

Fig. 11. Construction of the coordinate meter optics.

3.4.6.2. Parallel versus coaxial illumination

In principle, parallel and coaxial illumination provide the same signal level and contrast, since the beams from sheet reflectors are relatively wide (beam width from 30 to 300 mrad) and thus provide approximately the same irradiance at the receiver aperture for both constructions (Johnson NL 1979). Parallel optics will generally be a more attractive choice, however, due to simpler implementation. On the other hand, preliminary tests showed that the parallel system required uniform illumination and an accurately focused receiver in order not to introduce systematic pointing errors. In parallel illumination a reflector shifts laterally across the illuminating beam as its distance is varied and if the illumination beam is non-uniform, the apparent centroid position of the reflector changes according to the distance, as depicted in Fig. 12 (Fig. 5 in Paper II). Although a uniform illumination beam might be available, slight misfocusing would still cause pointing error due to non-uniform receiver lens illumination, as depicted in Fig. 13 (Fig. 6 in Paper II). This is caused by the fact that a sheet reflector reflects the highest intensity back towards the transmitter, and consequently illuminates the adjacent receiver aperture asymmetrically, which then makes the misfocused image spot non-uniform.

To avoid pointing errors related to parallel illumination, a coaxial transceiver construction with separate optical paths for the transmitter and receiver was used (Fig. 11). This made it possible to use axially symmetrical but otherwise non-uniform illumination beams such as those typical of fibre-coupled LEDs without introducing pointing errors. Pointing accuracy proved to be relatively insensitive to receiver focusing, too, and thus slight misfocusing, which might sometimes happen, could not cause any meaningful pointing errors (Mäkynen 1990). The construction also produced negligible crosstalk and good transmission. The low crosstalk was due to the totally separate transmitter and receiver optical paths, and the good transmission due to the small transmitter aperture, which blocked only about 5% of the receiver aperture.

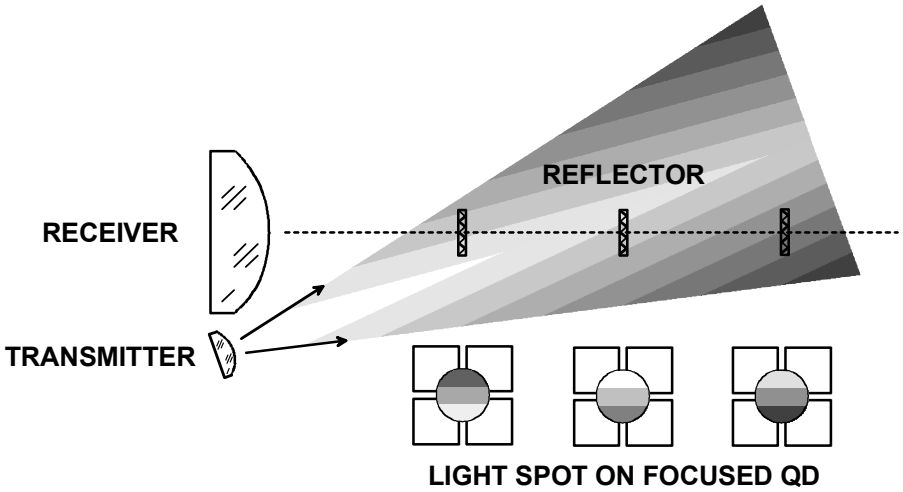

Fig. 12. Centroid position shift in the reflector image due to non-uniform parallel illumination.

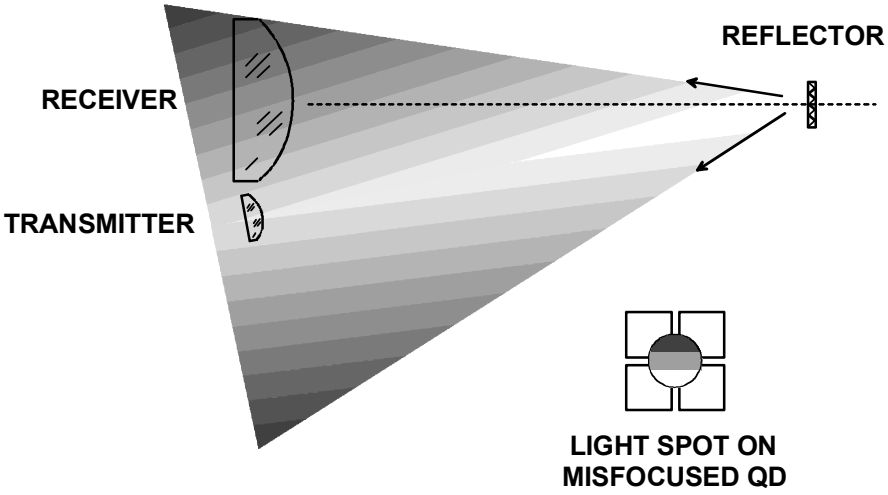

Fig. 13. Centroid position shift due to receiver misfocusing in the case of parallel illumination.

3.4.7. Performance of the tracking sensor prototypes

The tests were performed using a uniform diffuse background of low reflectivity ($\rho<0.1$) and a round reflector which was 10 mm in diameter and had a gain of about 800. The achievable precision and systematic errors due to various effects were measured when varying the reflector distance from 2 to 5 m and its observation angle between $\pm 45°$ according to the original specification set for the first prototype. The tests showed that a precision of a few micrometres is achievable as expected, and that a tracking accuracy of ± 0.1 mm is possible in case of a uniform background.

One of the main sources of error proved to be the non-uniform reflectivity of the reflector. This effect was clearly seen when the reflector was rotated around its central axis (Fig. 13 in Paper III). The error due to the non-zero observation angle (Fig. 11 in Paper III) included test equipment inaccuracy and the shading effect of the reflector mask, as depicted in Fig. 14. According to Zumbrunn (1995), a punched sheet reflector (reflector without a mask) results in better accuracy. A large (± 0.6 mm) but rarely evident error caused by specular reflection from the surface of the sheet reflector was encountered near the zero observation angle ($\pm 1°$). The measured accuracy including the error of the pointing mechanism was about ± 0.3 mm. No systematic tests concerning background induced errors were performed, but field tests with the second prototype showed that ± 1 mm pointing accuracy was achievable in an environment where the uniformity of the background was not controlled (Paper III).

Photographs of the automatic 3D coordinate meter prototypes are presented in Fig. 15.

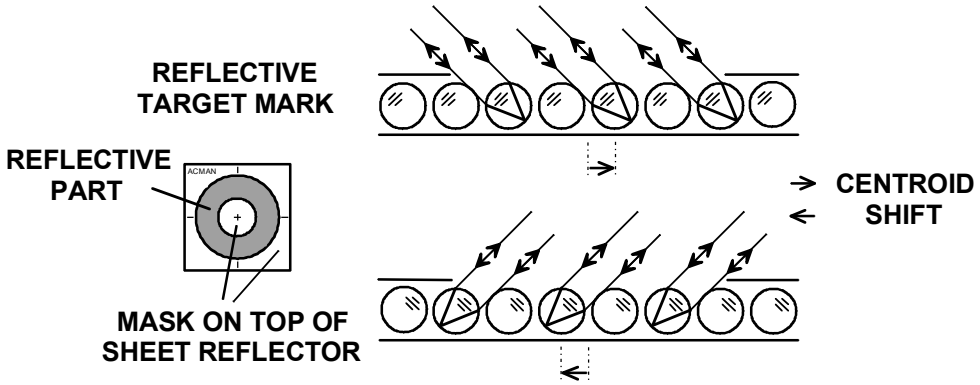

Fig. 14. Centroid position shift due to shading effect of the mask used in reflective marks.

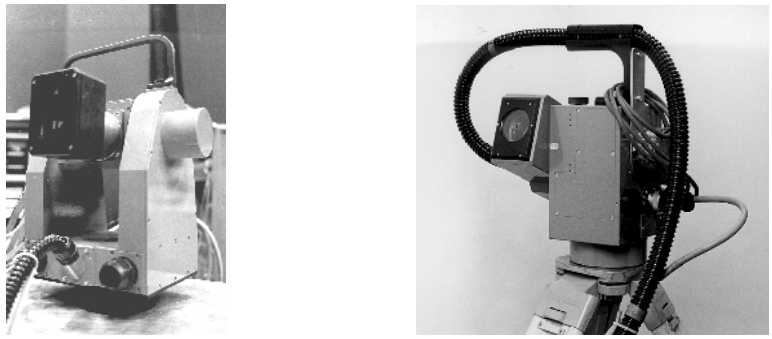

Fig. 15. Prototypes of the automatic 3D coordinate meter intended for checking the dimensions of large industrial objects.

3.4.8. Conclusions

The results show that a practical tracking sensor based on a coaxially illuminated sheet reflector and focused QD receiver is capable of providing performance which is essentially limited by the fundamental restrictions of the method, namely finite contrast and SNR, and that the accuracy is comparable to that of manual aiming in dimensional accuracy control applications. The latter presupposes, however, that specular background reflections caused by glossy metal surfaces etc. are eliminated in one way or another. Such backgrounds are typically present in shipyard applications where steel and aluminium objects are to be measured. Polarisation filtering is proposed in the following for improving the reflector background contrast in such cases.

3.5. Improving reflector background contrast by polarisation filtering

3.5.1. Applications of polarisation filtering and related work

Polarisation filtering is used in various kinds of displays, for example, to enhance contrast by reducing the amount of reflected ambient light and thereby increasing the visibility of the information displayed (Hewlett-Packard Company 1977). It is also used in some machine vision applications to avoid glare from specular surfaces (Melles Griot Inc. 1998). Yet another field of applications includes various isolator constructions in optical instruments to prevent unwanted feedback from optical components into lasers, for example, or to prevent crosstalk between the transmitter and receiver in common path optics (Gindele & Miller 1986).

Gaillet & Belleau (1985) patented a navigation method in which two cameras with crossed linear polarisers are used for enhancing the contrast of a scene which includes sources of linearly polarised light. Kunkel *et al.* (1985) suggested that a filtering based on linear polarisers and quarter wave retarder plates could be used for reflector coding in spacecraft docking sensors, and Sepp (1984) suggested a similar principle in order to discriminate between reflections from CCRs and those from the mirror-like spacecraft surface. Nobody provided any calculations or experimental results, however, to show the effectiveness of the method. We will look here at the effectiveness and suitability of polarisation filtering for lowering errors due to finite reflector background contrast in the case of sheet reflectors. The experimental results are reported in Paper IV.

3.5.2. Operating principle

The principle of using polarisation filtering to increase reflector background contrast is illustrated in Fig. 16. The system is composed of two crossed linear polarisers in front of the transmitter and receiver optics and a quarter wave ($\lambda/4$) retarder plate in front of the reflector. The reflection from a hollow CCR with three orthogonal metallic mirrors is studied first. The $\lambda/4$ plate converts the linearly polarised light used for illumination into circularly polarised light. This is achieved by setting the angle of the $\lambda/4$ plate crystalline axis to 45° with respect to the polarisation plane of the illumination beam. The circularly polarised light is then reflected three times, once from each mirror of the CCR. In each reflection the polarisation state is changed from left-handed to right-handed or vice versa, depending on the original situation, with the result that the polarisation of the retroreflected light is the opposite of the incoming light. After going through the $\lambda/4$ plate a second time, the light is converted to a linearly polarised state again, but this time the direction of polarisation is rotated through 90° relative to the incident light. This means that, due to the crossed polarisers in the transceiver optics, the light reflected from the CCR has the preferred plane of transmission with respect to the receiver polariser and is therefore effectively transmitted to the PSD, while the light reflected from CCR surroundings typically has another polarisation state and is therefore more or less blocked by the receiver polariser.

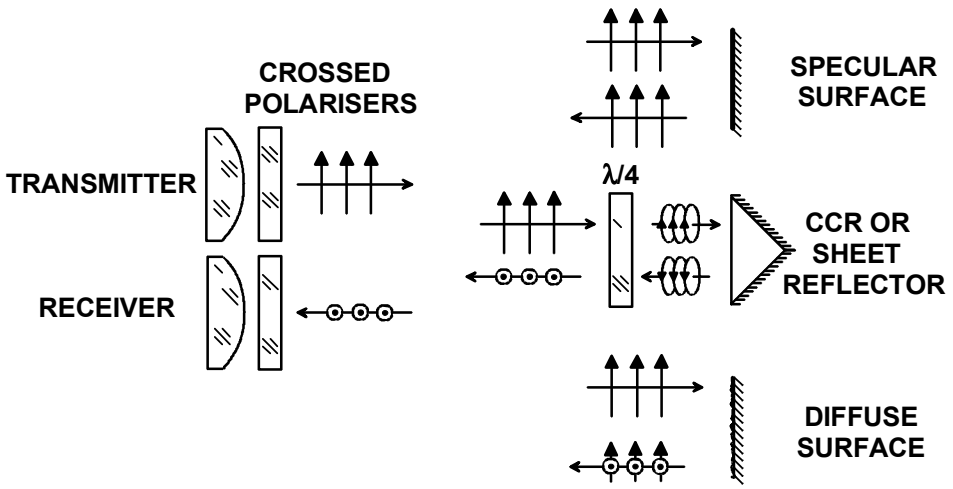

Fig. 16. Principle of using polarisation filtering to increase reflector background contrast.

The reflections from the reflector surroundings include two basic cases: reflection from a diffusing background material and that from a specularly reflecting metallic or dielectric material. Light, whether polarised or not, is generally considered to be randomly polarised after reflection from a diffusing surface. This means that diffuse background reflections are expected to be lowered to about half of that obtained without the crossed polarisers of the transceiver. According to Carmer & Bair (1969), the amount of light received from a diffuse background could be even smaller, since their experiments show that linearly polarised light reflected from a diffusing material, although apparently being randomly polarised, still has a dominant vector in the original direction of polarisation.

Reflection from a metallic or dielectric surface may dramatically change the state of polarisation of an electromagnetic wave, but due to the coaxial transceiver optics, the specular background reflections received include only beams that are essentially perpendicular to the reflecting surface and therefore maintain their original state of polarisation (Kraus 1992). Thus any specular reflections of the illuminating beam should have a plane of polarisation which is perpendicular to that of the preferred transmission of the receiver and should therefore be effectively blocked.

The method was found to operate as expected in the experiments reported in Paper IV. The reflector background contrast improved when polarisation filtering was introduced, and the error due to it decreased markedly. The method proved to be particularly effective when the background included mirror-like surfaces, as expected.

Polarisation filtering in the form presented here needs a reflector to maintain circular polarisation in reflection. Such reflectors include hollow CCRs with metal mirrors or solid glass CCRs with a metal coating, but not CCRs operating on the principle of total internal reflection (Lamekin 1988). It was found experimentally that polarisation filtering operated well with a sheet reflector composed of silver-coated glass spheres, but not with one based on a CCR structure employing total internal reflection (Paper IV).

3.5.3. Applicability to a tracking coordinate meter

Polarisation filtering provides one possible way of eliminating the contrast problem related to the tracking sensor proposed for automatic coordinate meters, since it very effectively eliminates the specular background reflections responsible for the most serious tracking errors in a practical operating environment, and since suitable retarder and reflector materials seem to be readily available. The practical implementation of reflective marks with a $\lambda/4$ retarder could be arranged, for example, by placing a low-cost (~0.1 \$/cm^2), thin (<0.3 mm) $\lambda/4$ retarder film on top of a sheet reflector composed of metal-coated glass spheres (Edmund Scientific Company 1999). Calculations using typical sensor parameters and a moderate polariser extinction ratio (10^{-4}) showed that the tracking accuracy of a sensor that incorporated polarisation filtering would be limited by the diffuse background case even if a reflector was positioned on a perfect mirror oriented perpendicularly to the optical axis of the receiver. A possible problem related to practical use of the method in coordinate measurement applications is that the $\lambda/4$ plate (reflector) must have a certain orientation with respect to the optical axis and the polarisation planes in order not to lower the effective gain of the reflector too much. This complicates target marking and restricts the observation angle of the marks. According to experimental results, the reflector gain is reduced by 50% at reflector rotational and observation angles of about $\pm 20°$ and $\pm 30°$, respectively. The half-gain observation angle is somewhat smaller than without polarisation filtering, but the gain loss could readily be compensated for by slightly increasing the reflector size. The tolerance in the rotational angle also seems to be large enough not to make target marking too inconvenient.

3.6. A rangefinder for measuring object position and orientation

This last part of the tracking rangefinder chapter deals with a rangefinding method that makes it possible to measure not only 3D coordinates but also the orientation of an object. Basically, the orientation of a stationary object can be determined simply by measuring the 3D coordinates of a few known points on it using a coordinate meter. With a moving object, however, very complicated constructions are needed (Lau *et al.* 1988). The rangefinding method proposed here provides a simple means for simultaneous detection of the position and orientation of a movable object at operating ranges of up to some tens of metres. It utilises an active target rangefinding principle, which includes small, fibre-coupled transmitters attached to the object. Its functionality was demonstrated by implementing a sensor system for the interactive teaching of robot paths and environments. A full description of the rangefinder, including constructional details and test results, is given in Paper V.

The background to robot teaching and optical sensors capable of 3D orientation determination is first reviewed, after which the operating principle and constructional details affecting the performance of the proposed device are explained. Finally the limits of its performance are discussed.

3.6.1. Interactive teaching of robot paths and environments

Teaching is necessary for industrial robots to carry out various tasks such as welding, spraying and assembling, for example, and this is typically performed either by directly writing a suitable control program or interactively using the robot in its teaching mode, i.e. the robot arm is moved by the operator through the desired sequence of 3D positions and orientations while movement information and other necessary data are simultaneously recorded by the robot controller (Shamash *et al.* 1988). Interactive teaching methods, including a special pointing tool for describing the working environment and the desired robot arm movements, have been proposed by Hasegawa (1982), Manninen (1984), Ishii *et al.* (1987) and Halme (1988). Suitable pointing tools for such a purpose are described by Kaisto *et al.* (1983), Hasegawa (1982), Ishii *et al.* (1984) and Adachi & Mita (1987), for example.

3.6.2. Sensor systems for position and orientation measurements

Sensors capable of measuring the orientation of a moving target are mostly found in the field of robotic performance measurements. These laser-based sensor systems are typically highly accurate and complicated. A tracking rangefinder with a second tracking assembly attached to the object, and another system composed of six rangefinder beams independently tracking a special assembly of three retroreflectors attached to the object have been proposed, for example (Lau *et al.* 1988). For robot teaching applications, however, more simple and less accurate techniques have been proposed since a movement sequence defined by teaching may be corrected during task execution using on-line sensors (Halme 1988). Optical sensor systems, including hand-held pointers, have been proposed by Ishii *et al.* (1984) and Adachi & Mita (1987), for example. The positions and orientations of a robot tool are taught simply by grasping the pointer and simulating the desired movements of the robot arm with the pointer by moving it in an appropriate orientation through the important passing points of the trajectory (Ishii *et al.* 1987). The sensor system consists of a stationary PSD camera and a pointer with multiple LEDs attached to it. The position and orientation determination of the pointer is based on the 2D coordinate values of the LEDs on the image plane of the camera and on the geometrical relationship among the 3D positions of the LEDs attached to the pointer. At close distances (~1 m) these sensors are reported to achieve position and orientation sensing accuracies of 3 to 5 mm and about 1 to 2°, respectively (Ishii *et al.* 1984, Adachi & Mita 1987). Due to the operating principle, depth information is less accurate than information on a lateral plane, and therefore the measurement accuracy of the pointer distance from the camera and its angle with respect to the camera's optical axis will decrease with increasing distance, thus limiting the applicable operating range of the sensor.

3.6.3. Sensor construction

A TOF rangefinder for measuring the 3D position and orientation of a hand-held pointing tool was proposed in Paper V. The pointer is used in a similar fashion to that proposed by Ishii *et al.* (1987), and its operating range and accuracy are specified to be 2 to 5 m and a few millimetres, respectively. The system is composed of a pointer with two fibre-coupled laser pulse transmitters and three LEDs attached to it, a tracking receiver, including a rangefinder receiver and a CCD camera, and a time interval measurement (TIM) unit (Fig. 17). The CCD camera is used to direct the receiver head continuously towards the pointer by detecting the position of the LEDs attached to the pointer arm. The 3D position and orientation of the pointer are obtained on the basis of the distances of the fibre-coupled laser pulse transmitters, the 2D positions of the LEDs in the camera image and the angles of the tracking receiver. The 2D positions of the LEDs in the camera image are used to detect the pointer angle on a plane perpendicular to the optical axis of the receiver (rotational angle), and the rangefinder to detect its angle with respect to the optical axis (depth angle) by measuring the difference in distances of the laser pulse transmitters positioned 20 cm apart on the pointer arm.

The general advantage of rangefinding over the camera-based techniques used by Ishii *et al.* (1984) and Adachi & Mita (1987) is that in principle a larger operating range is achievable without compromising on accuracy. This means in practice that millimetre-level accuracy should be achievable in the direction of the optical axis up to distances of a few tens of metres. This can be utilised not only when measuring the basic distance of the pointer but also when measuring its orientation (depth angle).

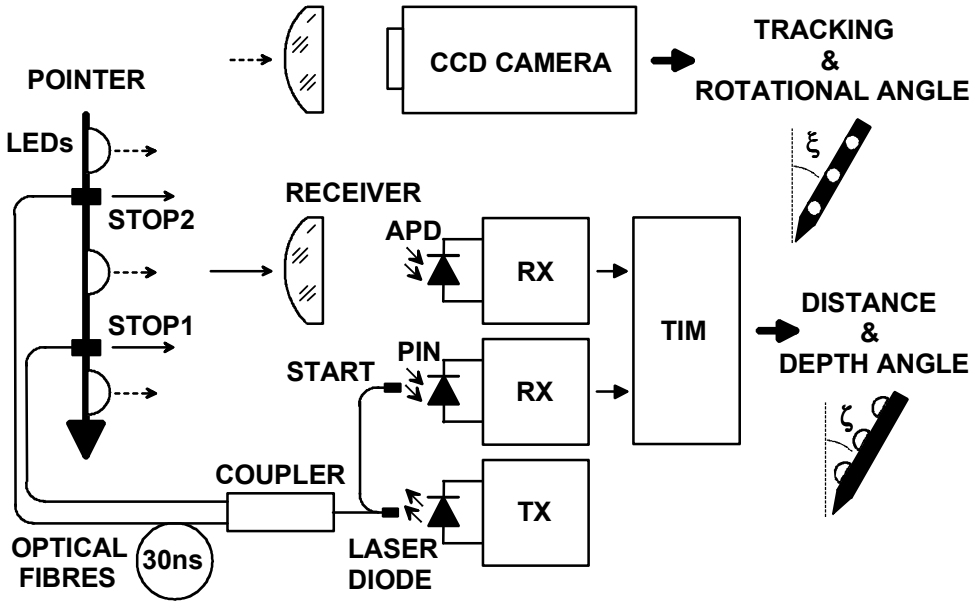

Fig. 17. Construction of the rangefinder intended for object orientation measurement.

3.6.4. Active target rangefinder

3.6.4.1. Operating principle

A conventional rangefinder has its transmitter and receiver optics in the same measuring head and the light pulse travels through the air to the object and back. In this application, however, use of the conventional principle would have led to a complicated sensor construction composing of two tracking rangefinders, for example. This was avoided by using a single rangefinder receiver with large FOV (~100 mrad) and two fibre-coupled radiators attached to the pointer arm. The light pulses travel via optical fibres to the pointer arm, from which they are radiated in a wide angle (120° x 80°) towards the receiver. The FOV of the receiver is large enough for the light pulses transmitted from both radiators to be detected simultaneously when the receiver is directed towards the centre of the pointer arm and the pointer is facing towards the receiver. The pointer could be rotated freely around the optical axis of the receiver but its angle with respect to the plane perpendicular to the optical axis and the rotational angle around its own mechanical axis were restricted to about ±40° and ±60°, respectively.

Simultaneous detection of two distances is implemented by appropriately delaying the transmitted pulses with respect to each other and then time-gating the received pulses accordingly. The timing of the start and stop pulses of the rangefinder is illustrated in Fig. 18. The START pulse is internally generated and detected a few nanoseconds after the light pulse is emitted from the laser. The basic distance of the pointer is obtained from the time interval between the START pulse and the first stop pulse, STOP1, which is received from the pointer tip and which travels for 35 ns in the fibre and from 7 to 17 ns in the air, depending on the distance (2 to 5 m).

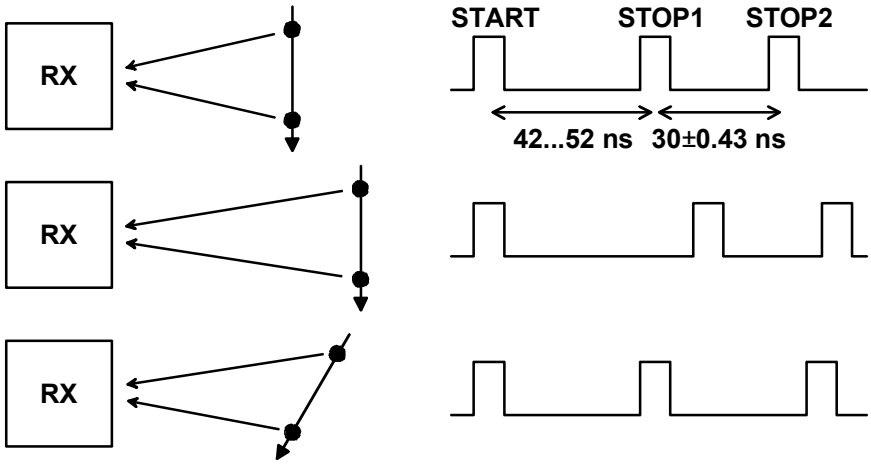

Fig. 18. Timing of the start and stop pulses of the rangefinder.

The distance difference is obtained by measuring the time interval between the STOP1 and STOP2 pulses transmitted from the opposite ends of the pointer arm. To be able to detect both stop pulses properly with a single receiver, STOP2 is delayed about 30 ns by using a longer coupling fibre. The time interval between the stop pulses varies ±430 ps as the angle of the pointer is varied in the range ±40°.

3.6.4.2. Miscellaneous phenomena and constructional details

The phenomena affecting the performance of an active target rangefinder include mode dispersion effects in fibres and multiple path propagation of light due to unwanted reflections. Since TOF rangefinding is based on accurate transit time measurement, any variations in the time needed for a light pulse to travel through a coupling fibre results in a measurement error. The large diameter (100 to 400 µm) multimode fibres used to maximise power coupling have high mode dispersion, and therefore transit time differences between individual light modes may cause errors of several centimetres when long (>10 m) fibres are used (Nissilä & Kostamovaara 1995). Distance measurement errors due to dispersion effects are mostly avoided in a conventional rangefinder by using a homogeneous diffuse target and coaxial optics with a constant numerical aperture (Kaisto *et al.* 1994, Nissilä & Kostamovaara 1995). This arrangement ensures that the selection of light modes propagating through the coupling fibres remains the same irrespective of the distance measured, and therefore the transit time of a light pulse in the fibre also remains constant.

With an active target the selection of received light modes varies substantially as a function of the observation angle of the radiator (fibre end), and therefore to maintain accuracy the radiators should be equipped with means of mixing the light modes so that the light received will be delayed equally in the fibre independent of the observation angle. The transit time was clearly observed to vary as a function of the radiator observation angle during preliminary tests with the rangefinder. The inaccuracies resulting from this phenomenon could be mostly eliminated, however, by covering the radiators with a transparent diffusing film (Fig. 10 in Paper V).

The wide divergence in the receiver FOV and in the transmitted beams also had an adverse effect on the sensor performance. In a conventional rangefinder the receiver is able to see basically only the area occupied by the transmitted light spot on the target surface, and therefore any secondary reflections from nearby surfaces will not be detected (Määttä & Kostamovaara 1992). In the present case, however, the receiver has a large FOV which also covers the surroundings of the radiators and is therefore capable of collecting not only the light coming directly from a radiator but also light pulses that are reflected from objects within the receiver FOV after being transmitted from the radiators. These reflections cause error in the distance results due to summing of the direct light pulse and its delayed reflection.

The radiators of the teaching device were originally designed to radiate cylinderically at an angle of 360°, so that the pointer could be rotated freely around its axis, but it turned out that background reflections were able to cause considerable distance measurement errors in certain situations, and therefore the divergence of the

radiators was reduced to about ±60° by ±40° to reduce the possibility of unwanted reflections. Despite the reduction in divergence it was observed that surfaces of area >10 cm^2, when located near the radiators (<10 cm), could still cause observable changes in the measured results. This was probably due to the fact that the diffusing films used for mode mixing enlarged the effective radiation angle of the radiators beyond the desired and enabled the light to reflect from nearby objects.

3.6.4.3. Measured performance

The test results showed that the distance and angle of the pointer could be measured with an accuracy of ±5 mm and ±5° within the specified ranges of 2 to 5 m and ±40°, respectively. The corresponding precisions were 1.3 mm and 0.3° (100 measurement results averaged using a pulse frequency of 4 kHz). The above performance was achieved using simple circuit implementation and without gain control.

3.6.5. Discussion

The sensor system was constructed ten years ago for demonstration purposes, and therefore the simplest possible construction was used (Mäkynen *et al.* 1988). The TIM unit included purely analogue time-to-distance converter circuitry and the received pulses were discriminated as such by the timing discriminators without any gain control. It is obvious that better accuracy could have been achieved if more sophisticated techniques had been used. Most of the state-of-the-art TOF rangefinding techniques reported in Määttä (1995), Kilpelä *et al.* (1998), Määttä & Kostamovaara (1998), Räisänen-Ruotsalainen (1998) and Ruotsalainen (1999), for example, could readily be used in constructing active target rangefinders, and therefore an accuracy of about ±3 mm and ±1° should in principle be achievable in the teaching device application, for example.

Errors related to mode dispersion and multiple path propagation effects could probably be eliminated by careful design of the radiators. Diffusing material could be used in front of the fibre end and simple collimating optics to direct the radiation to a well-defined angle in order to prevent reflections from nearby objects.

The operating range could be enlarged up to a few tens of metres simply by using a more powerful transmitter and by optimising the radiator and receiver construction. The transit time dependence of the fibres on temperature would probably be the main limiting factor when enlarging the operating range. The temperature dependence of the transit time delay in large diameter multimode fibres is reported to vary between 10 and 20 ps/C°100 m (Nissilä *et al.* 1991). Thus fibres longer than a couple of metres need temperature compensation in order to achieve millimetre accuracy. Such compensation is not straightforward, but has been successfully implemented within a limited temperature range (0 to +35 C°) for coordinate meters, which include 30 m of coupling fibres (Ylitalo 1994).

4. Sensors for lateral displacement measurements

The properties and performance of two reflected beam sensor constructions intended for displacement sensing applications are described here. The first utilises a focused QD receiver and a square-shaped sheet reflector to measure small lateral displacements (μm to cm) accurately from a distance of a few metres. The work was originally inspired by the fact that a QD-based reflected beam sensor provides high measurement-distance-to-precision ratios ($>10^6$) and simultaneously relatively high speeds (tens of kHz). Other advantages of the proposed sensor construction are that 2D displacement can be measured with one sensor and that the extent of the measurement field and measurement distance (stand-off distance) can vary within a large range. The sensing method is believed to be suitable for measuring various kinds of vibration in industrial machines and constructions, for example. The main purpose of the work was to demonstrate that the focused QD receiver provides position information which is proportional to the linear displacement of the reflector rather than its angular displacement and that its scaling is range-invariant and solely determined by the size of the reflector. The performance of a practical sensor composed of ordinary off-the-shelf components was also investigated. A full report on the sensor is presented in Paper VI.

The second sensor system is based on a focused LEP receiver and CCRs. This construction was found to be suitable for long-range outdoor measurements (>50 m) such as the aim point trajectory measurements needed in optical shooting practice. Special attention was paid to minimising the sensitivity of the receiver to atmospheric turbulence, since it is this that typically sets the upper bound for the precision achievable outdoors. The turbulence sensitivities of QD and LEP receivers were compared and it was found that a focused LEP receiver is less sensitive to atmospheric fluctuations and provides better precision despite its higher noise level. It was also found that fairly little can be done to further improve precision in turbulence-limited cases. Adjusting the receiver parameters or averaging successive measurement results typically has a negligible effect on precision. Some improvement was achieved, however, using a new method based on the averaging positions of multiple, laterally separated CCRs. The main precision optimisation results are reported in Papers VII, VIII and IX.

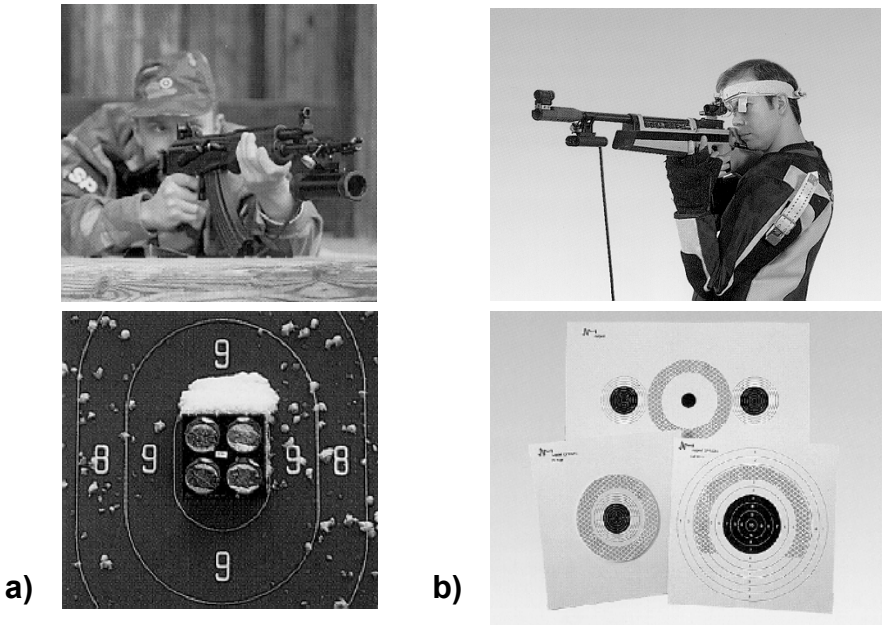

Fig. 19. Practice equipment intended for a) military and b) sports shooting (Noptel Oy 1997). Both pieces of equipment use the reflected beam sensing principle. The former uses CCR targets and the latter sheet reflectors.

The close-range sensor was constructed only to demonstrate the practical functionality of the idea. The original aim of the second experiment, however, was to find out whether it would be feasible to develop equipment for optical shooting practice using the reflected beam sensing principle (Fig. 19).

4.1. A reflected beam sensor for close-range displacement sensing

The properties and performance of a reflected beam sensor for close-range displacement sensing are described. Examples of methods used for small displacement sensing are presented first, and then the main properties of the sensing principle are described, after which the practical performance constraints are evaluated. Finally, conclusions and a discussion are provided.

4.1.1. Methods for small displacement sensing

Small displacements need to be detected in various measurements of vibration in industrial machines and constructions, for example, where frequencies typically vary from fractions of a Hz to several tens of kHz and amplitudes from a few tens of nanometres to several decimetres (Broch 1980). The vibratory displacements of mechanical bodies are typically measured using a piezoelectric accelerometer attached to them. Among the weak points of such electromechanical transducers in displacement sensing are the lack of dc-response, the lower corner frequency being 0.1 to 1 Hz, and the need for a cable to connect the transducer to the preamplifier, which makes it difficult to measure high frequency displacements of lightweight objects.

A number of non-contact optical sensors have been proposed for displacement sensing purposes. Their operation is generally based on interferometry (Strand 1985, Drain & Moss 1986), triangulation (Jarvis 1983), astigmatic focus error detection (Lou *et al.* 1984, Mitsui *et al.* 1988), or laser rangefinding (Kostamovaara *et al.* 1992). A common feature in these sensors is that they measure displacement in the direction of their optical axis, which means that they are capable of measuring one-dimensional displacement as such. The reflected beam sensor presented here detects object displacement in a plane which is perpendicular to the optical axis of the receiver and is therefore capable of measuring 2D displacement with one sensor head. Other types of optical displacement sensor capable of measuring multiple degrees of freedom have been proposed by Hutcheson (1976), Lou *et al.* (1984) and Francini *et al.* (1987), for example.

4.1.2. Main properties of the sensing principle

The proposed sensor has the same basic construction as the tracking sensor presented in section 2.4.1, with the exception that the non-linear transfer characteristics due to the circular shape of the reflector have been linearised by using a square reflector (Fig. 20). In its basic form, the reflected beam method provides information on the angular displacement of the reflector, but in the special case of a focused QD receiver the results can be shown to be proportional to the lateral (linear) displacement of the reflector. This is based on the fact that the size of its measurement field is determined solely by the size of the reflector image, which in the focused case corresponds exactly to that of the reflector in the object space at all distances. Arithmetically, the reflector displacement in the object space is

$$X = \frac{1}{m}\frac{d}{2}\frac{(i_a + i_b) - (i_c + i_d)}{i_a + i_b + i_c + i_d} = \frac{D}{2}\frac{(i_a + i_b) - (i_c + i_d)}{i_a + i_b + i_c + i_d}, \qquad (11)$$

where D is the side length of the square reflector, d (=d_s) the corresponding length in the image and m the magnification of the optics. The sensor provides inherently accurate and constant scaling independent of the reflector distance (magnification), and thus reflector displacement can be measured accurately as long as the reflector dimensions are known and the receiver is properly focused. The practical advantage of the above is that the extent of the measurement field can be tuned to a particular measurement task simply by choosing an appropriate size for the reflector, and that the stand-off distance can be freely selected.

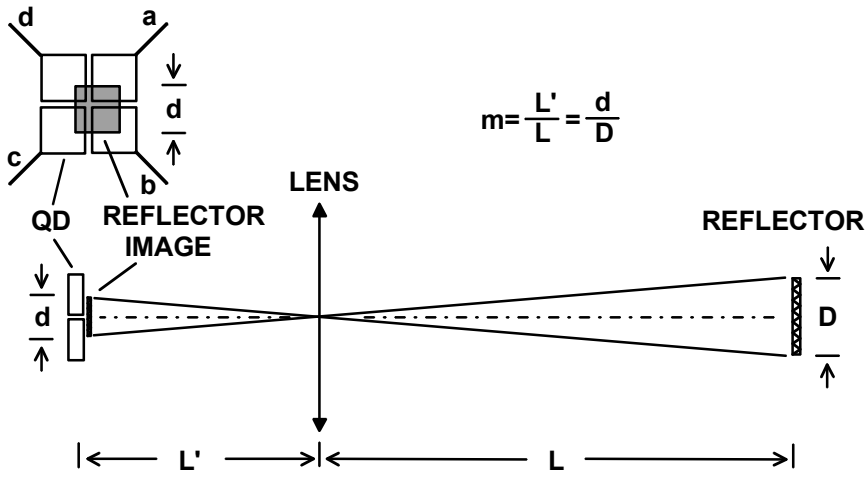

Fig. 20. Operating principle of the displacement sensor. Due to focusing, the size of the measurement field is determined by that of the reflector at all distances. The square shape of the reflector provides linear transfer characteristics.

The property of range-invariant scaling is unique to a focused QD receiver. With LEPs, for example, range-invariant scaling would require the use of special optics such as telecentric lenses, which provide constant magnification and perspective. Their working volumes are typically very limited, however, the distance range being a few tens of centimetres at most, and the lateral extent smaller than the receiver lens diameter (< 10 cm) (Häusler & Maul 1985, Melles Griot Inc. 1998). Similar limitations seem to exist in other range-invariant lens systems suitable for displacement sensing (Burch & Williams 1974, Hutcheson 1976). The working volume of the proposed sensing principle is substantially larger, being limited basically only by the reflector size and diffraction.

The ideas of using a square target for linearisation and utilising the range-invariance of a focused QD receiver measurement span for displacement sensing are believed to be new.

4.1.3. Performance of the experimental sensor

4.1.3.1. Precision

Important factors determining the applicability of the method to practical displacement sensing include the achievable precision, the accuracy of scaling and the linearity of the lateral transfer characteristics. As concluded earlier, typical sensor parameters yield submicron precision when a 1 cm^2 sheet reflector is used, even if the sensor bandwidth is several kHz and the measurement distance several metres. The pronounced distance dependence (~L^4) means, however, that such high precision is not achievable at long stand-off distances. In principle it is possible to achieve submicron precision at distances up to about 40 m using a bandwidth of 1 kHz and an optimally illuminated ($L\theta \sim 2\sqrt{2}D$) 40 mm high-gain sheet reflector, for example.

The experimental results showed the precision predicted by the calculations, but also emphasised that it is not possible to achieve submicron precision using stand-off distance of a few metres in a practical operating environment due to fluctuations caused by air currents. Without these fluctuations the precision of the experimental system using a stand-off distance of 2.5 m would have been about 0.02 μm at best (G~3000, D=10 mm, B=880 Hz, P_{ill}=0.38 mW, θ=12.5 mrad, ϕ=30 mm). The standard deviations measured in an ordinary indoor environment varied between 0.6 and 3.5 μm, however. Submicrometre precision was obtained only by limiting the air currents (Table I in Paper VI). The effect of fluctuations was stronger at longer stand-off distances, so that the achievable precision at a distance of 40 m, for example, was found to vary between 0.1 and 0.5 mm.

4.1.3.2. Accuracy of scaling

In practical implementations the scaling, which should be inherently accurate, is affected by image spot spreading due to diffraction, aberrations and misfocusing of the receiver optics, by non-optimal orientation of the reflector and its dimensional inaccuracies, by the gap width of the QD and crosstalk between its quadrants, and by the finite reflector background contrast. The effect of the above factors is summarised in the following for a small reflector. The small reflector case is interesting since it provides the best precision when optimally illuminated. A scaling accuracy of 1%, a diffuse background, a magnification of 0.1 and an f-number of 5 are assumed.

Diffraction and aberrations of the receiver optics increase the effective size of the reflector and the scale factor. Diffraction alone limits the minimum reflector side length to about 10 mm in the proposed case. If aberrations exist, the minimum reflector size obviously increases. Another reason for possible scaling inaccuracy is the finite reflector background contrast. Background reflections nevertheless cause a scaling error that is smaller than 1% when optimally illuminated high-gain (G~3000) reflectors are used with a diffuse background (Fig. 4 in Paper VI). With specularly reflecting backgrounds the scale factor errors can be minimised by using polarisation filtering, for example.

Other factors affecting the scaling accuracy are related to the practical construction of the QD. The gap between the quadrants has basically zero responsivity and thus reduces the apparent reflector size and the scale factor correspondingly. Using a 10 mm reflector, 1% scaling accuracy presupposes a gap width which is smaller than 10 µm. Crosstalk due to the common substrate of the quadrants should be less than 0.5% in order to achieve a better than 1% scaling accuracy. Note that this crosstalk depends on the gap width and decreases as the gap width increases, and that the effects of the gap and crosstalk are opposite and partly cancel one another out.

The demands set above for the receiver lens (diffraction limited near the optical axis) and the QD (10 µm gap and 0.5% crosstalk) are just low enough to be fulfilled using simple lenses and a standard QD. Experiments performed using a lens system (f/#~4) capable of producing a 30 µm focal spot within a ±1° angular FOV and a detector (SD085, Adcanced Photonix Inc. 2000) which had a 10 µm gap width and a crosstalk of about 0.6% (@850 nm) showed an error of 0 to –3% for 5 to 15 mm reflectors (G~800) when low reflectivity, a diffuse background and a magnification of 0.05 were used (Paper VI). Note that the results also include the dimensional inaccuracies of the reflectors.

4.1.3.3. Effect of receiver misfocus and reflector misorientation

Since a fast, easy sensor set-up without complicated auxiliary equipment would be an advantage, the accuracy needed in receiver focusing and reflector orientation in order to maintain scaling accuracy was studied in Paper VI. Scaling remains unchanged if the optical power per unit of spot displacement is not altered due to misfocus or reflector misorientation. According to the geometrical analysis and the experiments performed with a CCD camera and image analysis software, misfocusing first causes changes in irradiance at the edge of the reflector image, leaving the irradiance at the centre and the effective size of the reflector image essentially unaltered. This means that good scaling accuracy should be obtainable in slightly misfocused systems, but within a limited area at the centre of the measurement field. Use of a 10 mm reflector means that its distance could deviate about ±0.25 m from the best focus distance without detracting from accurate scaling (determined by the reflector size) within 50% (5 mm) of its total measurement field (f/#~5 and m~0.1). The experiments supported the above assumptions and showed that the average scale factor changes less than 0.1% within the central part (80%) of the measurement field when the reflector (D=15 mm) distance is altered by ±0.2 m from its best focus distance (f/#~4 and m~0.05) (Paper VI). In practice this means that only relatively coarse focusing is needed if oversized reflectors are used.

Accurate scaling presupposes proper orientation of the square reflector. A non-zero angle between the reflector normal and the optical axis (observation angle) will reduce the apparent size of the reflector, and thus the scale factor, in proportion to the cosine of this angle. Rotation of the reflector from its optimum orientation has a similar effect on the scale factor. Both angles have to be less than about 8° to ensure a smaller than 1% error contribution to scaling (Table II in Paper VI).

4.1.3.4. Linearity of the lateral transfer characteristics

The accuracy of displacement sensing is also affected by the linearity of the sensor transfer characteristics. The sources of non-linearity are the spatial non-uniformities of the detector responsivity, reflectivity of the reflector (specific radiance) and its illumination. A rough upper bound (ε_{srd}) for the non-linearity error related to the combined effect of these non-uniformities would simply be

$$\frac{\varepsilon_{srd}}{D} \approx \frac{\pm\frac{1}{2}\Delta S / S_{syst}}{2 \pm \Delta S / S_{syst}}, \tag{12}$$

where $\Delta S/S_{syst}$ is the maximum of the relative system responsivity difference in the areas occupied by the reflector and its image, and D the width of the reflector (Fig. 5 in Paper VI). The system responsivity includes the combined effect of illumination, reflectivity and the QD responsivity. According to Eq. (12), $\Delta S/S_{syst}$ should be less than 4% in order to achieve an integral non-linearity better than 1%. This places quite high demands on reflectivity and illumination uniformity in particular. The experimental results (Fig. 6 in Paper VI) nevertheless show better than 1% non-linearity for two different types of sheet reflector when illuminated with a collimated beam from an infrared LED. The differential non-linearity (Fig. 7 in Paper VI) was better than 7% when a measurement step of 200 μm was used. The main contributor to non-linearity proved to be the non-uniformity of the reflector materials, while the smallest contribution was due to spatial variation in QD responsivity.

4.1.4. Conclusions and discussion

The principle proposed here provides a potential means for implementing high-speed 2D displacement sensors with micrometre precision. Unlike a conventional reflected beam sensor, it provides position information which is proportional to the linear rather than angular displacement, and scaling which is range-invariant and solely determined by the size of the reflector. This means that the stand-off distance can vary within a large range and that the measurement field of the sensor can be tuned for a particular measurement task simply by using a square-shaped reflector of known side length that is long enough to cover the amplitude range of the displacements to be measured. In practice, the extent of the measurement field can range from a few millimetres to several decimetres and the stand-off distance from some decimetres up to several tens of metres. The results show that a sensor composed of standard components, having a measurement field of about 1 cm and using a stand-off distance of a few metres can provide a bandwidth of several kHz, a precision that is limited to the level of a few micrometres by atmospheric fluctuations, an inherent scaling accuracy of a few % and integral non-linearity better than 1%.

Only relatively coarse focusing and orienting of the reflector are needed when the sensor is set up. Accurate receiver focusing is not needed if oversized reflectors are used,

and thus the simplest means of focus adjustment should be sufficient. It is also relatively easy to set up proper rotational orientation for a reflector using coaxial viewing optics with a suitable reticle, for example. Setting up the observation angle may prove somewhat more complicated, however.

The main drawback concerning the practical performance of the proposed method was the powerful effect of atmospheric fluctuations on the achievable precision, which would have been one or two orders of magnitude better at a distance of a few metres without atmospheric effects. Note, however, that since the spectrum of atmospheric fluctuations is typically concentrated well below the 100 Hz region, it should be possible to measure vibratory displacements above 100 Hz with a precision determined by the electrical SNR simply by using high-pass filtering to remove the effect of atmospheric fluctuations (Fante 1975). Note also that averaging should provide an improvement in precision below the 100 Hz region if the measured displacement is repetitive.

The displacement of a sinusoidally vibrating loudspeaker coil measured with the experimental sensor system from a distance of 2.5 m is presented in Fig. 21 (Paper VI).

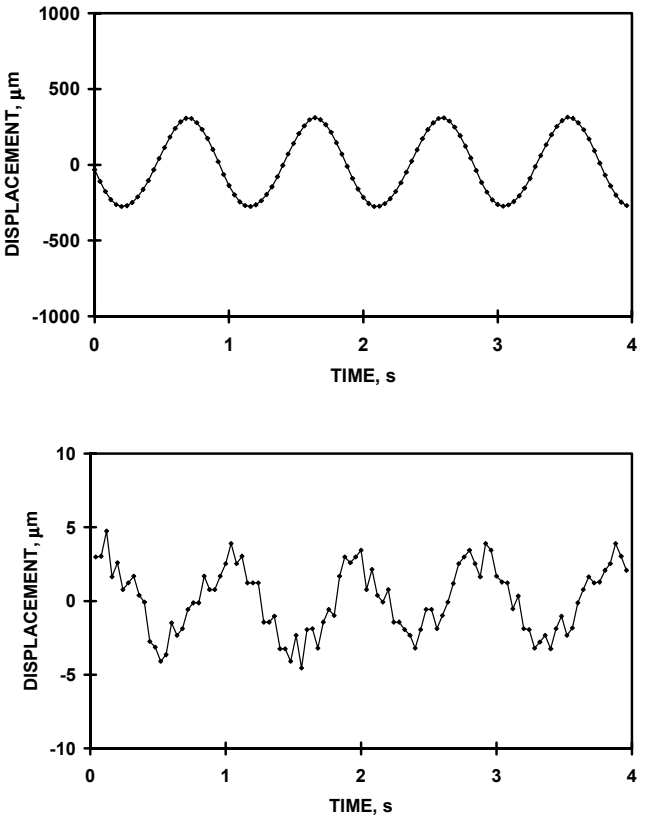

Fig. 21. Displacement of a sinusoidally vibrating loudspeaker coil measured with the experimental sensor system. No averaging or filtering was used to remove the effect of air currents.

4.2. A reflected beam sensor for long-range displacement sensing

A reflected beam sensor construction for long-range outdoor applications (>50 m) was proposed and its precision evaluated in Papers VII, VIII and IX. The original aim was to find out whether the reflected beam method could be used for aim point trajectory measurement in optical shooting practice. The previous sensing principle used in the shooting practice equipment had been based on the direct beam method, in which a laser transmitter was attached to the gun, and an active position-sensitive target was used to register the transmitter beam spot position during aiming and triggering. The main motivation for introducing reflected beam techniques was to be able to implement sensor systems for applications which needed such a large FOV that this would not have been feasible using an active target. The reflected beam method made it possible to replace a bulky and expensive active target with a small and inexpensive reflector.

The conventional tracking sensor construction based on a misfocused QD receiver is very sensitive to atmospheric turbulence and provides such poor precision in an outdoor environment that it cannot be used as such in shooting practice, for example. The reason for the poor precision proved to be the misfocusing needed for QD operation. A sensor construction based on a focused LEP receiver and CCR target was consequently proposed. This provides low sensitivity to atmospheric fluctuations, and despite its higher electrical noise, much better precision in a turbulent environment than the misfocused QD receiver.

The specifications for a sensor system intended for shooting practice are presented first after which possible sensor constructions. Since the measurement accuracy in an outdoor environment is determined by the atmospheric turbulence, the mechanisms by which atmospheric turbulence affects the precision of a reflected beam sensor are explained. Theoretical and experimental results on the achievable precision at intermediate levels of atmospheric turbulence are presented, and a method for improving the precision based on averaging the displacement results of multiple, laterally separated CCRs is proposed and its functionality demonstrated. Finally, the sensor construction required for the best precision is reviewed.

4.2.1. Requirements for a shooting practice sensor

The shooting training equipment considered here is intended for practising aiming and triggering with military firearms by optical means without ammunition. The main idea of such equipment is to improve the shooting skills of an ordinary soldier by making it possible to increase the amount and quality of the shooting practice available (Noptel Oy 1997). The requirements for the sensor in such equipment are based on a target-practice routine which involves use of a 150 m rifle range with square pieces of cardboard of side length one metre as targets and assault rifles as the weapons to be used.

To provide realistic aiming conditions, the optical target practice is performed in an outdoor environment with the cardboard targets, having suitable reflectors attached to them and positioned at a nominal distance of 150 m. The displacement sensing accuracy of the sensor system should be equal or better than the assumed width of the bullet hit

point distribution of a typical rifle when fired without aiming errors. The standard deviation in such a case is typically 1 to 2 cm at 150 m. This means that the sensor should provide better than 1% relative accuracy if a 10 mrad measurement FOV is used. According to experimental results, in order to record the aiming trajectory of a rifle accurately enough the measurement rate should be around 50 to 100 measurements/s, which corresponds to an analogue bandwidth of a few tens of Hz.

4.2.2. Possible sensor constructions

Although a reflected beam sensor primarily provides information on angular displacement, it can readily be used to detect the lateral displacement of the aiming trajectory in shooting practice, since the target distance is typically known. A conventional tracking sensor composed of a misfocused QD receiver and a CCR seems very suitable for the purpose, due to the good electrical sensitivity of the QD. Adequate linearity (1%) could be provided by restricting the effective measurement field to a fraction of the total field (Kazovsky 1983) or by using a square aperture (Carbonneau & Dubois 1986). According to the experimental results described in section 3.3.3, however, a misfocused QD receiver is very sensitive to atmospheric turbulence, which seriously detracts from the achievable measurement precision and makes a sensor based on a QD receiver and a CCR target unsuitable for the purpose.

As concluded in section 3.3.3, the use of a sheet reflector instead of a CCR would provide 20 times better precision in cases where intermediate atmospheric turbulence determined the precision. This means that low enough turbulence sensitivity with good enough electrical sensitivity and contrast could have been achieved simply by replacing the CCR with a high-gain sheet reflector having a diameter larger than about 30 cm and by using the conventional receiver construction.

The same techniques could be used as in close range displacement sensing. The square cardboard target could be fully covered with reflective sheeting and the QD receiver could be focused at the target distance. In addition to low turbulence sensitivity, good linearity and electrical sensitivity, this kind of a sensor would also provide lateral displacement directly without accurate knowledge of the target distance, as explained earlier.

4.2.3. Construction of the proposed sensor

Although sensor constructions based on a QD receiver and sheet reflector provide quite adequate performance for rifle practice, they are not satisfactory constructions for shooting training applications in general, because a reasonably sized sheet reflector (<1 m) would provide inadequate contrast and precision in applications requiring a long target distance (~1 km) or large FOV (~100 mrad), for example. A typical case of a long-range, wide FOV application of this kind is target practice with anti-armour weapons, in which an extensive lead is required for proper aiming.

The proposed sensor uses a CCR target to provide an adequate signal level and contrast irrespective of the target distance or the extent of the receiver FOV, and a focused LEP receiver to achieve low sensitivity to atmospheric fluctuations. Focusing is possible in the case of the LEP, since its signals are proportional only to the centroid position of the spot and are not affected by spot size. A LEP also provides better linearity than QDs, and thereby potentially better overall accuracy.

The main topic in the following is to analyse and compare the position sensing precision of the conventional QD-based sensor and the proposed sensor under outdoor conditions. The effect of electrical noise, and especially atmospheric fluctuations, is considered.

4.2.4. Effect of noise on measurement precision

The comparison of QD and LEP receivers in terms of sensitivity presented in section 2.3.1 and Paper VII shows that their relative superiority depends markedly on the noise contribution of the background illumination. Using one CCR and typical sensor parameters (R_{ie}=10 kΩ, B=30 Hz, ϕ=50 mm, P_{ill}=1 mW, τ=0.5, θ=0.01 rad, D=1.5 m) and assuming that the appropriate optical filtering (bandwidth ~10 nm) is used, it can be concluded that both sensors would provide electrically submillimetre precision in the described shooting practice application. A QD-based sensor would provide 6 to 12 times better incremental sensitivity, however, depending on its linearisation method, even in bright background illumination (spectral irradiance ~1300 W/m^{2}μm, background reflectivity ~0.3).

4.2.5. Atmospheric turbulence

Atmospheric turbulence causes phenomena commonly referred to as beam wander, scintillation and beam breathing, according to the effect produced on the beam spot as seen on the screen after travelling through a turbulent atmosphere. Beam wander means random changes in the position of the beam spot on the screen, scintillation illumination fluctuations within the beam and breathing expansion and contraction of the spot beyond the dimensions predicted by its geometry and diffraction. These effects are caused by index-of-refraction inhomogeneities which mainly arise from spatial temperature differences within the atmosphere.

A turbulent atmosphere can be thought to be composed of cells of various sizes that differ in their index of refraction. As these cells move across a beam of light, they result the effects described above. According to this ‘frozen’ atmosphere assumption, the velocity and direction of this uniform motion is determined by the mean wind speed (Fig. 22).

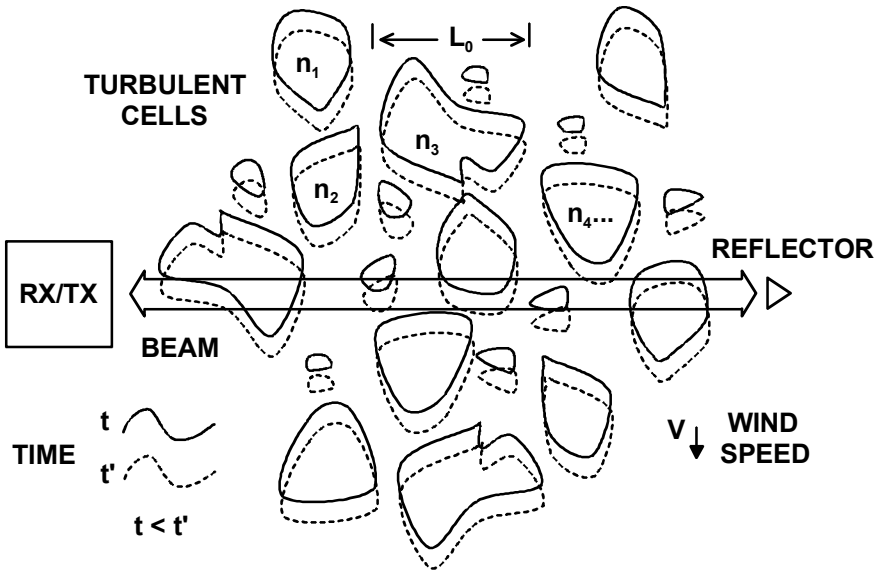

Fig. 22. According to the 'frozen' atmosphere assumption, the effects of atmospheric turbulence on beam propagation are caused by the uniform motion of turbulent cells of varying sizes and with a varying index of refraction.

Depending on the dominant cell size and beam diameter, turbulent cells affect light propagation in different ways. Cells that are larger than the beam diameter act like weak lenses and deflect the beam as a whole in a random way (angle of wave front) leaving its illumination distribution essentially unaltered (beam wander), but when the cell size is smaller than the diameter of the beam, refraction and diffraction take place and the illumination profile of the beam breaks up into small bright and dark areas as a result of refracted and diffracted wave front interference (scintillation). Depending on the relative strength of the turbulence either of the effects may be observed, or both simultaneously. The dominant effect is beam wander in weak turbulence and scintillation in strong turbulence (Weichel 1990). The outer scale of turbulence, L_0, describes the size of the largest turbulent cell and thus sets the limit for the lateral extent within which large-scale effects such as beam wander may be correlated. For horizontal beam paths near the ground, L_0 equals roughly 1/3 of the beam height (Lawrence & Strohbehn 1970).

The strength of atmospheric turbulence is described by the refractive index structure coefficient C_n, which is basically a measure of the spatial gradient of the refractive index (temperature) within the atmosphere. From the sensor point of view the strength of the turbulence also depends on the length of the path that the light traverses. The strength of path-integrated turbulence is described by the spherical wave coherence length $\rho_0=(0.545k^2LC_n^2)^{-3/5}$, where $k=2\pi/\lambda$ and λ is the wavelength. This describes the amount of scattering caused by atmospheric turbulence and is used to determine whether the turbulence in a particular case is considered weak or strong. Turbulence is considered to be weak if ρ_0 is larger than the diffraction patch size $\sqrt{L\lambda}$ and strong if it is smaller (Churnside & Lataitis 1989).

4.2.6. Effect of atmospheric turbulence on measurement precision

The effect of atmospheric turbulence on beam propagation is a result of complicated phenomena. In certain cases, however, it can be satisfactorily estimated using simple equations. Geometric optical formulation, for example, can be successfully used to predict large-scale effects such as angle-of-arrival fluctuations or beam wander (Lawrence & Strohbehn 1970, Chiba 1971, Dowling & Livingston 1973, Churnside & Lataitis 1987, Churnside 1989, Churnside & Lataitis 1990). This presupposes, however, that the beam diameter w should not be markedly altered by diffraction, or by scattering due to atmospheric turbulence. The first condition is fulfilled if the measurement distance is within the Fresnel diffraction range ($w>\sqrt{L\lambda}$) and the second condition if the path-integrated turbulence is weak ($\rho_0>\sqrt{L\lambda}$) (Churnside & Lataitis 1989).

The above conditions are not too restrictive when considering practical reflected beam sensors and the measurement conditions prevailing in shooting practice, for example, and thus equations developed for weak turbulence conditions in general should provide valid results when evaluating the effect of atmospheric turbulence on displacement sensing precision.

The various mechanisms by which the measurement precision of a reflected beam sensor is affected include angular fluctuations in the wave front, illumination fluctuations at a misfocused receiver aperture and illumination fluctuations within CCR arrays. Simple equations are presented below for estimating the magnitude of the above effects. The derivations were performed by combining the results of several publications. The experimental results concerning the effect of beam angular and illumination fluctuations on measurement precision in the case of a retroreflected beam are believed to be new. The results are reported in Papers VIII and IX.

4.2.6.1. Angle-of-arrival fluctuations

The angle of arrival is the average tilt of a wave front across the receiver aperture, and is thus the same as the angle (direction) of the received beam. A general form for the equation required to estimate the variance in angle-of-arrival fluctuations is

$$\sigma_\alpha^2 = \varphi C_n^2 \phi^{-\frac{1}{3}} L\,, \tag{13}$$

where φ is a constant, ϕ the aperture diameter and L the distance that the beam travels in a turbulent atmosphere before reaching the aperture.

Churnside (1989) has derived a set of complicated equations for angle-of-arrival fluctuations covering various illumination conditions and beam sizes of retroreflected light using a geometric optics approach, and concluded, like Aksenov *et al.* (1984), that when a CCR is illuminated with a diverging beam, the angle-of-arrival fluctuations in the reflected beam near the receiver are smaller than those in the illuminating beam near the CCR. This is attributed to the fact that wave front tilts induced on the way out to the CCR are partly removed on the way back due to phase-front inversion of the CCR.

According to numerical calculations, the long equations derived in Churnside (1989) can be simplified when the illumination is highly divergent (> 10 mrad). The equation describing the angle-of-arrival fluctuations at the CCR aperture reduces to the well-known spherical wave result in which φ is equal to ~1.1 (single-axis variance), and the ratio of the received beam angle-of-arrival variance to that present at the CCR reaches a constant value of about 0.57. Using these approximations, the variance in the angle-of-arrival fluctuations can be approximated with Eq. (13), in which φ is now 0.79.

The apparent variance in lateral displacement of the reflector at the target distance is equal to the angle-of-arrival variance multiplied by the square of the reflector distance, since the spot displacement at the detector is directly proportional to the average wave front tilt at the receiver aperture (Yura & Tavis 1985). The corresponding standard deviation of lateral displacement at the target is therefore

$$\sigma_{AOA} \approx 0.89 C_n L^{3/2} \phi^{-1/6} . \tag{14}$$

4.2.6.2. Effect of illumination fluctuations

Illumination fluctuations caused by atmospheric turbulence affect precision if the receiver is misfocused or if multiple reflectors are used. Atmospheric turbulence causes the received illumination to fluctuate across the receiver aperture. These fluctuations cause no problems in a focused case, because each elemental area of the receiver images the light collected by it onto the entire image spot. In this situation the illumination fluctuations related to the elemental area change the illumination of the image spot uniformly leaving its centroid unaltered. In a misfocused receiver, however, the illumination fluctuations across the receiver aperture are directly projected on the light spot on the PSD surface. These spatially uncorrelated fluctuations then cause variation in the light spot centroid and affect measurement precision. In the case of a misfocused QD receiver the standard deviation of the measured reflector position due to illumination fluctuations is

$$\sigma_{IFrec} \approx \frac{\pi \phi \delta}{16} \frac{L}{f} \frac{\sqrt{1-c}}{SFR} , \tag{15}$$

where δ is the relative misfocus (detector axial displacement from the image plane divided by the distance of the image plane from the receiver lens), c the correlation coefficient of the illumination fluctuations between crosswise quadrants of the circular receiver aperture, and SFR the signal-to-fluctuation ratio related to one quadrant of the receiver aperture defined as the average signal power divided by the rms value of its fluctuations (Andreev & Magind 1972).

In the case of narrow band laser illumination the spatial correlation depends on the effective distance of the crosswise receiver aperture quadrants in relation to the Fresnel zone size (√Lλ), and the SFR on the path-integrated turbulence strength and the averaging provided by the receiver aperture quadrant (Paper VIII). It can be concluded

from Lawrence & Strohbehn (1970), Fante (1975), Coles & Frelich 1982 and Churnside & Wilson (1993) that if the receiver is illuminated directly by a point source and two receiver points have a lateral separation larger than about $0.6\sqrt{L\lambda}$, c is essentially zero. This means that the illumination fluctuations of crosswise receiver quadrants should be uncorrelated when practical aperture sizes of a few cm and measurement distances up to a couple of hundred metres are used. In the case of retroreflected light, however, a slight positive or negative correlation ($-0.4 < c < 0.4$) may exist even beyond lateral distances of $\sqrt{L\lambda}$ (Banakh & Tikhomirova 1984). In the following illumination fluctuations of crosswise receiver quadrants are assumed to be uncorrelated ($c \sim 0$).

In the case of narrow band illumination, the SFR can be deduced in the following way. In weak turbulence the normalised illumination variance for a point receiver illuminated by a diverging beam is $\sigma_{Ipr}^2 = 0.496k^{7/6}L^{11/6}C_n^2$ (Weichel 1990). According to Churnside & Lataitis (1989) and Churnside & Wilson (1993) the corresponding variance with a retroreflected beam is σ_{Ipr}^2 if L is replaced with 2L. This magnitude of fluctuations is then reduced by aperture averaging $A=\sigma_{Ier}^2/\sigma_{Ipr}^2$, where σ_{Ier}^2 is the variance for the extended (averaging) receiver aperture. The extent of aperture averaging can be approximated using $A=[1+0.362\gamma^{7/3}]^{-1}$, where γ is the averaging aperture diameter divided by $\sqrt{L\lambda}$ (Churnside 1991). Now the SFR in Eq. (15) is simply $1/\sigma_{Ier}$.

When more than one CCR is used, the spatially uncorrelated fluctuation in illumination across the CCR array reduces the precision. This is because QD and LEP are capable of detecting only one centre of gravity and when multiple CCRs are used, the PSD detects their common centroid, the position of which is directly affected by the uncorrelated illumination variations of the separate image spots of the CCRs. If two reflectors are positioned equidistant from the centre of the measurement field, the standard deviation due to their mutual illumination fluctuations at the target is simply

$$\sigma_{IFref} \approx \frac{\Delta}{\sqrt{8}} \frac{\sqrt{1-c}}{SFR}, \tag{16}$$

where Δ is the distance separating the reflectors at the target, c the correlation coefficient of the illumination variation between the two reflectors and SFR the signal-to-fluctuation ratio related to one CCR (Paper IX). The values of SFR and c can be evaluated in a similar manner to that presented above. The averaging aperture diameter equals that of the receiver, and *c* becomes zero for all practical CCR separations.

4.2.7. Turbulence-limited precision of QD and LEP-based sensors

Angle-of-arrival fluctuations in the received wave front affect both sensor constructions equally, but the QD-based sensor suffers from additional precision deterioration due to receiver misfocusing. Also, precision degradation related to the multiple CCR target concerns both sensors, but multiple CCRs might be needed more often with the LEP-based sensor in order to compensate for its higher noise.

The contributions of the angle-of-arrival (σ_{AOA}) and illumination fluctuations (σ_{IFrec}, σ_{IFref}) to displacement sensing precision in the shooting practice application are estimated below assuming intermediate turbulence conditions and narrow band illumination. This means that $\sqrt{L\lambda}$ is roughly equal to ρ_0 (~ 1 cm), and that C_n is correspondingly about $5x10^{-7}$ $m^{-1/3}$. The total size of the measurement field is assumed to be 1.5 m (~ 150 m* 10 mrad) and the diameter of the coaxial transceiver aperture 50 mm.

According to Eq. (14), angle-of-arrival fluctuations should cause a standard deviation of about 1.3 mm when the reflector is positioned at a distance of 150 m. This is larger than that typically caused by electrical noise, and thus the precision of the QD and LEP-based sensors should in both cases be turbulence-limited. According to Eq. (15), the additional measurement uncertainty caused by illumination fluctuations in the case of a misfocused QD receiver may vary within a large range, depending on the correlation between the crosswise quadrants. Assuming that the signal fluctuations are uncorrelated, the standard deviation of the measured results should be about 10 cm. The minimum value for the contribution of illumination fluctuations at the target is obtained assuming that two CCRs have the smallest possible centre point separation (~25 mm). This should result in an additional measurement uncertainty of 2 mm.

According to the above, a focused LEP receiver should provide a precision of a few millimetres in intermediate atmospheric turbulence when the CCR distance is 150 m, while misfocused QD receiver seems to provide a precision of about ten centimetres.

4.2.8. Experimental results

A summary is presented of the experimental results reported in Papers VIII and IX. The experiments were performed mainly under what could be described as ‘typical worst-case operating conditions’ for optical shooting practice. This means daytime between sunrise and sunset with half-cloudy to sunny weather, moderate wind and a temperature above +20 °C. The beam path was set at a height of 1 to 1.5 m above a partly grassy and partly sand-covered pathway in the middle of a flat area. A direct beam sensor was used to estimate the strength of turbulence in the above conditions (Fig. 3 in Paper IX). An estimate for the refractive index structure coefficient C_n was calculated from the beam wander measured with the direct beam sensor using well-known and experimentally verified equations (Chiba 1971, Dowling & Livigston 1973, Churnside & Lataitis 1990). According to the measurements, the conditions described above correspond to that of intermediate path-integrated turbulence within the distance range 50 to 300 m.

4.2.8.1. Turbulence-limited precision of a QD-based sensor

The experimental results showed that the turbulence sensitivity of a QD receiver is not inherent to the detector but caused by misfocusing. This was verified by misfocusing a LEP receiver. The precision of a misfocused QD receiver was also found to scale linearly with the spot diameter (measurement field) as expected (Fig. 2 in Paper VIII, Fig. 6 in Paper IX). The relative standard deviations of a misfocused QD in strong and intermediate atmospheric turbulence were 5 to 7% and about 2% of the measurement field, respectively (Table I in Paper VIII, Fig. 5 in Paper IX), which correspond to about 10 cm and 3 cm at 150 m (D=1.5 m). The measured results have the same order of magnitude as those calculated using Eq. (15).

4.2.8.2. Turbulence-limited precision of a LEP-based sensor

Experiments with the LEP-based sensor confirmed that approximately one millimetre precision is achievable electrically using typical sensor parameters, that atmospheric turbulence restricts sensor precision under typical environmental conditions, and that the precision of a focused LEP receiver is roughly an order of magnitude better than that of the misfocused QD receiver (Table I and II in Paper VIII, Fig. 4 and 5 in Paper IX). In intermediate atmospheric turbulence a precision of 3 mm was achieved with the LEP receiver using a 150 m reflector distance and better than 1 cm up to 300 m (Fig. 3 in Paper VIII, Fig. 4 in Paper IX). No significant systematic differences were found between various CCR types, as expected. When an array of seven CCRs were positioned in contact with each other, the average precision was about the same as with a single CCR target (Fig. 8 in Paper IX), but separating them reduced the precision linearly in proportion to their lateral separation, as predicted (Fig. 9 in Paper IX). The experiments also showed that the performance of the optics cannot be neglected. The increase in minimum blur-spot size from the 30 μm of a multiple lens system to the 300 μm typical of a single planoconvex lens reduced the precision by a factor of 1.5 at a range of 300 m. This was presumably caused by intensity fluctuations as in the case of misfocusing.

The measured and calculated standard deviations in the case of one CCR and an accurately focused LEP receiver within a distance range from 50 to 300 m are depicted in Fig. 23. The results obtained with a direct beam sensor are also included for a reference. The experimental results for the reflected beam sensor are approximately twice as inaccurate as those predicted by Eq. (14), and also 1.4 to 2.1 times worse than those for the direct beam sensor, although the calculations suggested that they should have been slightly better (~20%).

Only a small part of the difference between the measured and calculated values was estimated to be due to the non-idealities of the measurement setup. A possible explanation for the difference could be that the geometric optics formulation, which is based on the assumption of weak turbulence, gives results that are too optimistic under the intermediate turbulence regime representing the upper boundary of the validity range. Another possible reason is that discussed by Churnside & Lataitis (1987) themselves, that beam wander off the receiver aperture occasionally reduces the effective aperture

size and thus may well affect the angle-of-arrival variance observed at the receiver. Comparison with other experimental results was not possible, since none seem to have been published before.

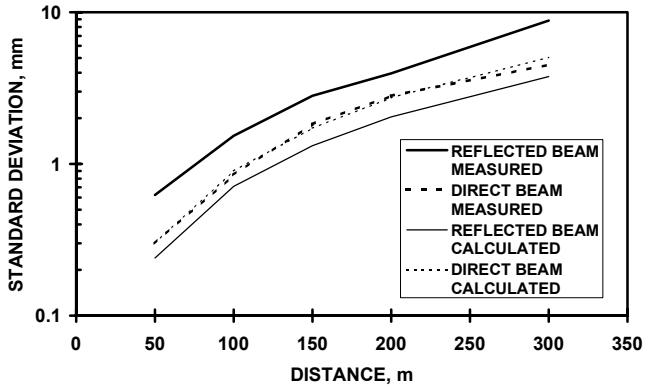

Fig. 23. Calculated and measured standard deviations in the lateral displacement results obtained with a direct beam sensor and a focused reflected beam sensor in intermediate atmospheric turbulence.

4.2.9. Improving turbulence-limited precision

According to Eq. (14), little can be done to improve turbulence-limited precision by adjusting the receiver parameters. The receiver diameter has a weak effect on angle-of-arrival fluctuations, but since the aperture size is typically already maximised in order to optimise the receiver SNR, practically no improvement is achievable. The effectiveness of averaging successive measurement results or multiple reflectors will be discussed below. The latter idea of using multiple, spatially separated beam paths for precision improvement is believed to be new.

4.2.9.1. Averaging successive measurement results

Assuming that atmospheric turbulence is stationary and homogeneous and that the angle-of-arrival fluctuations are normally distributed, the averaging of successive measurement results should reduce the standard deviation of the average proportionally to $1/\sqrt{n}$, where n is the number of results averaged. If individual measurement results are correlated, the efficiency of averaging drops and precision improves more slowly (Aumala *et al.* 1995).

In the case of turbulence-limited precision, uncorrelated results are obtained if the time interval between the measurements is long enough that a totally new set of inhomogeneities deflect the beam in each measurement. In principle, this means that the time between the measurements should be larger than L_0/V, where L_0 is the size of the

largest turbulent cell and V the mean cross-wind speed (Fig. 22). For a beam height of one metre L_0 should be approximately 30 cm, which results in a measurement interval >0.1 s if V is assumed to be 3 m/s. A similar conclusion can be reached by considering the frequency content of the angle-of-arrival fluctuations. According to Fante (1975), the spectrum of angle-of-arrival fluctuations reaches its maximum at the frequency $0.1V/2\pi\phi$, where ϕ is the diameter of the receiver aperture. The magnitude of the fluctuation drops to one tenth of its maximum at frequencies ~$0.02V/2\pi\phi$ and ~$3V/2\pi\phi$, respectively. Assuming an aperture diameter of 50 mm and a wind speed of about 3 m/s results in frequency band ranging from ~0.2 Hz to ~30 Hz, the maximum being at 1 Hz. Since the measurement rate needed for averaging in shooting practice is at least two orders of magnitude higher than the dominant frequency of the angle-of-arrival fluctuations, successive results tend to be correlated and averaging provides little improvement in precision. The experimental results presented in Fig. 24 (V~3 m/s, L=50 m and ϕ=50 mm) support the above and indicate that no rate higher than one measurement per second should be used in order to be able to average efficiently.

A method based on spatial averaging which can be used to improve precision when the necessary measurement rate is too high for efficient temporal averaging is proposed below.

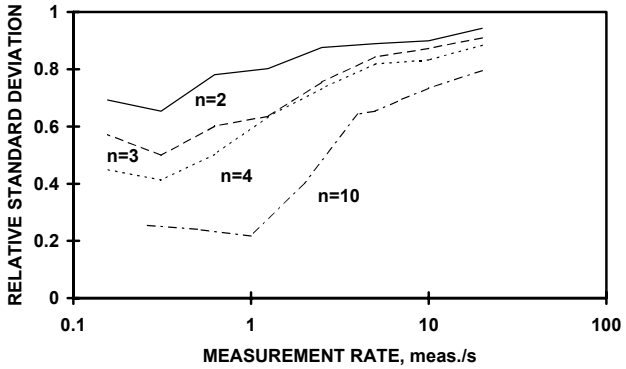

Fig. 24. Averaging efficiency as a function of measurement rate and the number of samples averaged.

4.2.9.2. Averaging using multiple reflectors

The idea of spatial averaging is to obtain uncorrelated results using multiple, spatially separated beam paths. An efficient improvement in precision should be obtained if the separation of the beams for most of their path length is larger than the size of the inhomogeneities responsible for the angle-of-arrival fluctuations. The averaging efficiency in this case should not depend on the measurement rate or wind speed as is the case when successive results are averaged but only on the spatial separation of the reflectors. In practice, averaging could be accomplished by attaching multiple reflectors

to the target, detecting their positions individually and calculating the average of these reflector positions (Fig 25).

Experimental results show that reasonable averaging efficiency is obtainable with tolerable reflector separations and using a relatively high measurement rate. The results in Table 3 (Table 1 in Paper IX), which were obtained using a rate of 20 measurements/s, show that as the lateral separation between two CCRs at 150 m is increased from 10 to 128 cm, the angle-of-arrival correlation decreases from +0.83 to +0.33 so that averaging provides an improvement in precision by a factor of 1.04 to 1.22 as compared with the use of a single CCR. Note that the angular fluctuations can never be totally uncorrelated, since the beams have a common starting point and end point at the transceiver.

It seems that an improvement in precision by a factor of two should be possible without increasing the number of reflectors (n ~ 5 to 10) or the illuminated FOV beyond reasonable limits. This presupposes, however, that the PSD is capable of detecting each CCR position individually instead of detecting their common centroid. Otherwise mutual illumination fluctuations in the CCRs will increase the target position variance more effectively than angle-of-arrival averaging can reduce it (Fig. 9 in Paper IX). One possible construction for such a PSD is presented in section 5.6.

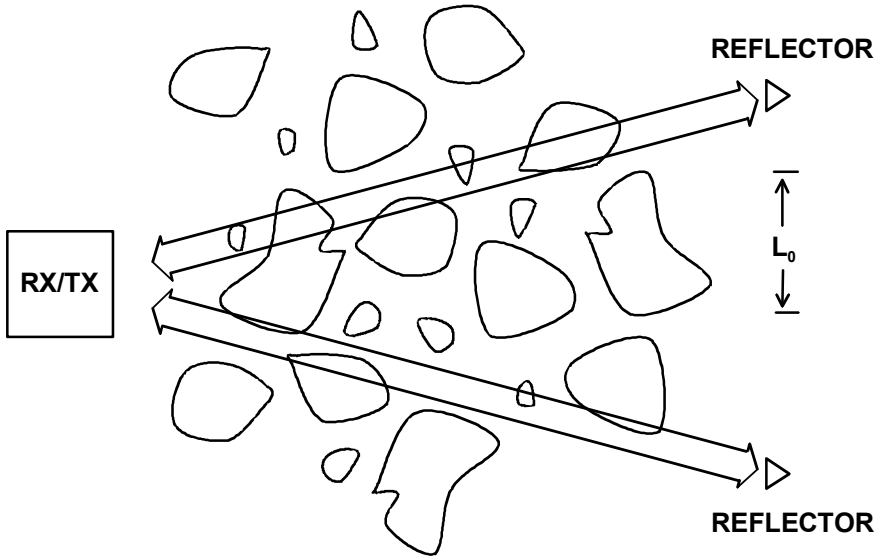

Fig. 25. The principle of spatial averaging using multiple, laterally separated reflectors.

Table 3. Precision improvement achieved by using two CCRs, detecting their displacement individually and then averaging the results. The improvement factor indicates the improvement in standard deviation relative to that of a single CCR measurement. The correlation coefficient between the two CCR displacements is also presented.

CCR separation, cm	Correlation of displacements	Improvement factor
10	+0.83	1.04
16	+0.71	1.08
32	+0.60	1.12
64	+0.49	1.16
128	+0.33	1.22

4.2.10. Sensor construction for the best precision

The optimal construction for a reflected beam sensor intended for long-range displacement detection as in outdoor shooting practice, can be deduced from the above results. CCRs should be used as reflectors in order to achieve good contrast and an adequate signal level, especially in applications requiring a long target distance or wide measurement field. A focused receiver should be used since it shows markedly lower sensitivity to atmospheric fluctuations than a misfocused one. A focused LEP receiver, for example, achieved better than 1 cm precision up to distance of 300 m in intermediate turbulence, while the precision of a QD receiver was typically an order of magnitude worse, due to the misfocusing inherently needed in its operation. Since the effect of misfocusing is substantial, the receiver should be carefully focused. The amount of misfocus caused by typical focal length tolerances (2%), for example, may increase the standard deviation of the measured results tenfold relative to an accurately focused situation. Consequently, the quality of the optics has an impact on the achievable precision, suggesting that a diffraction-limited receiver lens should preferably be used. If an array of CCRs is used to increase receiver SNR, they should have the smallest possible diameter providing efficient power coupling, and be placed in contact with each other in order to avoid precision degradation due to illumination fluctuations across the array. The reflector size can in turn be effectively minimised by using coaxial transceiver optics, in which case a CCR diameter corresponding to half of that of the receiver aperture is basically sufficient for efficient optical throughput. If precision improvement is needed in a turbulence-limited case, averaging can be used, and if the measurement rate is very slow (<< 1Hz), successive results can be averaged. When a faster rate is needed spatial averaging using multiple reflectors might provide better results, but in such a case the CCRs should have the largest possible lateral separation and a PSD should be used that is capable of individually detecting the positions of the CCR image spots.

5. Custom-designed position-sensitive devices

The last part of this thesis deals with position-sensitive devices designed to improve the performance of the reflected beam sensors used in long-range displacement sensing applications such as optical shooting practice. The most important aim was to implement PSDs with higher incremental sensitivity than LEPs, so that the illumination power (power consumption) or the receiver aperture size (sensor size) could be reduced, or the measurement field of the sensor increased without losing precision. Since the final aim also includes reduction of the size and power consumption of the receiver electronics by placing the front end circuitry on the same chip as the PSD, standard low-power IC technology was used for the PSD implementations. The work was originally inspired by the experiment of Kramer *et al.* (1992) in which they verified that a LEP manufactured with a standard industrial CMOS process can achieve comparable linearity to a LEP manufactured using dedicated technology.

A total of eight PSD constructions were implemented using 1.2 μm and 0.8 μm CMOS technology. The advantages of CMOS were its availability, low cost compared with other IC technologies and the fact that it provides a good means for implementing low-power front end circuitry. The first group of proposed PSDs utilise the current division principle, like LEPs and QDs, but are composed of a dense array of discrete photodetectors instead of a continuous structure. The second group consists of two digital PSDs composed of an area array of active pixels whose outputs assume binary values according to the illumination level falling on them. The idea of using an array of digital pixels for position sensing emanated from the work of Bose & Amir (1990) and Sklair *et al.* (1991), who verified that the centroid position of the binary image of a circular feature can be detected with an accuracy as high as 1/10 of a pixel simply by extending the image over five pixel widths.

All the PSDs tested were the first of their kind, and since they were designed without extensive optimisation, the performance reported here by no means represents the best achievable. Despite this, the array-based PSD prototypes showed much better sensitivity and linearity than a conventional LEP. The best performance was provided by an array PSD employing QD-type operation. It offered a 40-fold improvement in sensitivity and two-fold improvement in linearity. The digital PSD provided 10-fold improvement in sensitivity, a fully digital output, inherently better reflector background contrast and a possibility to measure multiple reflector positions simultaneously. The latter allows the

precision to be improved in the turbulence-limited case using averaging based on multiple spatially separated reflectors, for example. Unlike the other proposed PSDs and CMOS photodetectors in general, the performance of the QD-type array and the digital PSDs is also expected to improve as the minimum feature size of CMOS technology scales down.

After introducing related work on PSDs, the evolution and practical restrictions of the performance of a 2-axis LEP are described. The operating principles of the proposed PSDs are then explained and the sensitivity improvement they offer over conventional LEPs is estimated. After this the suitability of standard CMOS technology for implementing PSDs is discussed, followed by a description of the implemented PSDs and their performance. Finally the prototypes are compared in terms of performance and their suitability for long-range displacement sensing is discussed. Full descriptions of the PSDs and test results can be found in Papers X, XI, XII, XIII, XIV and XV.

5.1. Earlier work on PSDs manufactured using IC technologies

A few experiments have been reported on manufacturing LEPs by standard IC technologies. Noorlag & Middelhoek (1979) used standard planar silicon technology to implement their duolateral LEP, and Kramer *et al.* (1992) and Chowdhury *et al.* (1998) used standard CMOS technology. Muro & French (1990) and Smith & Huijsing (1991) implemented a single-axis LEP with appropriate signal processing circuits using bipolar IC technology, and Meijer *et al.* (1992) implemented a similar system using BiCMOS technology.

Several photodetector array based sensors have also been implemented using CMOS and BiCMOS technologies, but the main interest has been in the development of circuit architectures for light spot centroid computation, without paying attention to the performance of the photodetector array itself. DeWeerth & Mead (1988), Gonnason *et al.* (1990) and DeWeerth (1992) used an area array of vertical phototransistors, polysilicon resistors and tranconductance amplifiers in their centroid-computing CMOS chips, while Standley (1991) implemented a chip with an embedded photodetector area array which was capable of computing both position and orientation. Gruss *et al.* (1991) designed an analogue signal processor with an embedded 2D photodiode array for use in a light-stripe rangefinder. Based on the work of Bult & Geelen (1992), Tartagni & Perona (1993) proposed MOS transistors for current division in an array-type PSD and implemented the computational circuitry without photodetectors using general purpose CMOS. Venier *et al.* (1996) used the same idea and technology in their 2-axis position-sensitive array intended for solar illumination monitoring, while Umminger & Sodini (1995) realised an integrated sensor for automatic alignment using a segmented photodiode and BiCMOS technology. Work related to the proposed digital PSD has been reported by Langenbacher *et al.* (1993), who implemented a 32 x 32 array of thresholding phototransistor cells using standard CMOS.

5.2. Conventional 2-axis LEP

5.2.1. Evolution

Analogue position-sensitive photodetectors using the lateral photoelectric effect have been around in existence since the early 1960s. The first LEP, described by Walmark (1957), was a 2-axis device consisting of four point contact electrodes placed on a common resistive sheet (Fig. 26a). The device exhibited large non-linearity, which was later lessened by introducing extended strip-like contacts. This tetralateral LEP (Fig. 26b) was reasonably linear in its central region but still severely non-linear over most of the active area. Woltring (1975) showed theoretically that the reason for this was the interference that crosswise electrodes cause to each other. Owen & Awcock (1968) proposed a double-sided (duolateral) LEP structure in which one pair of electrodes and a resistive sheet were positioned on each side of the device (Fig. 26c). Woltring (1975) showed that the steady-state lateral response of the duolateral LEP is inherently linear. Besides much better linearity, the duolateral structure also provided an improvement in precision by a factor of two due to the fact that the photocurrent was now split into two parts rather than four as was the case with the tetralateral structure.

After this research interest turned to fabrication issues. Petersson & Lindholm (1978) and Noorlag (1982) analysed the effect of non-idealities on position sensing linearity, as in the case of an inhomogeneous resistive layer or finite electrode conductance, for example, and verified that it was possible to manufacture duolateral LEPs with an integral non-linearity of about 0.2%. Since the main disadvantage of the duolateral construction was the high fabrication costs due to double-sided wafer processing, alternative ways of manufacturing linear 2-axis LEPs were also studied. Based on the theorem of Gear (1969), Yamamoto *et al.* (1985) suggested a ‘pincushion’ electrode geometry to reduce the interference between the four electrodes in the basic tetralateral structure (Fig. 26d). Wang & Busch-Vishniac (1989) proposed a tetralateral structure called clover, and Morikawa & Kawamura (1992) proposed a tetralateral device which included MOSFET switches to make its lateral response linear by changing it momentarily to a single-axis device. All of these devices could be manufactured using single side processing and offered better linearity than the basic tetralateral LEP. They have not gained much popularity among manufacturers, however.

The duolateral structure is almost solely used in high-performance 2-axis LEPs nowadays. The manufacturing processes are carefully optimised to provide the LEP with the highest possible responsivity and linearity, and also with low capacitance. Silicon planar processes with a diffusion or ion implantation method employed for doping are mostly used (Lindholm 1999). A modified duolateral LEP with a floating backside layer suitable for single side wafer processing has also been developed (Lindholm & Edwards 1991).

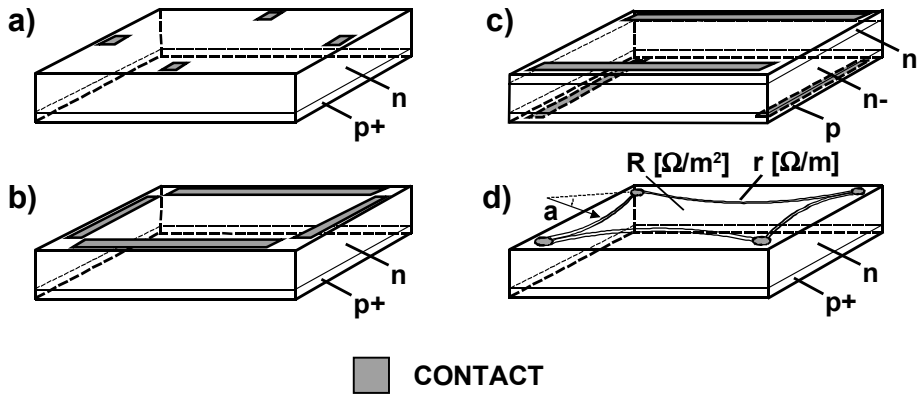

Fig. 26. Structures of 2-axis LEPs: a) Wallmark b) tetralateral c) duolateral and d) pincushion. In the case of the pincushion LEP, the radius of curvature of the active area boundary a should be equal to R/r, where R is the sheet resistance within the active area and r the boundary resistance.

5.2.2. Performance of a duolateral LEP

The duolateral LEP provides basically a highly accurate means of detecting the position of the light spot centroid. Its lateral position response is inherently linear, and due to the continuous structure, its accuracy is not affected by spot truncation or non-optimal spatial sampling, as may be the case with devices composed of discrete photodetectors (Woltring 1975, Noorlag & Middelhoek 1979, Petersson & Lindholm 1978, Alexander & Ng 1991). Due to non-idealities in the process technology, however, the resistance of the current dividing layer is not uniform, and thus perfectly linear LEPs cannot be manufactured. A state-of-the-art 2-axis LEP typically provides 0.3% integral non-linearity (Fig. 27), which is defined as the standard deviation of the error divided by the span used for measurement, which is typically 80% of the active area dimensions (SiTek Electro Optics 1996, Hamamatsu Photonics K.K. 1997, UDT Sensors Inc. 1998).

The low value for the current dividing resistance makes a LEP noisy. Its incremental sensitivity can be described by the noise equivalent power (NEP), which is defined here as the optical power providing *SNR*~1 simultaneously at each output terminal. The NEP of a 2-axis LEP is typically about 5 pW/√Hz (R_{ie}~10 kΩ, S~0.5 A/W) (SiTek Electro Optics 1996, Hamamatsu Photonics K.K. 1997, UDT Sensors Inc. 1998). This means that if a small spot size (~0.1 mm) is used to eliminate turbulence effects and the maximum allowable power density is 10 mW/cm^2, the best possible precision is about 1/300000/√Hz of the measurement span.

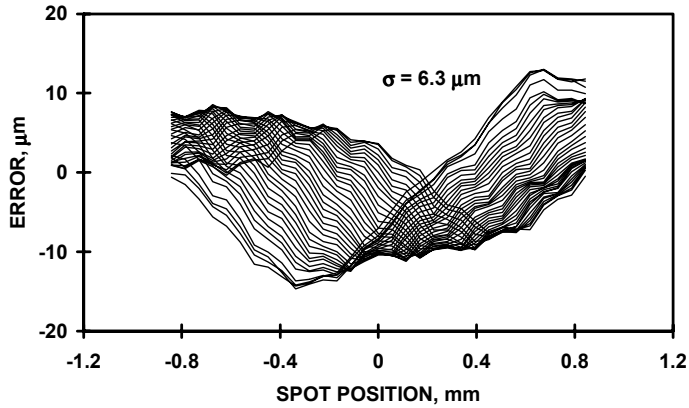

Fig. 27. Measured position-sensing error of a high-quality 2-axis LEP with 2 x 2 mm^2 area.

5.2.3. Precision optimisation and its practical restrictions

Since the main goal of the work was to design a PSD of high sensitivity, the factors restricting the sensitivity of the conventional 2-axis LEP structure are first described. The precision of a LEP is typically determined by the high thermal noise of the interelectrode resistance, and thus the highest possible value of the resistance should be used in order to maximise sensitivity. The fundamental upper bound for the interelectrode resistance is determined by the desired bandwidth, since linearity deterioration will take place if the received signal contains frequency components that exceed the bandwidth of the LEP. This occurs because the bandwidth of a PSD terminal depends on the spot position, due to the different resistance and capacitance seen by the photocurrent excitation between itself and the output terminals. According to Klein & Bierig (1974), the bandwidth of a LEP can be calculated from $\pi/2R_{ie}C_d$, in which R_{ie} is the interelectrode resistance and C_d the total capacitance of the LEP. Consequently, there exists an optimal value of R_{ie} for a given bandwidth which provides the best achievable precision without impairing the inherent linearity of the LEP. Assuming a pulse-modulated signal, the available precision in the case of optimal interelectrode resistance can be approximated using

$$\frac{\sigma_{\min}}{d} \approx \frac{B\sqrt{4kTC_d}}{P_r S}. \tag{17}$$

The fundamental limit for the achievable precision is set by the device responsivity S and capacitance C_d (Paper XV). The process technology used for LEP production provides such high responsivity (>0.5 A/W) and low capacitance (1 to 10 aF/µm^2) that it should in principle be possible to improve the sensitivity of LEPs 10 to 100-fold if R_{ie} were

optimised for the frequency band of a few kHz that is used in the shooting practice applications, for example. The problem is, however, that a relatively low value for the sheet resistance (10 kΩ/□) must be used in 2-axis devices to guarantee good resistance homogeneity and device linearity (Noorlag 1982, Lindholm & Edwards 1991, Lindholm 1999). All the main manufacturers use the same sheet resistance value and provide the same performance level in their 2-axis standard products (SiTek Electro Optics 1996, Hamamatsu Photonics K.K. 1997, UDT Sensors Inc. 1998). Attempts have been made to manufacture small batches of special 2-axis LEPs with a sheet resistance markedly higher than 10 kΩ/□, but they have not been successful, since the production of these using conventional (affordable) process technology is a highly elaborate business (Lindholm 1999)[2]. Consequently, it seems practically impossible to improve the sensitivity of 2-axis LEPs if good linearity is required simultaneously, and that if one wishes to do so totally new device structures must be used. PSDs based on photodetector arrays are proposed here.

5.2.4. Receiver power consumption

In addition to high noise, the low interelectrode resistance of a 2-axis LEP makes the power consumption of transimpedance front end circuitry relatively high. Operational amplifiers meeting the voltage noise specifications of a LEP preamplifier (5 nV/√Hz) have a current consumption of few mA at the lowest, while otherwise similar amplifiers having low enough noise specifications for an ordinary photodiode or QD front end (20 nV/√Hz) consume typically only one tenth of the above amount. The reason for this is that low voltage noise and low current consumption are contradictory requirements and thus difficult to combine (Lee 1999). The power consumption of the LEP front end may even dominate the total power consumption of a reflected beam sensor. Thus, besides better sensitivity, the new PSD structure should preferably make it possible to replace the conventional front end circuitry with a low power equivalent in order to be able truly to reduce the power consumption of the sensor.

5.3. Aims of the PSD experiments

The most important aim of the PSD experiments was to implement CMOS-compatible 2-axis PSDs with better incremental sensitivity than LEPs and equal or better linearity. Good sensitivity is needed when trying to realise reflected beam sensors with wide FOV, since the precision is heavily dependent on the diameter of the measurement field (~D^3

[2] When the manufacturers were asked to produce a customised LEP with the highest possible interelectrode resistance, SiTek Electro Optics replied that no higher than 30 kΩ could be provided, UDT Sensors offered 50 kΩ resistance but could not reach this specification, and Hamamatsu indicated that they supply a LEP S4744 as a standard product which has an interelectrode resistance of 180 kΩ but about five times worse linearity than best 2-axis LEPs.

in the case of a CCR). Enhanced sensitivity could obviously also be utilised to reduce power consumption and the size of the sensor by cutting down the illumination power and the size of the receiver aperture. To achieve the best possible precision in a turbulent environment, it was also important that the desired performance should be achievable with a small spot size (<0.1 mm). PSDs based on photodetector arrays were experimented with as means of achieving these goals. The operating principles of the proposed PSDs are explained below and the sensitivity improvement they offer relative to LEPs is estimated.

5.4. Array PSDs employing LEP-type current division

5.4.1. A photodiode array PSD

The main advantage of the array PSD composed of separate photodiodes and current dividing resistors as depicted in Fig. 28 is that relatively low sheet resistance values can be used to obtain high interelectrode resistance for the PSD. This is due to the possibility of using a much lower aspect ratio (width/length) for the current dividing resistors than in the case of a conventional 2-axis LEP. Therefore, assuming that a constraint exists between resistor homogeneity and the sheet resistance value, as concluded in section 5.2.3, the photodiode array PSD should provide lower noise than a LEP (higher interelectrode resistance) with equal non-linearity. Note that since the constraint between resistor homogeneity and the sheet resistance value is determined by the type of resistor used and the quality of the manufacturing technology, there is no guarantee that an array PSD implemented in a standard CMOS process, for example, would provide any better combination of noise and linearity than LEPs manufactured in dedicated processes.

The idea of using an array of photodiodes together with resistive current division for position sensing is not new, having been used earlier by Tartagni & Perona (1993) and Venier *et al.* (1996), for example. Their work did not consider the sensitivity issues, however, which were the main focus of this study.

5.4.2. A phototransistor PSD

A phototransistor array PSD is basically similar to a photodiode array, but phototransistors are used instead of photodiodes to improve sensitivity by amplifying the signal before noisy current division. In such a case the precision for a single-axis device is roughly

$$\frac{\sigma_{PTPSD}}{d} \approx \frac{\sqrt{4kTB/R + q(P_r + P_b)S\beta^2 B}}{P_r S\beta}, \tag{18}$$

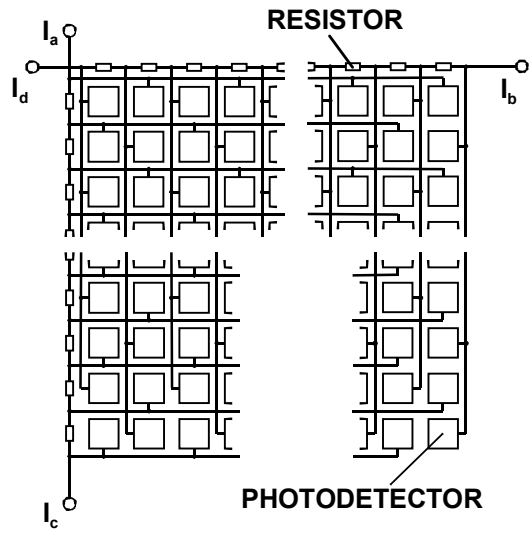

Fig. 28. Construction of an array PSD employing LEP-type current division. Various types of resistors and photodetectors may be used.

where β is the current gain of the phototransistors and P_b the background illumination power (Paper XI, De La Modena *et al.* 1971). Comparing Eqs. (5) and (18), it can be concluded that if the background illumination is low, the incremental sensitivity of a phototransistor PSD should be β times higher than that of a LEP. The main disadvantage of phototransistors is that without bias their bandwidth tends to be fairly low and if bias is used to increase the bandwidth, the noise level increases due to the bias current, reducing the incremental sensitivity fairly rapidly.

Phototransistor arrays have been used in several centroid computing circuits but the proposed idea of increasing the sensitivity of a PSD by using phototransistors and LEP-type current division has not been reported before (DeWeerth & Mead 1988, Gonnason *et al.* 1990, Standley 1991, DeWeerth 1992, Langenbacher *et al.* 1993).

5.4.3. Effect of a discrete photodetector array on accuracy

The use of discrete photodetectors causes additional centroiding error, which obviously does not exist in the case of a LEP owing to its continuous structure. This spatial digitising error becomes meaningful when the spot size approaches that of a single photodetector, and thus it was particularly important to take it to account in the present case, where the smallest possible spot size should be used in order to minimise the deterioration in precision due to atmospheric turbulence.

An optimal compromise between the digitising error and turbulence sensitivity is achieved by using the smallest spot diameter that allows subpixel centroiding accuracy. According to Cox (1986, 1989), the optimum spot diameter for the most common spot profiles is about two pixel widths. The digitising error in such a case for an array having a fill factor (photodetector area divided by the total area) of 70% typically varies from 1/20 to 1/10 of the pixel width, depending on whether the illumination profile of the light spot is closer to a uniform or a diffraction one (Cox 1986, Cox 1989). For the proposed array PSDs, in which only every second pixel takes part in centroid computation, the rms error is about 1/8 of a pixel width at best. The construction of photodetector arrays with a reasonable fill factor (>0.5) using one-micron CMOS technology results in a photodetector size of 20 to 30 μm, which means that the error due to the discrete photodetector structure becomes comparable to the non-linearity error of a LEP, and thus should be taken into account if linearity improvement with respect to LEPs is desired.

5.4.4. Lowering the digitising error by spatial filtering

Alexander & Ng (1991) have shown that the centroid of a spatially digitised light spot is free of systematic error if the highest spatial frequency component of that spot is less than the sampling frequency of the array. This means that the systematic error caused by digitisation can be lowered simply by lowpass filtering of the illumination profile of the light spot before digitisation. Optical filtering methods include misfocusing and the use of high f-number optics, in which the blur-spot size is increased by diffraction (Alexander & Ng 1991). In the present case neither of these methods is optimal, since a high f-number (>10) typically reduces the received optical power too much, while misfocusing detracts from the precision in a turbulent environment.

Electrical filtering methods do not have the above drawbacks. They are typically based on a simple resistive grid or a more sophisticated active network connected between the photodetectors. In the case of a resistive grid each node shares its input current with its neighbours according to the resistor values used in the grid, and forms an exponentially decaying spatial impulse response (Mead 1989). Active networks are used to provide more optimal responses, such as a Gaussian one (Kobayashi *et al.* 1991).

The filtering effect in the proposed array PSDs is based on crosstalk between photodetectors. This crosstalk is caused by the narrow depletion region width, which gives rise to carrier generation within the bulk material outside the depletion region and makes it possible for these bulk-generated carriers to diffuse laterally to neighbouring photodetectors. The spatial response of a filter based on this diffusion coupling effect is similar to that of a resistive grid. Its potential advantage is that arrays with a higher fill factor can be implemented, since no additional devices are needed for the filter implementation. Its disadvantage, however, is that the response is not readily controllable but more or less fixed by the process technology and illumination wavelength used. The experimental results concerning the effect of diffusion coupling on the spatial digitisation error are presented in section 5.7.3.

5.5. An array PSD employing QD-type current division

As concluded earlier, a QD provides much better electrical sensitivity than a LEP but cannot be used outdoors since its precision is severely hampered by atmospheric turbulence, due to receiver misfocusing. The main idea here was to utilise the high electrical sensitivity of a QD and combine it with the low turbulence sensitivity of a LEP. This was accomplished by dynamically partitioning the 2-dimensional PSD array into four quadrants according to the spot position on the array so that a focused spot could be used in QD operation. The idea evolved partly from the principles used in military tracking equipment (Sparrius 1981, Gerson *et al.* 1989) and partly from those proposed for intersatellite telecommunication links (Boytemy 1987, Perez *et al.* 1989), but the idea and its realisation as such are believed to be new.

The operation of this tracking PSD is similar to that of the QD with the exception that the gap tracks the light spot electrically within the active area of the PSD (Fig. 29). The gap is moved in discrete steps, and thus the high accuracy (<<μm) of the photodetector array geometry can be used to establish good integral linearity. High precision is based on 'subspot' interpolation performed using the inherently non-linear but highly sensitive QD principle. The tracking feature allows a small spot to be used, which lessens the sensitivity to atmospheric turbulence.

The scale factor of a LEP is determined by the extent of the active dimensions d (measurement span) of the device, whereas in the tracking PSD the scale factor of the interpolation function is determined by the size of the light spot d_s, which is only a small fraction of the active dimensions. This means that, besides having lower noise due to the lack of interelectrode resistance, the noise sensitivity of a tracking PSD is markedly lower than that of a LEP (factor d/d_s). Thus the precision of the tracking PSD relative to that of the LEP (σ_{LEP}), assuming equal responsivity and size of the active areas, is

$$\sigma_{TRPSD} \approx \frac{\pi}{4}\frac{d_s}{d}\frac{i_n}{i_{nLEP}}\sigma_{LEP}, \tag{19}$$

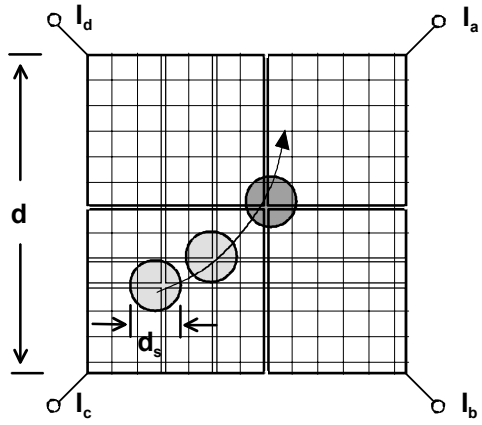

Fig. 29. Operating principle of the tracking PSD.

where i_n and i_{nLEP} are the noises of the tracking PSD and LEP receivers, respectively (Paper XII). Since d_s/d is typically <0.1 and i_n/i_{nLEP}~0.1 for a receiver suitable for shooting practice, for example (ϕ=50 mm, f=100 mm, θ=0.01 rad), the sensitivity of the tracking PSD should be at least two orders of magnitude better. Even when the sensitivity is limited due to background-induced noise, a situation which might be encountered in large FOV applications, the tracking PSD should still provide a roughly d/d_s-fold improvement in sensitivity ($\sigma_{TRPSD} \sim \sqrt{3\pi} d_s \sigma_{LEP}/4d$).

Another advantage of the tracking PSD over array PSDs employing LEP-type operation is that the improvement in sensitivity is mostly based on geometrical scaling rather than on the electrical characteristics of the devices. This means that an improvement in performance with respect to a LEP should be achievable despite possible shortcomings in photodetector responsivity or resistor homogeneity, for example, and that the performance should continuously improve as the feature size of the implementation technology decreases.

5.6. An array PSD composed of digital pixels

The operating principle and construction of a digital PSD resembles that of a conventional electronic camera, in which the outputs of all pixels are separately quantified and processed. The advantages of the camera-based approach in position sensing are lower sensitivity to background-induced noise, better tolerance of low reflector background contrast and the possibility of measuring the position of multiple reflectors simultaneously, all of which are consequences of the individual processing of pixel signals. The purpose here was to make the camera-based approach feasible for position sensing applications by lowering the relatively high signal processing load and current consumption characteristic of grey-scale camera sensors to a level which would be more appropriate for low-power, microcontroller-based sensors. To accomplish this, the proposed digital PSDs generate a low resolution binary image of the target reflector and contain simple preprocessing hardware to reduce the signal processing effort needed for image readout and centroid computation. The idea was simply to make use of the small feature size of CMOS technology and construct arrays with a small enough pixel size that centroid calculation from the binary image of the reflector would provide good enough positional accuracy and sensitivity for long-range displacement sensing applications.

5.6.1. Accuracy of binary detection

Bose & Amir (1990) and Sklair *et al.* (1991) verified that the centre of a binary image of a circular feature can be detected with subpixel accuracy by a simple centroiding method, and that centroiding accuracy is in direct proportion to the square-root of the spot diameter. The accuracy is restricted by the spatial digitisation error, rms value of which for a round, uniform light spot is roughly

$$\sigma_{DPSD} \approx 0.21\frac{p}{\sqrt{q}} = 0.21\frac{p^{3/2}}{\sqrt{d_s}}, \qquad (20)$$

where the spot diameter d_s equals qp and p is the pixel width (Paper XIII). The method is reasonably effective up to an accuracy of about 1/10 of a pixel, which is achieved by extending the spot diameter over approximately five pixel widths. When better accuracy is needed, the total number of triggered pixels, and accordingly the total signal energy, rises rapidly, reducing the sensitivity of the PSD.

5.6.2. Optimal pixel size

Achieving a small pixel size is important not only for optimising the digitisation accuracy and sensitivity but also due to the necessity for minimising the effect of atmospheric turbulence. Assuming that the spot diameter needed to obtain the desired digitisation accuracy is adjusted by misfocusing the receiver, and that the error contributions of intermediate atmospheric turbulence and digitisation are set to be equal, the pixel width should be approximately ten times larger than the rms value of a tolerable error. This means that in the shooting practice application, for example, the optimal pixel size would be about 70 μm (f~100 mm). A much smaller pixel would reduce the fill factor and sensitivity accordingly, and a larger pixel size would obviously increase the digitisation and turbulence-induced error beyond the desired level. Note that the optimum spot size becomes relatively large (~350 μm) and if atmospheric turbulence is strong, the desired accuracy is not achieved[3]. A digital PSD prototype fulfilling the above requirement (p=50 μm, K_F=30%) has been constructed as reported in Paper XIII.

5.6.3. Construction and operating principles of a digital pixel

A digital PSD is composed of an area array of active pixels, circuits for triggering and illumination control of the pixels, and standard readout circuits. Computational circuitry such as edge detectors may also be included to speed up image readout and centroid calculation.

The pixels include a photodiode and a simple comparator circuit for one-bit amplitude quantification (Fig. 30), and an adjustable threshold current is used to prevent triggering due to background illumination. A pixel is triggered when the signal current (+ background current) exceeds the threshold current and the voltage U_{in} across C_{pix} due to the discharging current $I_s+I_b-I_t$ goes below half of the operating voltage U_{dd}.

[3] The error contribution of intensity fluctuations in intermediate path-integrated turbulence is about 2% of the misfocused spot diameter. Angle-of-arrival fluctuations are disregarded.

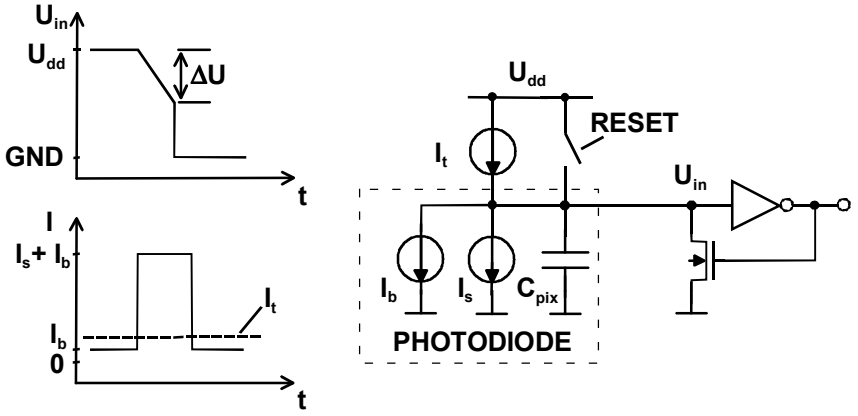

Fig. 30. Operating principle of the digital pixel.

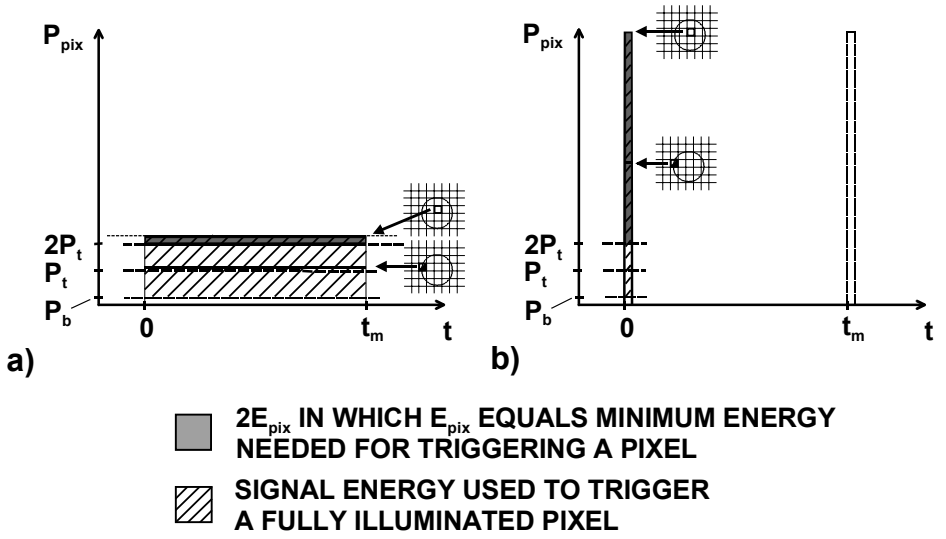

Fig. 31. Minimum signal power levels required to trigger fully and half-illuminated pixels as a function of time in a) continuous current mode and b) pulsed mode.

The digital PSD can be operated either in continuous current mode or in pulsed mode. In order to achieve the accuracy predicted by Eq. (20), a pixel should be triggered when half-illuminated with a uniform spot. The signal power (P_{pix}) falling on fully and half-illuminated pixels is depicted in Fig. 31 as a function of time in both operating modes. In the continuous mode the illumination is not modulated and P_{pix} is constant (Fig. 31a). Assuming an infinitely long measurement period t_m, the minimum power level impinging on a fully illuminated pixel becomes twice that of the threshold power P_t. The level of P_t is determined by the threshold current I_t, which again is set high

enough to prevent triggering due to background illumination. Taking into account the finite time between measurements, $2P_t$ is still increased by $2E_{pix}/t_m$, in which E_{pix} is the energy needed to discharge the input capacitance C_{pix} of a pixel. The power level used to trigger a fully illuminated pixel now becomes $2(P_t+E_{pix}/t_m)$.

In the pulsed mode the target is illuminated using short but powerful pulses repeated every t_m seconds. The average signal power needed for triggering is much smaller, since the signal is used almost solely to discharge the input capacitance of a pixel, as depicted in Fig. 31b. Consequently, the pulsed mode provides better sensitivity.

5.6.4. Sensitivity in pulsed mode

The minimum energy needed to achieve digitisation-limited accuracy in pulsed mode is deduced here. Assuming that the threshold level is negligible compared with the amplitude of the signal pulse, the sensitivity in pulsed mode is determined purely by the optical energy needed for discharging the input capacitance of a pixel, which is

$$E_{pix} \approx \frac{C_{pix}\Delta U}{SK_F}, \tag{21}$$

where C_{pix} is the total input capacitance of a pixel, comprising the photodiode and circuit input capacitances, ΔU the voltage change at the input needed to set the output, S the photodiode responsivity and K_F the fill factor. The fact that the minimum operating voltage for conventional CMOS digital circuits is twice the threshold voltage U_T of the MOS transistors makes ΔU roughly equal to U_T. For a pixel manufactured using 1.2 µm CMOS technology and measuring 50 µm by 50 µm U_T, K_F, C_{pix} and S are approximately 0.75 V, 30%, 100 fF and 0.4 A/W, respectively, and E_{pix} is correspondingly around 0.6 pJ. The total energy per measurement for a uniform spot can now be estimated by calculating the number of pixels occupied by the spot and assuming that energy used per pixel is $2E_{pix}$.

Spatial and temporal noise cause triggering uncertainty, which may increase the digitisation error beyond that predicted by Eq. (20). Partially illuminated edge pixels are the most susceptible to noise. Noise alters the triggering energy needed, causing uncertainty on triggering and consequently an additional centroiding error. According to the calculations and experiments presented in Paper XIII, the rms value of the variation in triggering energy E_{pix} can be as high as 30% without affecting the digitisation accuracy. Experiments show that the temporal noise remains well below this (Paper XIII and XIV). The contribution of spatial noise to the triggering uncertainty in pulsed mode can be readily estimated by determining the variation in U_T, K_F, C_{pix} and S. The use of typical parameter variations results in small enough variation in E_{pix} and thus an energy level of $2E_{pix}$ per pixel should result in the accuracy predicted by Eq. (20).

5.6.5. Sensitivity comparison with LEP

Sensitivity comparison with a LEP is not a straightforward matter, since the operating principles of PSDs are quite different. A digital PSD is best operated in pulsed mode, while LEPs are typically operated in continuous current mode. The sensitivity of a digital PSD is not dependent on the size of the active area as is the case with a LEP, but on the pixel and spot sizes, which means that the receiver parameters must be fixed before any comparison can be made. Due to the different relationships between the achievable precision and SNR, the desired precision must be fixed as well. The sensitivity of the digital PSD is estimated here using the parameters of a 50 µm pixel (E_{pix}~0.6 pJ) and sensor parameters typical of the shooting practice application (t_m=10 ms, θ=10 mrad, f=100 mm).

Assuming that the noise equivalent bandwidth of an LEP receiver is roughly $1/2t_m$ and that fully illuminated pixels receive $2E_{pix}$ energy, the relation in terms of the total energy needed for one measurement result is

$$\frac{E_{DPSD}}{E_{LEP}} \approx 0.0043 \frac{p^4 E_{pix}}{\sigma_{PSD}^3 d \sqrt{4kTt_m / R_{ie}}}, \tag{22}$$

where σ_{PSD} is the tolerated standard deviation in the position sensing results reduced to the PSD surface. According to Eq. (22), a digital PSD with 50 µm pixels should provide the accuracy needed in the shooting practice application (σ_{PSD}~7 µm) with 10 times less energy per sample than a LEP. Note also that according to Eq. (22), downscaling of the pixel size will enhance the relative sensitivity of a digital PSD fairly rapidly as the feature size of the implementation technology decreases.

5.7. Suitability of CMOS technology for PSD realisations

Standard CMOS technology was used here to implement the PSDs. CMOS is the dominant technology for VLSI implementations and thus well established, easily accessible and also of relatively low cost. In general, it also provides the best means for implementing signal processing circuits with low power consumption. The main disadvantage regarding PSD realisations is obviously that CMOS processes are not designed for photodetector production and that photodetectors are not characterised in any of the processes. The compatibility of CMOS technology for PSD implementations is discussed below.

5.7.1. Properties of CMOS photodetectors

The properties of industrial CMOS processes are dictated by the requirements of digital electronics, and thus CMOS is far from being ideal for implementing photodetectors. Many experiments show, however, that CMOS-compatible photodetectors, such as the well-substrate photodiode depicted in Fig. 32, are fully adequate for visible and near infrared optical sensing where a responsivity from 0.2 to 0.4 A/W is sufficient, where relatively large spatial and spectral non-uniformity in its responsivity can be tolerated (~ 5% standard deviation), and where low crosstalk and extremely high speed are not of importance (Figs. 2 and 3 in Paper X, Aubert *et al.* 1988, Sayles & Uyemura 1991, Soncini *et al.* 1991, Sandage & Connelly 1996, Palojärvi *et al.* 1997). Note also that the dark current of CMOS photodiodes, and hence their noise level, is comparable with those of ordinary photodiodes (Paper X, Aubert *et al.* 1988) and that phototransistors with responsivities better than 20 A/W can be implemented in standard CMOS (Paper X, Paper XI, Vidal *et al.* 1991, Sandage & Connelly 1996).

The variation in the spatial responsivity of CMOS photodetectors directly alters the 'electrical' centroid position of a light spot, and thus may potentially have detrimental effects on PSD linearity. Experimental studies have shown, however, that both CMOS LEPs and array-based PSDs offer a linearity that is comparable to that of high-quality LEPs (<0.5%) (Paper X, DeWeerth & Mead 1988, Kramer *et al.* 1992). The above implies that although CMOS photodetectors may not be as good as those manufactured with dedicated processes in terms of performance, there are no fundamental obstacles to achieving reasonable performance when realising PSDs using CMOS.

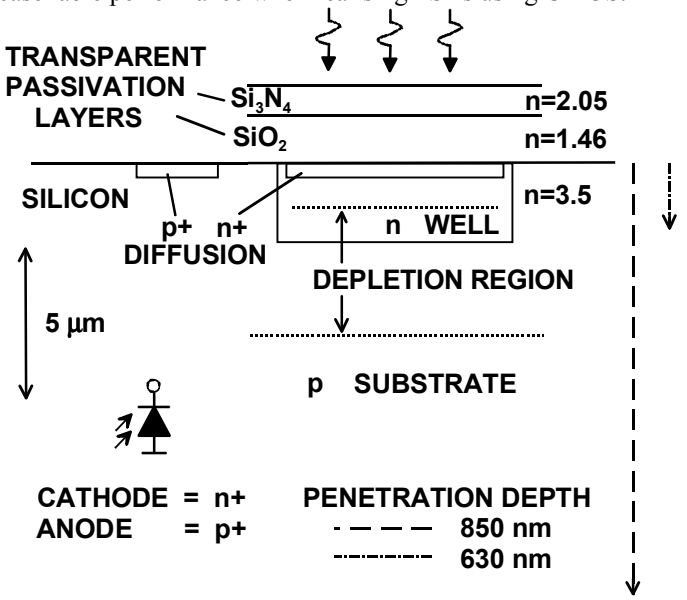

Fig. 32. Cross-section of a CMOS-compatible well-substrate photodiode in a 1.2 µm CMOS process. The shallow depletion region reduces responsivity at longer wavelengths and the temporal response is slowed down by the relatively high amount of diffusion current. Variations in spectral and spatial responses are caused by light interference within passivation layers.

5.7.2. 2-axis LEP realisations using CMOS

CMOS technology provides photodetectors and resistive layers which have a good enough responsivity and homogeneity for implementing linear single-axis LEPs (Paper X, Paper XIV, Kramer *et al.* 1992). The weak points of CMOS regarding 2-axis LEP devices, however, are related to the sensitivity and linearity that can be achieved. Problems in noise optimisation are caused by the large junction capacitance of the CMOS photodiodes (10 to 100 aF/μm^2) and the low sheet resistance (a few kΩ/□) available for current division as compared with the values of 1 to 10 aF/μm^2 and ~10 kΩ/□ used in dedicated processes (SiTek Electro Optics 1996, Hamamatsu Photonics K.K. 1997, UDT Sensors Inc. 1998). The former reduces the sensitivity achievable in high bandwidth applications (>100 kHz) and the latter when low bandwidths are used (<10 kHz). Linear structures, such as pincushion and duolateral, are difficult to implement in standard CMOS due to the lack of layers with a suitable sheet resistance. Two-axis LEPs could be readily implemented using a tetralateral structure but they would not provide satisfactory performance due to the inherent non-linearity of this structure. Thus it is difficult to achieve even comparable performance with conventional duolateral LEPs when using CMOS for 2-axis LEP realisations.

5.7.3. Effect of crosstalk on spatial digitisation error

Suitable photodetectors for PSD realisations in CMOS are those based on the well-substrate junction, for example, since they provide a good combination of responsivity and capacitance. They also provide a relatively high level of crosstalk due to the common substrate contact, which means good possibilities for lowering the spatial digitisation error based on the diffusion coupling effect, as explained in section 5.4.4. Crosstalk is caused by the shallow junction depth (1 to 3 μm) and narrow depletion region width (< 3 μm) of a well-substrate junction, which results in a large amount of carriers residing within the substrate below a depletion region. This is true especially when photodetectors are illuminated with near infrared wavelengths, in which case the penetration depth is larger than 10 μm (Sze 1981).

The experiments presented in Paper XIV demonstrate that there exists a fairly large amount of crosstalk between the well-substrate photodiodes in an area array of photodetectors with 25 μm spacing (Fig. 33). Only half of the photogenerated carriers contributed to the current in the illuminated photodiode when 850 nm illumination was used, while the other half was detected by the rest of the array. Comparison of simulations and experimental results shows that crosstalk reduces the digitisation error of a 50 μm spot in such an array from >1/8 of pixel width to about 1/36 (Paper XIV). This result suggests that a significant decrease in digitisation error is achievable due to crosstalk and that in this sense CMOS technology provides a clear advantage over dedicated photodetector array processes, which are typically optimised to provide low crosstalk for high spatial resolution. From the application point of view, the above means that the digitisation error is lowered to a negligible level (<1μm) in array PSDs utilising LEP-type current division.

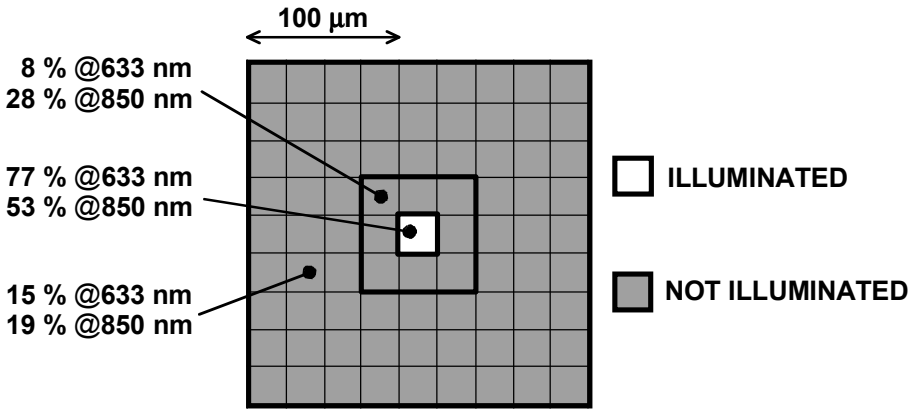

Fig. 33. Measured photocurrent distribution in a well-substrate photodiode array at two wavelengths when only one photodiode (25 x 25 µm^2) is illuminated.

5.8. PSD prototypes

Eight PSD prototypes were implemented using 1.2 µm and 0.8 µm CMOS technology. These included two single-axis and one 2-axis LEP, 2-axis photodiode and phototransistor arrays utilising LEP-type current division, a 2-axis PSD using QD-type operation and two digital PSDs. Summaries of their construction and performance are presented below.

5.8.1. Single-axis LEPs

Two single-axis LEPs with active areas of 1.0 x 0.15 mm^2 and 5.0 x 0.2 mm^2 were implemented first. The n-well p-substrate junction was used as the photodetector and the well as the current dividing layer. In the second device a pinched well was used to increase sheet resistance (2.5-fold) relative to a simple well (Fig. 34). The measured responsivities (~0.4 A/W at 850 nm) and interelectrode resistances (16.8 kΩ and 152 kΩ) corresponded to the values expected on the basis of typical process parameters. The NEPs of the devices were 5 pW/√Hz and 1.6 pW/√Hz, respectively, and the integral non-linearities 0.1% and 0.2%. The linearities achieved are comparable to those of conventional LEPs, but the NEPs are worse (Papers X and XIV).

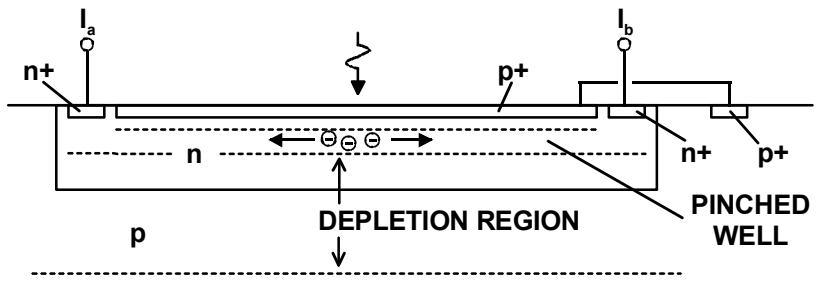

Fig. 34. Cross-section of a CMOS-compatible LEP using a pinched well for current division and a well-substrate junction for photodetection.

5.8.2. 2-axis LEP

The 2-axis LEP was implemented using a pinched well construction, which provides the best combination of responsivity and interelectrode resistance in CMOS. The inherent non-linearity of the tetralateral geometry was linearised by changing the 2-axis LEP effectively to a single-axis device using switchable electrodes. The 2-axis measurements could then be performed as two successive single-axis measurements. The idea was originally proposed by Morikawa & Kawamura (1992), who demonstrated it using dedicated MOS technology. The device presented here is a modified version of Morikawa's which is suitable for implementation in a standard CMOS process. The main difference is that it uses electrodes composed of multiple point contacts instead of continuous strip contacts. Each electrode is composed of a row of 100 minimum-sized contacts positioned 25 μm apart. Each of the contact spots is then connected to a common signal rail by a MOS switch. The single-axis operation is set up by alternately disconnecting one opposite pair of the electrodes using these switches (Fig. 35).

Besides improving linearity, the alternate operating principle and the usage of multiple contact electrodes also improved the sensitivity as compared with the conventional tetralateral structure. The interelectrode resistance seen by each preamplifier increases when the virtual ground of the transimpedance preamplifier inputs of the obsolete electrode pair is disconnected. This is due to the fact that the low-resistive path formed by this pair of electrodes breaks when switched off.

The measured non-linearity in the alternate mode (0.14%) was half of that of a conventional duolateral LEP. In the tetralateral mode the non-linearity (7.2%) corresponded to that of a conventional tetralateral LEP, as expected. An interelectrode resistance of 4.5 kΩ and a NEP of 10 pW/√Hz were achieved in the alternate mode, while the values in the tetralateral mode were 0.85 kΩ and 47 pW/√Hz. The NEP in the alternate mode is twice that of a conventional 2-axis LEP.

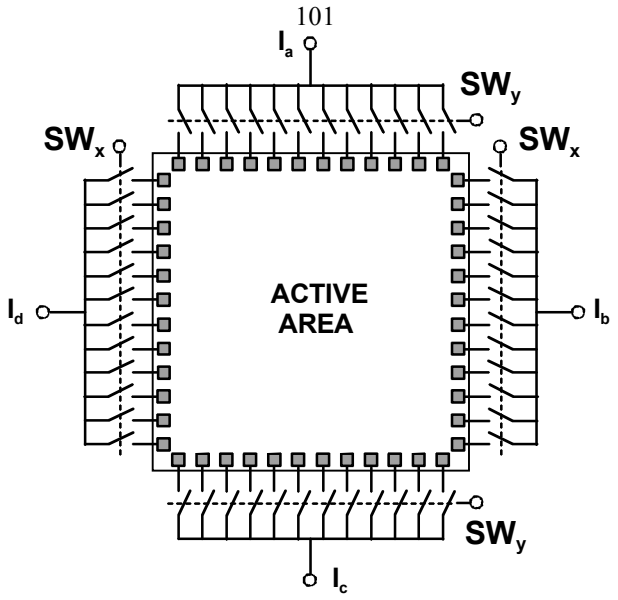

Fig. 35. Simplified outline of the 2-axis CMOS LEP. SW_x and SW_y are used to switch the opposite contact pairs on and off alternately.

5.8.3. Photodiode array PSD

The PSD comprises an area array of discrete well-substrate photodiodes and two linear arrays of MOS transistors residing outside the photosensing area. The practical advantage of MOS transistor current division is that it provides an area-efficient method for implementing high resistance values and a possibility for electrical adjustment of this resistance by changing the network bias voltage. The idea of using MOS transistors for current division in PSDs was originally proposed by Tartagni & Perona (1993). They did not consider sensitivity issues, but demonstrated that the achievable non-linearity of MOS current division without photodiodes is better than 0.3%.

The PSD, the basic construction of which is was depicted in Fig. 28, is composed of 100 x 100 well-substrate photodiodes occupying a total area of 2.5 x 2.5 mm^2. The array pitch is 25 μm and the fill factor about 70%. The current-dividing MOS transistor arrays consist of 100 PMOS transistors each. To obtain good matching, relatively large-area transistors were used (100 x 20 μm^2). The transistors were designed to give an interelectrode resistance of a few hundred kΩ and a bandwidth of about 10 kHz.

The interelectrode resistance of the PSD was 250 kΩ and the corresponding noise level 1/5 of that of a LEP (R_{ie}~10 kΩ), but the NEP (3.5 pW/√Hz) and the measured position sensing precision were only 1.4 times better. The apparent discrepancy between the noise levels and the precision is explained by the lower effective responsivity and the fact that the total signal current is divided into four parts instead of two, as is the case with the conventional 2-axis duolateral LEP. The sensitivity of the PSD could in principle be increased 3 to 4-fold by minimising the area (capacitance) of the current-

dividing transistors, the contribution of which to the total capacitance (C_d~400 to 500 pF) was substantial (~300 pF). The measured integral non-linearity (0.14%) was a half of that measured for a conventional LEP. The symmetrical S-shape of the error curves (Fig. 4 in Paper XV) suggests that the error is mostly due to the finite bandwidth, and that responsivity non-uniformity and MOS transistor mismatch make only minor contributions. The highest signal frequency providing the measured performance was about 5 kHz (Fig. 6 in Paper XV).

5.8.4. Phototransistor PSD

The construction of the phototransistor PSD depicted in Fig. 36 resembles that of the photodiode PSD. It is composed of 100 x 100 CMOS-compatible vertical phototransistors (pitch 25 μm and K_F~70%), the emitters of which are connected to the row and column current lines, which in turn are connected to two arrays each composed of one hundred 30 Ω polysilicon resistors. Polysilicon resistors provided lower capacitance and a more compact design in this case than MOS resistors.

Experimental comparison with a LEP (R_{ie}~10 kΩ) shows that up to a bandwidth of about 2 kHz the responsivity of the phototransistor PSD is high enough to provide approximately seven times better precision at best (P_r~10 nW), and that equal precision (σ/d~0.1%) is achieved using ten times less signal power at best, corresponding to a NEP of 0.5 pW/√Hz (Fig. 2 in Paper XI). Responsivity could still be increased at low signal levels by using the background or signal to optically bias the transistors. The latter results in a lower total bias current, and thus in lower noise due to the smaller area illuminated. A signal prebias of 100 pW gave a responsivity better than 10 A/W even at very low signal levels (<10 pW).

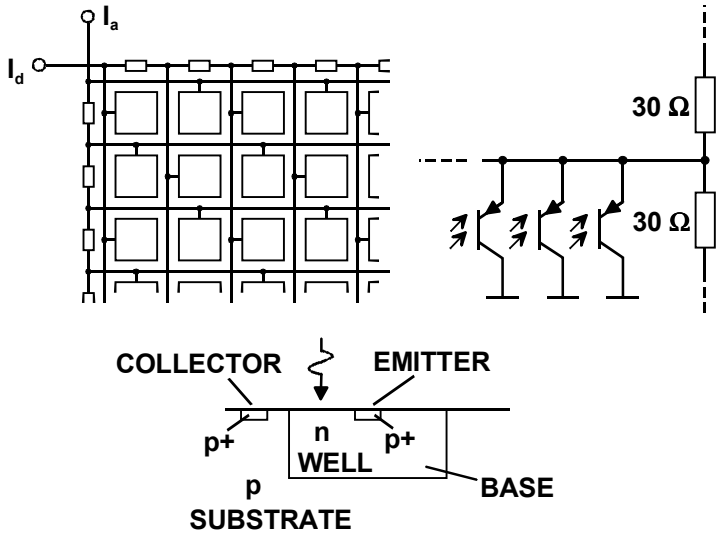

Fig. 36. Construction of the phototransistor PSD.

The integral non-linearity was 0.06% when a 50 µm spot was used, which is about five times better than that of a LEP (Fig. 3 in Paper XI). Enlarging the spot to 300 µm resulted in 0.03% non-linearity (Fig. 4 in Paper XI). The error curves suggest that non-linearity due to the finite PSD bandwidth is negligible and that the deviations from linear behaviour are mostly due to the discrete photodetector structure in the case of the 50 µm spot. With the 300 µm spot most errors are probably caused by the resistor mismatch and the non-uniformity of the responsivity.

5.8.5. Tracking PSD

The tracking PSD depicted in Fig. 37 is similar in construction to the photodiode array PSD. This time the transistors are used to divide the array into four separate areas by switching a few adjacent transistors off and keeping others fully open in both transistor arrays. In the prototype, four adjacent PMOS transistors had a common gate drive, and thus the smallest possible gap width and gap step were 100 µm. Somewhat better accuracy was achieved than with a LEP of equal size. The measured position sensing error was about 3 µm (Fig. 4 in Paper XII), which was mainly caused by the non-linearity of the interpolation function (Fig. 3 in Paper XII). Note that the absolute value of the error should not increase when the device size (measurement span) is increased, as is the case with the LEP, and that the position sensing error could be readily lowered by using a smaller gap width and spot diameter. The measured NEP was 1.3 pW/√Hz and the precision 40 times better than that of an equally sized LEP. Owing to the low effective responsivity of the CMOS PSD, the difference is slightly smaller than that predicted by Eq. (19).

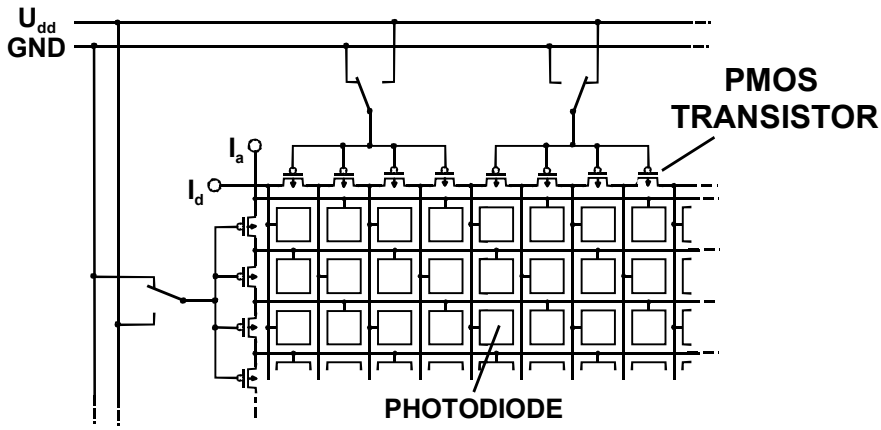

Fig. 37. Construction of the tracking PSD.

5.8.6. Digital PSDs

The digital PSD concept was experimented with by implementing two arrays and a couple of pixel prototypes. The block diagrams of the PSDs are presented in Fig. 38. The first of them was implemented using 1.2 μm CMOS technology and consisted of a 16 x 16 pixel array and circuitry for threshold setting, resetting and readout. A schematic diagram of a pixel is presented in Fig. 39a. The threshold current is set by the transistor M1, which has a low aspect ratio to provide reasonable matching for the low threshold currents (<1nA). The threshold level is set either automatically with the aid of auxiliary photodiodes positioned on the same chip (internal reference), or by using an external current input (external reference). Transistors M3, M4 and M5 form a comparator (latch) and transistors M2, M6 and M7 are used for resetting and readout. Transistors M8 and M9 were not included in the first version of the digital PSD.

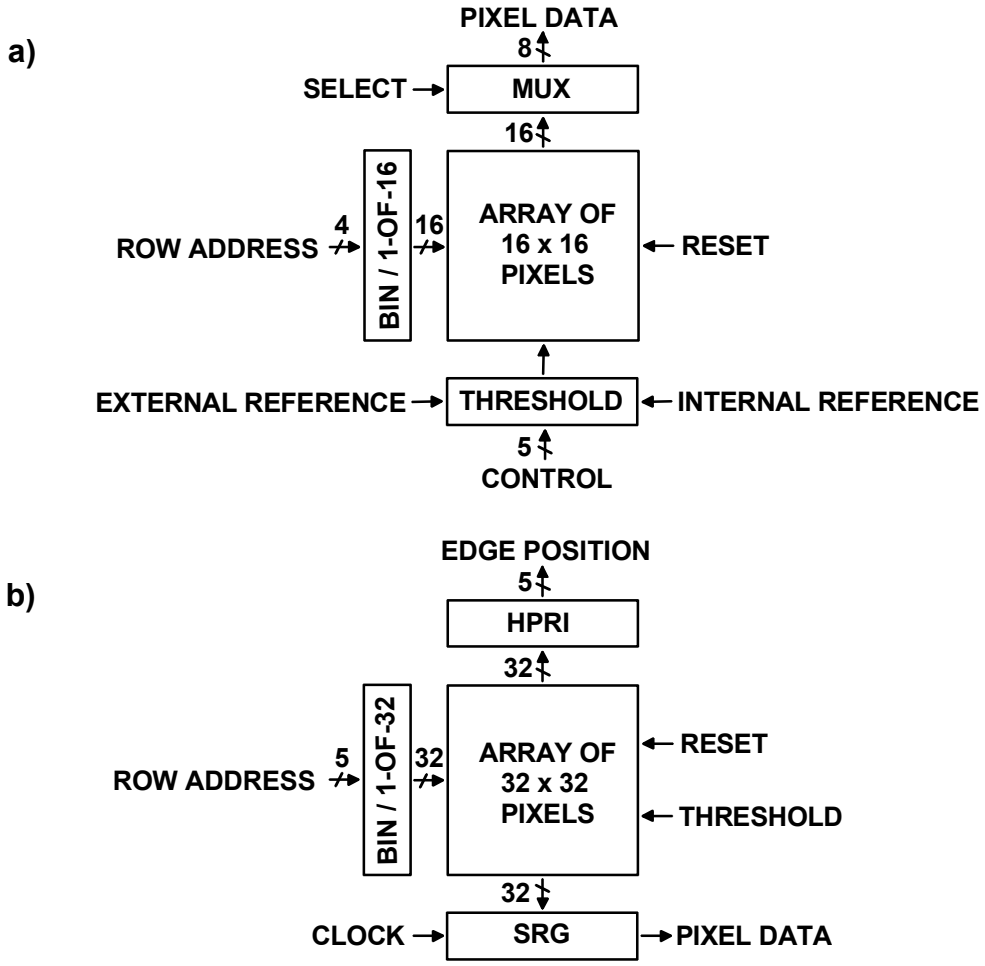

Fig. 38. Block diagrams of the a) 16 x 16 and b) 32x 32 digital PSDs.

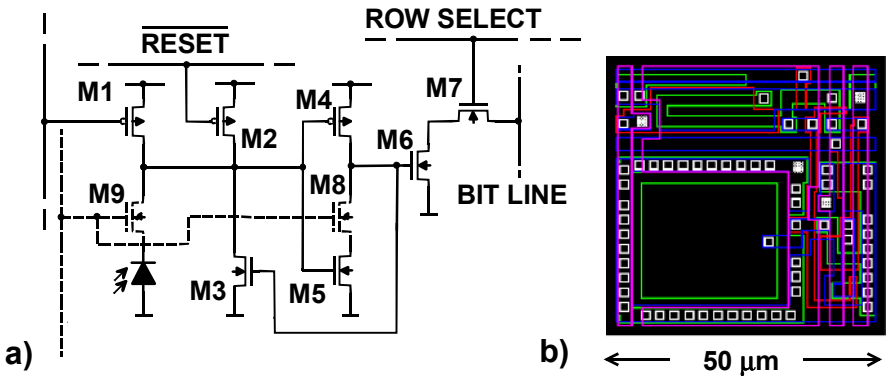

Fig. 39. a) Schematic diagram and b) layout of a digital pixel.

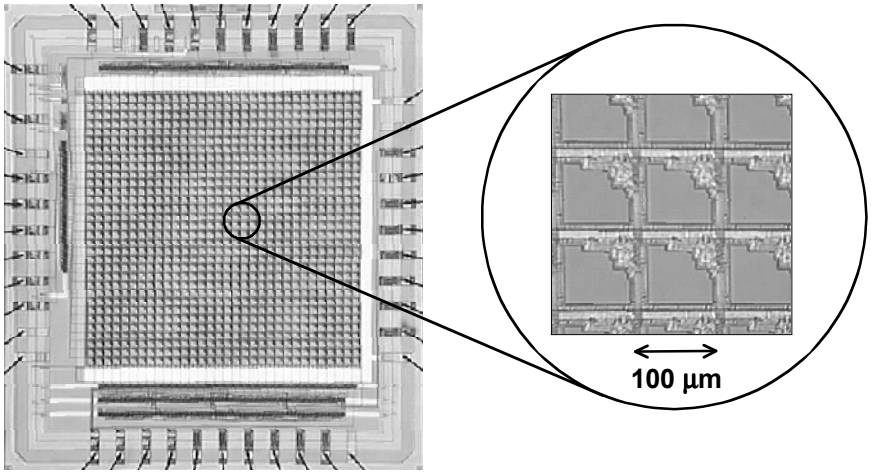

Fig. 40. Photograph of the 32x32 digital PSD chip.

The layout of a pixel is depicted in Fig. 39b. The photodiode and pixel sizes achieved were 30 μm x 25 μm and 50 μm x 50 μm, respectively, corresponding to a fill factor of 30%. The circuitry other than the photodiode was shielded from direct illumination using either of the two metal layers.

The digitisation error measured for the 16 x 16 array agreed with the results reported by Bose & Amir (1990) and Sklair *et al.* (1991). A standard deviation of 4.3 μm (~1/10 of the pixel width) was achieved using a spot of 280 μm in diameter (5 to 6 pixel widths) and full pixel SNR higher than seven. Since the PSD was tested in the continuous current mode, spatial noise due to mismatch of the transistors M1 determined the sensitivity. By

using the lowest possible threshold current providing digitisation-limited performance and equating the error contributions of a LEP with those of the digital PSD, it could be concluded that the sensitivity of the digital PSD in the continuous current mode is comparable with that of a small-area LEP (~10 mm^2).

Before designing the second area array, separate pixels were implemented to measure their sensitivity and speed in pulsed mode (Paper XIV). The basic pixel structure used in the 16 x 16 array was compared with a pixel which included the transistors M8 and M9 (Fig. 39a). M8 was used to reduce ΔU and M9 to reduce C_{pix} by isolating the capacitance of the photodetector from the pixel input. The energy needed for triggering the basic pixel with a 38 μm x 38 μm well-substrate photodiode was 1 pJ (without the effect of K_F) when operated with a supply voltage of 5V. The inclusion of M8 and M9 lowered the triggering energy to 0.23 pJ. The measured triggering energy agreed with the calculations and was also found to be independent of the pulse width and pulse repetition rate, as expected.

The second area array, implemented using a 0.8 μm CMOS process (Fig. 38b), was composed of 32 x 32 pixels, which included the transistors M8 and M9, measured 100 μm x 100 μm each and had a fill factor of 70%. The chip also included simple priority encoders (HPRI) for detecting the position of a light spot edge in each row, and circuitry for detecting the number of triggered pixels in order to minimise the total energy per sample. The measured E_{pix} and current consumption were 0.5 pJ and 0.1 mA, respectively (U_{dd}=5 V, t_m=10 ms). Note that the current consumption is only a small fraction of that of a conventional LEP front end (a few mA) or that of a typical imaging array (a few 10 mA). A photograph of the chip is presented in Fig. 40.

5.9. Comparison of the performance of the PSDs

The performance improvement factors and test results of the implemented PSDs are summarised in Tables 4 and 5, respectively. Table 4 contains the improvement factors describing the enhancement achieved in incremental sensitivity and linearity as compared with a conventional small-area LEP (2.5 x 2.5 mm^2). The sensitivity of a digital PSD was evaluated by assuming that the spot size was adjusted to provide a digitisation error equal to the non-linearity error of a LEP (linearity improvement factor 1). Sensitivity was calculated assuming that the first digital PSD was operated in pulsed mode.

According to Table 4, the best candidates for long-range displacement sensing applications are the phototransistor PSD, tracking PSD and digital PSD. The tracking PSD provided the best overall performance, with a 40-fold improvement in sensitivity and two-fold improvement in linearity over a LEP. The phototransistor PSD and the digital PSD provided 10-fold improvement in sensitivity along with equal or better linearity. Since the prototypes were designed without extensive optimisation, the performance reported is believed to indicate a safe underestimation in each case.

This topic is brought to a close below by discussing the feasibility of the proposed PSD concepts as starting points for the development of actual sensors for long-range displacement sensing applications.

Table 4. Performance improvement factors of the 2-axis PSDs. The factors describe the improvement achieved in incremental sensitivity and linearity relative to a conventional small-area LEP (2.5 x 2.5 mm^2).

	CMOS LEP	Photodiode PSD	Phototran. PSD	Tracking PSD	Digital PSD
Sensitivity	0.5	1.4	10	40	10
Linearity	2	2	5	2	1

Table 5. Results of the tests on the PSD prototypes. Conventional LEPs (1-axis and 2-axis, d=2.5 mm) have typical characteristics deduced from the main manufacturer's datasheets. The dimensions of the single-axis and 2-axis LEPs are 5 x 0.2 mm^2 and 2.5 x 2.5 mm^2, respectively. The characteristics of the digital PSD are those of the 16 x 16 pixel array when operated in the pulsed mode.

Property		Conven-tional LEP	1-axis CMOS LEP	2-axis CMOS LEP	Photo-diode PSD	Photo-transis-tor PSD	Track-ing PSD	Digital PSD
Responsivity, A/W		0.5 – 0.7	0.42	0.38	0.3 [3]	>20 [4]	0.3 [3]	0.4
Fill factor, %		100	100	100	70	70	70	30
Sheet resistance, kΩ/□		10	6	6				
Interelectrode Resistance, kΩ	1-axis	250	152	4.5 [2]				
	2-axis	10		0.85 [1]	250	3		
NEP, pW/√Hz	1-axis	~1	1.6	10 [2]				
	2-axis	~5		47 [1]	3.5	0.5	1.3	
Triggering energy, pJ								~1 [5]
Capacitance, pF	1-axis	1 – 10	160					
	2-axis	6 – 60		1300	~400			
Time constant RC/π^2, ns	1-axis	25 – 250	2500	600 [2]				
	2-axis	6 – 60		110 [1]	~10 k	~100 k		~200
Non-linearity, % [6]	1-axis	~0.1	0.2	0.14 [2]				
	2-axis	~0.3		7.2 [1]	0.14	0.06 [4]	0.15	
Digitisation error, % [6]								0.22 [7]

[1] tetralateral mode
[2] alternate mode
[3] includes fill factor
[4] total signal power >1 nW, spot diameter 50 µm
[5] for one pixel, including fill factor
[6] of full scale, FS = 0.8 x d
[7] spot diameter 280 µm, total triggering energy about 25 pJ

5.9.1. Effects of technology and device scaling

An important factor affecting the feasibility of the proposed PSD concepts is the fast development of CMOS technology. The evolution of CMOS at the pace of 0.7x of the minimum feature size every three years means that one-micron CMOS technology will soon cease to exist and the proposed PSDs, if found feasible, must be designed using submicron technology. Many important device characteristics change as the technology is scaled, thus causing changes in PSD performance. The most important parameters that affect the performance of the proposed PSDs include pixel (photodetector) size, responsivity, capacitance and the threshold voltage of MOS transistors. According to Wong (1996), pixel size in photodetector arrays will decrease in direct proportion to the minimum feature size. Sheet capacitance will increase, but as the area of a pixel is scaled down, the total pixel capacitance will diminish in proportion to the minimum feature size as well. As the minimum feature size decreases to 1/4, the responsivity of a well-substrate photodiode is expected to decline to 1/2 or 1/3 depending on the wavelength used (Moini 2000). The MOS transistor threshold voltage will be approximately halved as the minimum feature size decrease to 1/5 (Wong 1996).

The sensitivity of all PSDs will obviously suffer from the reduction in responsivity. The sensitivity of the photodiode PSD will also decline due to increased sheet capacitance, which will increase the total capacitance of the array and thereby reduce the maximum usable value of the current-dividing resistance. The sensitivity of the phototransistor PSD will probably decline most, since the gain of the vertical bipolar transistor used as a phototransistor tends to become lower in proportion to the minimum feature size (AMS International AG 1999). The digitisation errors of the photodiode and phototransistor PSDs will be reduced due to the smaller pixel size. The ratio between diffusion length and photodetector size will remain constant, and therefore the relative reduction in digitisation error due to diffusion coupling (crosstalk) is expected to remain unchanged (Wong 1996). The tracking PSD will suffer from the responsivity reduction, but its effect on sensitivity will probably be more than compensated for by the possibility of reducing the spot size due to the decreasing photodiode size. The digital PSD is expected to benefit from technology downscaling. The smaller pixel size will reduce the total number of pixels needed to achieve a certain level of accuracy and the triggering energy of a pixel will be reduced due to the lower pixel capacitance and lower threshold voltage, which together are expected to be more than enough to compensate for the reduction in photodetector responsivity.

5.9.2. Applicability to long-range displacement sensing

The photodiode array PSD provided some improvement in terms of sensitivity and linearity as compared with a LEP. The large sheet capacitance and low responsivity of CMOS photodiodes made the sensitivity improvement relatively modest, however. If the capacitance of the current-dividing MOS transistors had been properly optimised, the sensitivity improvement factor (1.4) would have been around 3 or 4. Its non-linearity was half of that of a LEP and was dominated by the error due to bandwidth limitation.

The photodiode array PSD will suffer from the increasing capacitance of photodiodes and the lowering of their responsivity as CMOS is scaled down. This will probably reduce its sensitivity gradually to below that of the LEP and thus make the approach unattractive.

The phototransistor PSD provided 10-fold and 5-fold improvements in sensitivity and linearity, respectively, which as such would provide a good starting point for the single chip PSD development work. Unfortunately, the gain of CMOS-compatible phototransistors seems to degenerate rapidly as the feature size of CMOS technology decreases, which together with the lowering of primary responsivity also makes the phototransistor PSD obsolete. The excellent linearity and sensitivity, however, prove the feasibility of the basic concept and mean that successful use of it would simply call for other means of signal amplification.

The tracking PSD provided the best overall performance of all prototypes by providing a 40-fold improvement in sensitivity and two-fold improvement in linearity relative to a LEP. An additional improvement in sensitivity and linearity by a factor of four may be achieved if the minimum gap step is set to one pixel width instead of the four pixel widths used in the prototype. This would also effectively minimise the turbulence sensitivity of the PSD by making it possible to reduce the spot size below 0.1 mm. The performance of the tracking PSD will suffer from a responsivity reduction as the feature size of CMOS technology becomes smaller, but due to the fact that the sensitivity improvement is mostly based on geometrical scaling (d vs. d_s), the responsivity reduction will probably be more than compensated for by the possibility of reducing the spot size as the photodiodes become smaller. Low preamplifier power consumption should also be achievable, since the voltage noise specification for the preamplifier core amplifier is relaxed compared with a LEP due to the high-impedance nature of the PSD. The main disadvantage of the tracking PSD is that it does not solve the fundamental problem related to simple PSDs, that is sensitivity to low reflector background contrast.

Although the tracking PSD provided the best overall performance, the digital PSD is considered to be the most promising candidate for displacement sensing applications in general. Besides providing better sensitivity and lower front end power consumption than a LEP, it tolerates much lower reflector background contrast due to individual pixel processing than the other PSDs and makes it also possible to measure multiple spot positions simultaneously. The latter could be used to improve precision in the turbulence-limited case by averaging the positions of multiple reflectors, for example, or to measure lateral displacement without knowing the target distance by attaching two or more reflectors with known lateral separation to the target. The performance of the digital PSDs is also expected to improve as the minimum feature size of CMOS technology decreases. The one-micron technology used for implementing the prototypes provided a 10-fold improvement in sensitivity relative to a conventional LEP, but the present leading edge technologies (<0.2 μm) should facilitate 10 μm pixel size and basically a 40-fold improvement in sensitivity simultaneously with a 5-fold improvement in measurement accuracy. The 20 μm spot diameter needed in such a case would also optimise measurement precision in a turbulent environment. Further experimental work is needed, however, to confirm the estimated performance.

6. Discussion

Discussions related to the various applications have already been entered into separately in each chapter. The purpose here is to discuss which contributions of the thesis are believed to be the most important and which will probably be of more general significance beyond their association with the presented applications. The starting point for the work was to apply the reflected beam method used in military and aerospace applications to certain industrial applications. It was readily found that the conventional laser spot tracker as such could not provide sufficient performance in industrial applications, and therefore various modifications were proposed to improve its performance. The main scientific contribution of the thesis comprises these modifications, of which the most important ones, namely ways to improve precision in a turbulent environment, reflector background contrast and the performance of a PSD, are discussed below.

6.1.Ways to reduce the effect of atmospheric turbulence

The conventional reflected beam sensor, which includes a misfocused QD receiver, is very sensitive to atmospheric turbulence. Alongside fluctuations in beam direction (angle-of-arrival), fluctuations in illumination within the received beam are especially important in detracting from precision. The use of a sheet reflector instead of a CCR improved the precision by reducing spatial variations in illumination. This is believed to be due to the averaging effect of the thousands of small reflective cells that make up the sheet. The second method used to avoid the effect of illumination fluctuations was simply to focus the receiver. In the focused case atmospheric fluctuations change the illumination within the image spot uniformly leaving the centroid of the spot unaltered. In the second case a LEP was used as the PSD instead of a QD, since its operation is not dependent on the size of the light spot.

Both modifications provided roughly an order of magnitude improvement in precision in the presence of intermediate atmospheric turbulence. Due to the low gain of the sheet reflector, the first method is best suited for relatively short target distances, while the second one is also applicable for longer distances. The sheet reflector used in

the first case makes it possible to construct accurate targets with an omnidirectional observation angle. In the second case the target observation angle is basically restricted to that of a single CCR. The tracking precision achieved in both cases appeared to be comparable to those indicated for the commercial tracking stations used in surveying applications.

The precision of the reflected beam sensors with a focused receiver might be restricted by the angle-of-arrival fluctuations caused by atmospheric turbulence. In certain cases these fluctuations may be reduced using basic signal conditioning methods such as averaging, for example. If the measured signal is non-repetitive, however, and the signal band overlaps with that of the atmospheric fluctuations, averaging typically becomes inefficient due to the correlation between successive results. A new way to improve precision in such a case was proposed here. The idea was to average the angle-of-arrival fluctuations of multiple, spatially separated beam paths. The basic advantage of the method compared with temporal averaging is that the precision improvement should not be dependent on the measurement rate but only on the spatial separation of the beam paths. It was realised that an improvement in precision could be obtained if the separation of the beams was larger than the largest of the turbulent inhomogeneities responsible for the angle-of-arrival fluctuations. Since the size of these fluctuations is typically only a few tens of centimetres for near-ground paths, precision improvement is possible. The averaging efficiency is restricted by the fact that the beams have a common starting point and end point at the transceiver and thus angular fluctuations can never be totally uncorrelated. It seems that an improvement in precision by a factor of two is possible without increasing the number of reflectors and the extent of the illuminated FOV beyond reasonable limits.

The adverse effect of misfocus on the precision of the reflected beam sensor in a turbulent environment is a generally known fact, but it seems that no experimental results have been reported before. Neither have them been reported on angle-of-arrival fluctuations although some theoretical studies has been published. The ideas of using a sheet reflector instead of a CCR or using multiple laterally separated CCRs for precision improvement are believed to be new, too.

6.2. Improving reflector background contrast

Finite reflector background contrast causes measurement errors in reflected beam sensing, since simple PSDs cannot distinguish between the reflector and background reflections. Contrast improvement has not been studied much, since the CCRs used in a conventional laser spot tracker tend to provide adequate contrast. For practical reasons, CCRs are not suitable for all industrial applications, and sheet reflectors must be used instead. Due to the lower gain of the sheet reflectors, the contrast may easily become poor, especially if the reflectors are placed on specularly reflecting objects. Polarisation filtering was proposed to increase the contrast in such cases, and this was found effective, as expected, provided that the reflection process within the reflector did not include total internal reflections. It was concluded that irrespective of the background properties, polarisation filtering should provide a contrast which is limited by the diffuse

background case. The main shortcoming of polarisation filtering is that the reflector should have an appropriate rotational orientation with respect to the transceiver in order to maintain its gain. It was concluded, however, that this should not be a problem in manufacturing accuracy control applications, for example.

Further contrast improvement could be achieved using a digital PSD instead of a conventional PSD. Individual pixel processing in the digital PSD could be used to remove the contribution of background reflections from the centroid calculation on the basis of the intensity difference between the reflector and the background. Combining polarisation filtering with the digital PSD would make sure that specular reflections from background are not mixed up with that from the reflector.

Polarisation filtering is a well-known method for eliminating specular reflections, but its use for contrast enhancement in a reflected beam sensor including sheet reflectors is believed to be new.

6.3. Custom-designed PSDs

The properties of the PSD affect the performance of a reflected beam sensor quite markedly. The main drawbacks of the LEP, for example, are its high noise and the non-linearity of its transfer characteristics. The non-linearity is mainly due to the inhomogeneity of the interelectrode resistance, and the noise is due to the low interelectrode resistance needed in order to obtain the desired linearity (resistor homogeneity) at tolerable manufacturing costs.

CMOS technology was used to implement various types of optical position-sensitive photodetectors. The proposed array-type PSDs provided clear improvement in sensitivity and accuracy relative to LEPs. The photodetector performance in CMOS is not as good as in dedicated photodetector processes but the array construction made it possible to more than compensate for this deficiency in all cases. The additional error due to the discrete photodetectors and small spot size needed to maintain good precision in atmospheric turbulence was rendered small enough by the crosstalk inherent to CMOS-compatible photodetectors. The best performance was provided by the tracking PSD, phototransistor PSD and digital PSD, which provided improvements in sensitivity by factors of 10 to 40 along with equal or better linearity. The phototransistor PSD has a LEP-type operation in which improved sensitivity is achieved using the gain of the phototransistors to amplify the signal before noisy current division. The tracking and digital PSDs utilise the accurate geometry and small feature size of CMOS technology to establish good position-sensing performance. In view of this it seems possible to improve the performance of the tracking and digital PSDs further as the feature size of CMOS decreases. Although the tracking PSD provided the best overall performance, the digital PSD was considered the most promising candidate for the long-range displacement sensing application, mainly due to its fully digital connection and the advantages to be gained from individual pixel processing.

Active pixel image sensors, when operated in binary image mode, provide basically the same features as the proposed digital PSD. The main difference between imaging detectors and the digital PSD is that in the latter digitisation is performed in parallel fashion in each pixel while in imaging detectors it is performed more or less serially outside the array. The advantage of parallel digitisation is that the real time exposure control and spot tracking needed to minimise the illumination energy and the number of pixels to be read can be easily implemented (Langenbacher *et al.* 1993). Also filtering can be readily performed at the pixel level using simple Boolean operators, for example (Bernard *et al.* 1993). Due to its simple construction the power consumption of a digital PSD should also be much less than that of imaging detectors, and its operating speed should be much higher, too. Frame rates up to one MHz should basically be possible. An imaging detector provides much better sensitivity than the digital PSD, however, and thus an important aim for future work will be to enhance the sensitivity of the digital PSD. Ways of improving the sensitivity of photodetection could possibly be derived from the work of Brockherde *et al.* (1998), Biber & Seitz (1998) and Kindt (1999), for example.

Photodetector arrays used for position-sensing purposes have been discussed in many papers, but sensitivity issues have not been addressed in any of them. The tracking PSD, however, seems to be the only totally new PSD construction proposed. Despite the fact that long-range displacement sensing such as optical shooting practice was the target application, it seems clear that the proposed PSDs might well be used in various other applications, too, such as those listed in section 1.1.

7. Summary

This thesis discusses optical position-sensitive devices (PSDs) and reflected beam sensors developed mainly for automatic pointing of a laser beam and for measuring object displacement from a reference point. The beam pointing sensor was developed for industrial dimensional accuracy control application, and the displacement sensor for measuring the aiming trajectory in optical shooting practice. In the proposed sensors a target equipped with a reflector is illuminated and a PSD is used to measure the displacement of the target reflection in a plane perpendicular to the direction of observation. The sensing method is similar to that of the laser spot trackers commonly used in aerospace and military applications. The main contribution of the work is related to modifications to the construction of a conventional laser spot tracker in order to be able to use it for industrial applications that require a few millimetre to submillimetre accuracy. This work includes modifications in the optical construction of the sensors and the designing of new types of PSDs.

A reflected beam sensor construction for a tracking laser rangefinder intended for vehicle positioning was described first. A conventional laser spot tracker composed of a misfocused QD receiver and a CCR is highly susceptible to atmospheric turbulence and has inadequate precision for this purpose. The main reason for the deterioration in precision proved to be the sensitivity of the misfocused receiver to spatially uncorrelated illumination fluctuations caused by atmospheric turbulence. Improved precision was obtained by replacing the corner cube reflector with a sheet reflector, which provided negligible fluctuations due to the averaging effect of the multiple overlapping beams reflected from it. The proposed sensor construction was estimated to provide subcentimetre tracking accuracy up to the distance of about a 100 m in most outdoor conditions, i.e. an accuracy compatible with that of a pulsed TOF method used for target distance measurement. Comparable accuracy was achieved with a focused LEP and a CCR proposed later for long-range displacement sensing applications. The spherical sheet reflector was considered more suitable for vehicle positioning, however, due to its wide observation angle and the low systematic error inherent in its spherical shape. The main drawback of the proposed construction is its relatively short operating range due to the low gain of the sheet reflector as compared with a conventional tracking sensor using CCR targets.

Another tracking sensor prototype was implemented for a rangefinding 3D coordinate meter, to point its measurement beam automatically towards a marked point on the object surface. This was intended to automate and speed up the performing of measurements in dimensional accuracy control applications. A sensor based on a focused QD receiver, coaxial illumination and a small sheet reflector placed on the point to be measured provided comparable accuracy to manual aiming when the object had diffuse reflectance properties. The main drawback of the sensor construction in a practical operating environment was its sensitivity to the specular background reflections typically confronted in shipyard applications, for example, where the dimensions of steel and aluminium objects are to be measured. Polarisation filtering was proposed in order to increase the reflector background contrast in such a case. The method proved to be effective and seems technically feasible. Even a moderate polariser extinction ratio should provide tracking accuracy, which is limited by the diffuse background case. The main problem related to the practical use of the method is that the reflector must have a certain orientation with respect to the receiver in order to maintain its gain. This affects target marking and restricts the observation angle of the marks. This was thought not to be a problem in typical accuracy control measurements, however.

The last part of Chapter 3 dealt with a rangefinding method for object distance and orientation measurements in which small fibre-coupled transmitters are attached to the target object and their distances from a tracking receiver are measured using a pulsed TOF rangefinder. The results are used to determine the basic distance from the target and its orientation with respect to the optical axis of the receiver. The measurement principle was demonstrated by constructing an experimental pointing device for short-range robot teaching purposes. Mode dispersion in the optical fibres and multiple path propagation effects due to the wide FOV of the transmitters and the receiver were the most critical factors affecting the accuracy of the method, but mode mixing using diffusers and collimation of the transmitted radiation reduced these errors. The dependence of the transit time on temperature in the coupling fibres was estimated to be the main factor limiting measurement accuracy if the operating range was to be enlarged beyond a few metres. Using state-of-the-art rangefinding techniques, however, a distance range of some tens of metres should in principle be possible with an accuracy of a few millimetres.

The properties and performance of two reflected beam sensors intended for displacement sensing applications were described in Chapter 4. The first of these employs a focused QD receiver and a square sheet reflector to measure small displacements accurately over a distance of a few metres. Unlike the conventional tracking sensor, this construction provides position information which is proportional to linear rather than angular displacement, and scaling which is range-invariant and determined solely by the size of the reflector. The main advantage of the method compared with other range insensitive methods such as telecentric gauging, for example, is its large working volume. The extent of the measurement field can range basically from a few millimetres to some decimetres, and the stand-off distance from several decimetres up to tens of metres. The experimental results show that a sensor composed of standard components and having a measurement field of 10 mm and stand-off distance of a few metres provides a bandwidth of several kHz, precision that is limited by atmospheric fluctuations to the level of a few micrometres, an inherent scaling

accuracy of a few % and integral non-linearity better than 1%. The effect of atmospheric fluctuations on precision could probably be reduced by filtering or averaging in some cases.

The second displacement sensor was composed of a focused LEP receiver and a CCR and intended for long-range outdoor displacement sensing such as the aim point trajectory measurements needed in optical shooting practice. Ways of minimising receiver sensitivity to atmospheric turbulence, which determines the measurement precision outdoors, were studied. The turbulence sensitivities of a misfocused QD receiver and a focused LEP receiver were compared theoretically and experimentally, and it was found that the LEP receiver is less sensitive to atmospheric fluctuations, since it can be focused. A precision better than 1 cm was achieved over a distance range of up to 300 m in intermediate atmospheric turbulence with the focused LEP receiver, while the precision of the QD receiver was an order of magnitude worse. Although precision of the focused LEP receiver is good enough for the aim point trajectory measurement, for example, possibilities for improving the turbulence-limited precision further were also studied. The averaging of successive measurement results proved to be inefficient, since fluctuations between successive results were found to be highly correlated when the measurement rate exceeded a few Hz. A method for improving the turbulence-limited precision based on averaging of the positions of multiple, laterally separated reflectors was proposed, and precision improvement proved to be achievable, since the beams reflected from the CCRs have a lateral separation larger than the average size of the inhomogeneities responsible for the fluctuations in measurement results. The experiments indicate that the averaging efficiency seems not to be dependent on the measurement rate but only on the spatial separation of the reflectors, and improves as their separation increases. An optimal sensor construction for long-range outdoor displacement sensing applications was finally deduced.

Chapter 5 describes various types of PSD designed particularly for long-range, outdoor displacement sensing applications. The main goal was to design a PSD with a higher electrical sensitivity than a LEP. It was important for any performance improvements to be achieved with a small spot size, to ensure that the best possible precision was available in a turbulent environment, too. The problem with a conventional 2-axis LEP is that a relatively low sheet resistance must be used to guarantee good linearity, which then leads to high noise and high front end power consumption. To solve this problem, several PSD constructions based on photodetector arrays were implemented using standard CMOS technology.

Two of the array PSDs used LEP-type current division, the first having an area array of small-sized photodiodes and high interelectrode resistance, while in the second the sensitivity was improved by using phototransistors instead of photodiodes in order to increase the signal level before noisy current division. The spatial digitisation error due to the discrete photodetector structure was rendered negligible by the filtering effect of the crosstalk which is inherent to CMOS-compatible photodetectors having a common substrate contact. This made it possible to use the small spot size without increasing the digitisation error beyond the desired level. The idea of the third PSD was to utilise the high electrical sensitivity of a QD and combine it with the low turbulence sensitivity of a LEP-type PSD. This was accomplished by partitioning a PSD array into four quadrants according to the position of the spot on the array, so that a focused spot could be used in

QD operation. The fourth PSD resembles that of a conventional electronic camera, in which the outputs of all the pixels are separately quantified and processed. The camera-based approach was made feasible for position sensing applications by lowering the signal processing load compared with actual camera sensors. To accomplish this, the proposed digital PSD generates a low-resolution binary image of the target reflector and includes simple hardware to reduce the signal processing effort.

The implemented prototypes showed that by using dense photodetector arrays it is possible to obtain equally low sensitivity to atmospheric turbulence as with the LEP but better linearity and incremental sensitivity. The tracking PSD prototype provided the best overall performance by offering a 40-fold improvement in sensitivity and two-fold improvement in linearity as compared with a LEP. The digital PSD was considered to be most promising. This was estimated to provide a 10-fold improvement in sensitivity and a clear decrease in power consumption relative to a LEP receiver, in addition to which it seems to provide a solution to the contrast problem inherent in simple PSDs and also a practical means of improving precision in the turbulence-limited case using the multiple beam method. Since the tracking and digital PSDs utilise mainly the accurate geometry and small feature size of CMOS technology to establish a good position-sensing performance, it seems possible to continue to improve their performance as the feature size of CMOS processes decreases. The development work of the digital PSD is continuing.

The results presented in this thesis show that, with certain modifications, the laser spot trackers used in military and aerospace applications can be used successfully in industrial measurement applications, too. The main scientific contribution of the thesis comprises these modifications the most important of which are the methods and constructions that can be used to improve measurement precision in a turbulent environment, to improve reflector background contrast and to improve the performance of a PSD.

References

Adachi T & Mita T (1987) Detecting methods for the position/direction of a robot hand using PSD and its applications. Advanced Robotics 1(4): 357–370.

Advanced Photonix Inc. (2000) Bi-cell and Quadrant position sensing photodetectors. Product data sheet. http://www.advancedphotonix.com/Bi-Cell/quad1.htm (20 March 2000).

Ailisto H (1997) CAD model-based planning and vision guidance for optical 3D co-ordinate measurement. VTT Publications 298.

Aksenov VP, Banakh VA & Chen BN (1984) Variance of displacements of the image of objects during optical location in a turbulent atmosphere. Optics and Spectroscopy 56(5): 529–532.

Alexander BF & Ng KC (1991) Elimination of systematic error in subpixel accuracy centroid estimation. Optical Engineering 30(9): 1320–1331.

Ammon G & Russel S (1970) A laser tracking and ranging system. Applied Optics 9(10): 2256–2260.

AMS International AG (1999) 0.35, 0.6, 0.8, 1.2 µm CMOS process parameters. Unterpremstätten, Austria.

Andreev GA & Magind RM (1972) Influence of intensity fluctuations on the measurement of angular position of radiation source by optical-electron monopulse method. Izvestiya Vysshikh Uchebnykh Zavedenii Radiofizika 15(1): 55–61.

Aubert P, Oguey HJ & Vuilleumier R (1988) Monilithic optical position encoder with on-chip photodiodes. IEEE Journal of Solid-State Circuits 23(2): 465–473.

Aumala O, Ihalainen H, Jokinen H & Kortelainen J (1995) Mittaussignaalien käsittely. Pressus, Tampere, Finland.

Automated Precision Inc. (1996) Precision measurement and sensing instruments for manufacturing. Product information, Gaithersburg, Maryland, USA.

Banakh VA & Tikhomirova OV (1984) Variance and spatial correlation of the intensity of laser beams reflected in a turbulent atmosphere. Optics and Spectroscopy 56(5): 524–528.

Bernard TM, Zavidovique BY & Devos FJ (1993) A programmable artificial retina. IEEE Journal of Solid-State Circuits 28(7): 789–798.

Biber A & Seitz P (1998) CMOS compatible avalanche photodiodes. Proceedings of SPIE 3410: 10–20.

Bose CB & Amir I (1990) Design of fiducials for accurate registration using machine vision. IEEE Transactions on Pattern Analysis and Machine Intelligence 12(12): 1196–1200.

Boytemy J-C (1987) Use of CCD arrays for optical link acquisition and tracking. Proceedings of SPIE 810: 215–222.

Broch JT (1980) Mechanical vibrations and shock measurements. Bruel & Kjaer, Berlin, FRG, p 97–108.

Brockherde W, Hosticka BJ, Petermann M, Schanz M & Spors R (1998) Smart 2048-pixel linear CMOS image sensor. Proceedings of the 24th European Solid-State Circuits Conference, Hague, Netherlands: 212–215.

Brown LB, Merry JB & Wells DN (1986) Coordinate measurement with a tracking laser interferometer. Lasers & Applications 5(10): 69–71.
Bult K & Geelen GJGM (1992) An inherently linear and compact MOST-only current division technique. IEEE Journal of Solid-State Circuits 27(12): 1730–1735.
Burch JM & Williams DC (1974) Afocal lens systems for straightness measurement. Optics and Laser Technology 6(4): 166–168.
Burr-Brown Corp. (1994) Comparison of noise performance between a FET transimpedance amplifier and a switched integrator. Application Bulletin AB-057A.
Carbonneau R & Dubois J (1986) An optical gun muzzle sensor to improve firing accuracy. Proceedings of SPIE 661: 352–358.
Carmer DC & Bair ME (1969) Some polarization characteristics of magnesium oxide and other diffuse reflectors. Applied Optics 8(8): 1597–1605.
Chiba T (1971) Spot dancing of the laser beam propagated through the turbulent atmosphere. Applied Optics 10(11): 2456–2461.
Chowdhury MF, Davies PA & Lee P (1998) CMOS 1D and 2D n-well tetra-lateral position sensitive detectors. Proceedings of IEEE International Symposium on Circuits and Systems, Monterey, California, USA, 6: 606–609.
Churnside JH & Lataitis RJ (1987) Angle-of-arrival fluctuations of a reflected beam in atmospheric turbulence. Journal of Optical Society of America A 4(7): 1264–1272.
Churnside JH (1989) Angle-of-arrival fluctuations of retroreflected light in the turbulent atmosphere. Journal of Optical Society of America A 6(2): 275–279.
Churnside JH & Lataitis RJ (1989) Statistics of a reflected beam in the turbulent atmosphere (Path correaltion). NOAA Technical Memorandum ERL WPL-172, National Oceanic and Atmospheric Administration, Environmental Research Laboratories, Wave Propagation Laboratory, Boulder, Colorado, USA.
Churnside JH & Lataitis RJ (1990) Wander of an optical beam in the turbulent atmosphere. Applied Optics 29(7): 926–930.
Churnside JH (1991) Aperture averaging of optical scintillations in the turbulent atmosphere. Applied Optics 30(15): 1982–1994.
Churnside JH & Wilson JJ (1993) Enhanced backscatter of a reflected beam in atmospheric turbulence. Applied Optics 32(15): 2651–2655.
Coles WA & Frechlich RG (1982) Simultaneous measurement of angular scattering and intensity scintillation in the atmosphere. Journal of Optical Society of America 72(8): 1042–1048.
Cooke CR & Speck JP (1971) Precision aircraft tracking system. Proceedings of a Seminar on Optical Tracking Systems, El Paso, USA: 39–50.
Cox JA (1986) Point source location sensitivity analysis. Proceedings of SPIE 686: 130–137.
Cox JA (1989) Advantages of hexagonal detectors and variable focus for point-source sensors. Optical Engineering 28(11): 1145–1150.
Cyran EJ (1986) Airborne inertial surveying using laser tracking and profiling techniques. Proceedings of SPIE 644: 54–59.
De La Moneda FH, Chenette ER & Van Der Ziel A (1971) Noise in phototransitors. IEEE Transactions on Electron Devices 18(6): 340–346.
Degnan JJ, Kahn WD & Englar TS (1983) Centimeter precision airborne laser ranging system. Journal of Surveying Engineering 109(2): 99–115.
Degnan J & McGarry J (1997) SLR2000: eyesafe and autonomous single photoelectron satellite laser ranging at kiloherz rates. Proceedings of SPIE 3218: 63–77.
DeWeerth SP & Mead CA (1988) A two-dimensional visual tracking array. Proceedings of the 5th MIT Conference on Very Large Scale Integration, Cambridge, Massachusetts, USA: 259–275.
DeWeerth SP (1992) Analog VLSI circuits for stimulus localization and centroid computation. International Journal of Computer Vision 8(2): 191–202.
Dowling JA & Livingston PM (1973) Behavior of focused beams in atmospheric turbulence: Measurements and comments on the theory. Journal of the Optical Society of America 63(7): 846–858.
Drain LE & Moss BC (1986) Laser measurement of vibration. Proceedings of IEE Colloquium on Optical Techniques for NDT, London, England: 4/1–4/4.

Edmund Scientific Company (1999) Optics and optical instruments catalog, USA, p 69.
Fante RL (1975) Electromagnetic beam propagation in turbulent media. Proceedings of the IEEE 63(12): 1669–1692.
Feige E, Clegg TB & Poulton JW (1983) A new optical transducer to measure damped harmonic motion. Americam Journal of Physics 51(10): 954–955.
Francini F, Macchiarulo M, Tiribilli B & Buah-Bassuah PK (1987) Opto-electronic system for displacement and vibration measurements. Review of Scientific Instruments 58(9): 1678–1681.
Gaillet A & Belleau B (1985) Automatic guiding method and apparatus for moving objects especially for driverless self-propelled vehicles. EP patent 146428.
Gear CW (1969) Graphics in a time sharing environment. Proceedings for Skytop Conference on Computer Systems in Experimental Nuclear Physics: 552–565.
Gerson G, Rue AK & Caplan LC (1989) Tracking systems. In: Wolfe WL & Zissis GJ (eds) The Infrared Handbook. Prepared by The Infrared Information Analysis Center, Environmental Research Institute of Michigan. Office of Naval Research, Department of Navy, Washington D.C., USA, p 22-1–22-108.
Gindele EB & Miller TL (1986) Polarization effects in optical free space communications. Proceedings of the IEEE Military Communications Conference, Monterey, California, USA 3: 45.4/1–6.
Gonnason WR, Haslett JW & Trofimenkoff FN (1990) A low cost high resolution optical position sensor. IEEE Transactions on Instrumentation and Measurement 39(4): 658–663.
Gottwald R & Berner W (1987) A new angle on 3-D coordinate determination. Sensor Review 7(3): 143–146.
Gottwald R (1988) Kern Space: An automated non contact 3-D measuring system for industrial applications. Proceedings of the 7th International Conference on Robot Vision and Sensory Controls, Zurich, Switzerland: 3–12.
Graeme JG (1996) Photodiode amplifiers – Op Amp Solutions. McGraw-Hill, USA, p 31–61.
Gruss A, Carley LR & Kanade T (1991) Integrated sensor and range-finding analog signal processor. IEEE Journal of Solid-State Circuits 26(3): 184–191.
Halme A (1988) A task level control and simulation system for interactive robotics. In: Kopacek P, Troch I & Desoyer K (eds) Theory of Robots. Pergamon, Oxford, UK, p 289–296.
Hamamatsu Photonics K.K. (1997) One, two-dimensional PSDs (Position sensitive detectors). Product data sheet, Cat. No. KPSD1003E04, Hamamatsu City, Japan.
Hasegawa T (1982) An interactive system for modelling and monitoring a manipulation environment. IEEE Transactions on Systems, Man and Cybernetics 12(3): 250–258.
Heikkilä R (1996) The applicability of an electro-optical coordinate measuring technique to the dimensional control of precast concrete facade panel production. Acta Universitatis Ouluensis C Technica 86.
Hewlett-Packard Company (1977) Optoelectronics applications manual. Chapter 6. Contrast enhancement for LED displays. Optoelectronics division, USA.
Horsmon AW & Lupica CJ (1990) Advanced industrial measurement systems for productive shipbuilding. Proceedings of NSRP Ship Production Symposium, Milwaukee, Wisconsin, USA, 3A-1: 1–16.
Hutcheson LD (1976) Practical electro-optic deflection measurement system. Optical Engineering 15(1): 61–63.
Häusler G & Maul M (1985) Telecentric scanner for 3-D sensing. Optical Engineering 15(6): 978-980.
IBEO GmbH (1987) NAVITRACK 1000, Bedienungsanleitung N870615-D (Anwendung in der hydrographie), Hamburg, Germany.
IEEE (1996) The IEEE standard dictionary of electrical and electronics terms. IEEE Standard 100-1996. IEEE Standards Office, Piscataway, New Jersey, USA.
Ishii M, Sakane S & Kakikura M (1984) A New 3D sensor for teaching robot paths and environments. Proceedings of the 4th International Conference on Robot Vision and Sensory Controls, London, UK: 155–164.

Ishii M, Sakane S, Mikami Y & Kakikura M (1987) Teaching robot operations and environments by using a 3-D visual sensor system. Proceedings of the International Conference on Intelligent Autonomous Systems (IAS), Amsterdam, Netherlands: 283–289.

Jarvis RA (1983) A perspective on range finding techniques for computer vision. IEEE Transactions on Pattern Analysis and Machine Intelligence 5(2): 122–139.

Johnson NL (1979) Accuracy in the photometry of retroreflectors. Proceedings of SPIE 193: 136-146.

Johnson RE (1979) Optical engineering of first- and second-generation automatic tracking/laser designator pods. Optical Engineering 18(4): 370–375.

Kaisto I, Kostamovaara K, Manninen M & Myllylä R (1983) Optical rangefinder for 1.5-10-m distances. Applied Optics 22(20): 3258–3264.

Kaisto I, Kostamovaara J, Manninen M & Myllylä R (1994) Laser radar based measuring systems for large scale assembly applications. Proceedings of SPIE 2088: 121–131.

Kazovsky LG (1983) Theory of tracking accuracy of laser systems. Optical Engineering 22(3): 339–347.

Kelly BO & Nemhauser RI (1973) Techniques for using the position sensitivity of silicon photodetectors to provide remote machine control. Proceedings of the 21st Annual IEEE Machine Tool Conference, Hartford, Connecticut, USA.

Kilpelä A, Ylitalo J, Määttä K & Kostamovaara J (1998) Timing discriminator for pulsed time-of-flight laser rangefinding measurements. Review of Scientific Instruments 69(5): 1978–1984.

Kindt WJ (1999) Geiger mode avalanche photodiode arrays. Delft University Press, Netherlands.

Kingsley S & Quegan S (1992) Understanding radar systems. McGraw-Hill, London, UK, p 48–61.

Kinnard KF, Dempsey DJ & Mitchell RD (1978) Laser ranging and tracking. Proceedings of the Technical Program on Electro Optics and Laser 75 Conference: 317–320.

Klein CA & Bierig RW (1974) Pulse-response characteristics of position-sensitive photodetectors. IEEE Transactions on Electron Devices 21(8): 532–537.

Kobayashi H, White JL & Abidi AA (1991) An active resistor network for gaussian filtering of images. IEEE Journal of Solid-State Circuits 26(5): 738–748.

Kostamovaara J, Määttä K, Koskinen M & Myllylä R (1992) Pulsed laser radars with high-modulation-frequency in industrial applications. Proceedings of SPIE 1633: 114–127.

Kramer J, Seitz P & Baltes H (1992) Industrial CMOS technology for the integration of optical metrology systems (photo-ASICs). Sensor and Actuators A 34(1): 21–30.

Kraus JD (1992) Electromagnetics. McGraw-Hill, New York, NY, USA, p 599–630.

Kunkel B, Lutz R & Manhart S (1985) Advanced opto-electronical sensors for autonomous rendezvous, docking and proximity operations in space. Proceedings of SPIE 591: 138–148.

Lamekin PI (1988) Polarization properties of corner reflectors. Sovjet Journal of Optical Technology 55(1): 16–19.

Langenbacher H, Chao TH, Shaw T & Yu J (1993) 64 x 64 Thresholding photodetctor array for optical pattern recognition. Proceedings of SPIE 1959: 350–358.

Lau K, Hocken R and Haynes L (1985) Robot performance measurements using automatic laser tracking techniques. Robotics and Computer-Integrated Manufacturing 2(3/4): 227–236.

Lau K, Dakalakis N & Myers D (1988) Testing. In: Dorf RC & Nof SY (eds) International Encyclopedia of Robotics: Applications and Automation. Wiley, New York, USA 3: 1753–1769.

Lawrence RS & Strohbehn JW (1970) A survey of clear-air propagation effects relevant to optical communications. Proceedings of the IEEE 58(10): 1523–1545.

Lee B (1999) Private communications. Senior application engineer, Burr-Brown Europe Ltd.

Leica Geosystems AG (1998) TPS5000 – Electronic precision theodolites for industrial applications. Product information. Heerbrugg, Switzerland.

Leica Geosystems AG (1999a) Leica TC2003/TCA2003 – High-performance total station for precision surveying to millimetre accuracies with quality certificate. Product information. Heerbrugg, Switzerland.

Leica Geosystems AG (1999b) Leica laser tracker system – Portable coordinate measuring machine for small and large objects. Product information. Heerbrugg, Switzerland.

Light W (1982) Non-contact optical position sensing using silicon photodetectors. Application Note, United Detector Technology, Hawthorne, California, USA, 24 p.

Lindholm L & Edwards IK (1991) Analog position-sensing photodetectors: New life for an old technology. Photonics Spectra 25(11): 149–156.

Lindholm L (1999) Private communications. R & D manager, SiTek Electro Optics, Partille, Sweden.

Lou DY, Martinez A & Stanton D (1984) Surface profile measurement with dual-beam optical system. Applied Optics 23(5): 746–751.

Mackenthun D & Muller R (1987) High accuracy marine positioning for dredging surveys at the port of Hamburg. Proceedings of the International Symposium on Marine Positioning, Dordrecht, Netherlands: 409–414.

Manninen M (1984) Task-oriented approach to interactive control of heavy duty manipulators based on coarse scene description. Acta Polytechnica Scandinavica, Ma 42, Helsinki, Finland.

Manninen M & Jaatinen J (1992) Productive method and system to control dimensional uncertainties at final assembly stages in ship production. Journal of Ship Production 8(4): 244–249.

Manninen M, Torvikoski T, Kaisto I, Ailisto H and Moring I (1992) ACMETER PROG – A new method and system for shape control. Proceedings of 2nd Nordic Workshop on Industrial Machine Vision, Kuusamo, Finland.

Martin Marietta Aerospace (1974) Active optical seeker. Final report prepared for US Army Missile Research, Development and Engineering Laboratory. Contract number DAAH01-74-C-0412, Orlando, Florida, USA, 61 p.

Mayer JRR & Parker GA (1994) A portable instrument for 3-D dynamic robot measurements using triangulation and laser tracking. IEEE Transactions on Robotics and Automation 10(4): 504–516.

Mead C (1989) Analog VLSI and neural systems. Addison-Wesley, USA.

Meijer GCM, van Drecht J, de Jong C & Neuteboom H (1992) New concepts for smart signal processors and their applications to PSD displacement transducers. Sensor and Actuators A 35(1): 23–30.

Melles Griot Inc. (1998) Machine vision product guide – Optical systems. MVPG 4/98, USA.

Mitsui K, Sakai M & Kizuka Y (1988) Development of a high resolution sensor for surface roughness. Optical Engineering 27(6): 498–502.

Moini A (2000) Vision chips or seeing silicon. http://www.eleceng.adelaide.edu.au/Groups/GAAS/Bugeye/visionchips/index.html (20 March 2000).

Morikawa Y & Kawamura K (1992) A small-distortion two-dimensional position-sensitive detector (PSD) with on-chip MOSFET switches. Sensors and Actuators A 34(2): 123–129.

Muro H & French PJ (1990) An integrated position sensor using JFETs as a buffer for PSD output signal. Sensors and Actuators A 22(1-3): 544–552.

Mäkynen A, Kostamovaara J & Myllylä R (1988) A laser-based 3D sensor for teaching robot paths. Proceedings of SPIE 954: 702–709.

Mäkynen A (1990) Paikkaherkkään detektoriin perustuva suuntaustekniikka, Licentiate thesis, University of Oulu, Department of Electrical Engineering.

Mäkynen AJ, Kostamovaara JT & Myllylä RA (1991) Small angle measurement in a turbulent environment using position-sensitive detectors. In: Tzafestas SG (ed) Engineering Systems with Intelligence. Kluwer, Dordrecht, Netherlands, p 275–284.

Määttä K & Kostamovaara J (1992) The effect of measurement spot size on the accuracy of laser radar devices in industrial metrology. Proceedings of SPIE 1821: 332–342.

Määttä K, Kostamovaara J & Myllylä R (1993) Profiling of hot surfaces by pulsed time-of-flight laser range finder techniques. Applied Optics 32(27): 5334–5347.

Määttä K (1995) Pulsed time-of-flight rangefinding techniques and devices for hot surface profiling and other industrial applications. Acta Universitatis Ouluensis C Technica 81.

Määttä K & Kostamovaara J (1998) A high-precision time-to-digital converter for pulsed time-of-flight laser radar applications. IEEE Transactions on Instrumentation and Measurement 47(2): 521–536.

Nakamura O, Goto M, Toyoda K, Takai N, Kurosawa T & Nakamata T (1994) A laser tracking robot-performance calibration system using ball-seated bearing mechanisms and a spherically shaped cat's-eye retroreflector. Review of Scientific Instruments 65(4): 1006–1011.

New BM (1974) Versatile electro-optic alignment system for field applications. Applied Optics 13(4): 937–941.

Nishimura T (1986) Laser rotary encoder. Robot (54): 77–83.

Nissilä S, Kostamovaara J & Myllylä R (1991) Thermal characteristics of optical delay in fibers used in pulsed laser rangefinding. Journal of Lightwave Technology 9(11): 1464–1466.

Nissilä S & Kostamovaara J (1995) On the use of optical fibres in a pulsed time-of-flight laser rangefinder. Robotica 13(1): 45–53.

Noorlag DJW & Middelhoek S (1979) Two-dimensional position-sensitive photodetector with high linearity made with standard IC-technology. Solid-State and Electron Devices 3(3): 57–82.

Noorlag DJW (1982) Quantitative analysis of effects causing nonlinear position response in position-sensitive photodetectors. IEEE Transactions on Electron Devices 29(1): 158–161.

Noptel Oy (1997) Optical marksmanship training and analysis systems. Product information.

Owen RB & Awcock ML (1968) One and two dimensional position sensing semiconductor detectors. IEEE Transactions on Nuclear Science 15(3): 290–303.

Palojärvi P, Ruotsalainen T, Simin G & Kostamovaara J (1997) Photodiodes for high frequency applications implemented in CMOS and BiCMOS processes. Proceedings of SPIE 3100: 119–126.

Perez E, Bailly M & Pairot JM (1989) Pointing acquisition and tracking systems for Silex intersatellite optical link. Proceedings of SPIE 1111: 277–288.

Petersson GP & Lindholm LE (1978) Position sensitive light detectors with high linearity. IEEE Journal of Solid-State Circuits 13(3): 392–399.

Pohlmann K (1992) The compact disk handbook. The Computer Music and Digital Audio Series, Volume 5. A-R Editions.

Prometrics Ltd. (1993a) ACMAN 2000 Automatic 3D dimensional control system. Product information.

Prometrics Ltd. (1993b) ACMAN 1000 3D dimensional control system. Product information.

Ruotsalainen R (1999) Integrated receiver channel circuits and structures for a pulsed time-of-flight laser radar. Acta Universitatis Ouluensis C Technica 136.

Räisänen-Ruotsalainen E (1998) Integrated time-to-digital converter implementations. Acta Universitatis Ouluensis C Technica 122.

Sandage RW & Connelly JA (1996) Producing phototransistors in a standard digital CMOS technology. Proceedings of IEEE International Symposium on Circuits and Systems, Atlanta, Georgia, USA 1: 369–372.

Sayles AH & Uyemura JP (1991) An optoelectronic CMOS memory circuit for parallel detection and storage of optical data. IEEE Journal of Solid-State Circuits 26(8): 1110–1115.

Schuda FJ (1983) High-precision, wide-range, dual-axis, angle monitoring system. Review of Scientific Instruments 54(12): 1648–1652.

Seikosha Corp. (1994) X-126 Distance sensor module. Product data sheet.

Sepp G (1984) CW diode laser instrumentation for rendez-vous and docking manoeuvers in geosynchronous orbits. Proceedings of ESA Workshop on Space Laser Applications and Technology. ESA, Paris, France: 249–254.

Shamash Y, Yang Y & Roth Z (1988) Teaching a robot. In: Dorf RC & Nof SY (eds) International Encyclopedia of Robotics: Applications and Automation. Wiley, USA, 3: 1753–1769.

Sharp Corp. (1997) GP2D12/GP2D15 – Distance measuring sensors. Product data sheet U970501, Japan.

SiTek Electro Optics (1996) PSD user's manual – Position sensing detectors. Partille, Sweden, 51 p.

Sklair C, Hoff W & Gatrell L (1991) Accuracy of locating circular features using machine vision. Proceedings of SPIE 1612: 222–234.

Smith JG (1983) A new high precision range/azimuth position fixing system. Sea Technology 24(3): 33–36.

Smith T & Huijsing JH (1991) An integrated linear position sensitive detector with digital output. IEEE International Conference on Solid-State Sensors and Actuators. Digest of Technical Papers. IEEE, New York, USA: 719–722.

Soncini G, Zen M, Rudan M & Verzellesi G (1991) On the electro-optical characteristics of CMOS compatible photodiodes. Proceedings of the 6th Mediterranean Electrotechnical Conference, Ljubjana, Yugoslavia: 111–113.

Sparrius AJA (1981) Electro-optical imaging target trackers. Transactions of the South African Institute of Electrical Engineers 72(11): 278–284.

Spectra-Physics VisionTech (1996) LR-2000 Delta. Product information. Oulu, Finland.

Spectra Precision AB (1998a) Geodimeter 600 ATS. Product information. Publication No 571740311, Danderyd, Sweden.

Spectra Precision AB (1998b) Geodimeter System 600 Pro. Product information. Publication No 571710541, Danderyd, Sweden.

Spiess S, Vincze M & Ayromlou M (1998) On the calibration of a 6-D laser tracking system for dynamic robot measurements. IEEE Transactions on Instrumentation and Measurement 47(1): 270–274.

Standley DL (1991) An object position and orientation IC with embedded imager. IEEE Journal of Solid-State Circuits 26(12): 1853–1859.

Stenberg L (1999) SiTek's PSD-school. Non-Contact – People, Products & News 1995-2000. Newsletter SiTek Electro Optics, Partille, Sweden.

Strand TC (1985) Optical three dimensional sensing for machine vision. Optical Engineering 24(1): 33–40.

Symmons Industries Inc. (1999) Ultra-sense, sensor faucets with position sensitive detection. Product information. Braintree, Massachusetts, USA.

Sze SM (1981) Physics of semiconductor devices. Wiley, USA, p 750.

Tartagni M & Perona P (1993) Computing centroids in current-mode technique. Electronics Letters 29(21): 1811–1813.

UDT Sensors Inc. (1998) Standard photodetector component catalog, Hawthorne, California, USA.

Umminger CB & Sodini CG (1995) An integrated analog sensor for automatic alignment. IEEE Journal of Solid-State Circuits 30(12): 1382–1390.

Venier P, Landolt O, Debergh P & Arreguit X (1996) Analog CMOS photosensitive array for solar illumination monitoring. IEEE International Solid-State Circuits Conference, San Francisco, California, USA. Digest of Technical Papers. IEEE, New York, USA 1: 96–97.

Vidal MP, Bafleur M, Buxo J & Sarrabayrouse G (1991) A bipolar photodetector compatible with standard CMOS technology. Solid-State Electronics 34(8): 809–814.

Wallmark JT (1957) A new semiconductor photocell using lateral photoeffect. Proceedings of the IRE 45: 474–483.

Walter JF (1976) Prospects for precision active tracking using a quadrant detector. Technical Memorandum APL/JHU TG 1290, The Johns Hopkins University, Applied Physics Laboratory, Laurel, Maryland, USA, 61 p.

Wang W & Busch-Vishniac IJ (1989) The linearity and sensitivity of lateral effect position sensitive devices – An improved geometry. IEEE Transactions on Electron Devices 36(11): 2475–2480.

Weichel H (1990) Laser beam propagation in the atmosphere. SPIE, Bellingham, Washington, USA, p 45–66.

Woltring HJ (1975) Single- and dual-axis lateral photodetectors of rectangular shape. IEEE Transactions on Electron Devices 22(8): 581–590.

Wong HS (1996) Technology and device scaling considerations for CMOS imagers. IEEE Transactions on Electron Devices 43(12): 2131–2142.

Yamamoto K, Yamaguchi S & Terada Y (1985) New structure of two-dimensional position sensitive semiconductor detector and applications. IEEE Transactions on Nuclear Science 32(1): 438–442.

Yanhai Y (1986) The design of echo spot and optical focusing in automatic laser tracking. Optics and Laser Technology 18(2): 75–79.

Ylitalo J (1994) Private communications. R & D engineer, Prometrics Ltd., Finland.

Young PW, German LM & Nelson R (1986) Pointing, acquisition and tracking subsystems for space-based laser communications. Proceedings of SPIE 616: 118–128.

Yura HT & Tavis MT (1985) Centroid anisoplanatism. Journal of Optical Society of America A 2(5): 765–773.

Zumbrunn R (1995) Systematic pointing errors with retroreflective targets. Optical Engineering 34(9): 2691–2695.